



LODZ UNIVERSITY OF TECHNOLOGY
FACULTY OF MECHANICAL ENGINEERING
Division of Dynamics



Łukasz Borkowski

PHD DISSERTATION

**NUMERICAL AND EXPERIMENTAL ANALYSIS
OF COUPLING AND DELAY EFFECTS IN THE ARRAY
OF NONLINEAR OSCILLATORS**

SUPERVISOR:
Prof. Andrzej Stefański, Ph.D., D.Sc.



EUROPEAN UNION
EUROPEAN REGIONAL
DEVELOPMENT FUND



ŁÓDŹ 2013

CONTENTS

1. INTRODUCTION.....	3
1.1. Scenarios of a transition to chaos	4
1.2. 3D torus	6
1.3. Ring of coupled oscillators – a rotating wave	8
1.4. Systems with time delay	9
1.5. Subject of the work – oscillators under analysis	10
1.6. Aims and thesis.....	13
2. RING OF SEVEN UNIDIRECTIONALLY COUPLED NONLINEAR DUFFING OSCILLATORS – STABILITY ANALYSIS OF STATIONARY STATES	15
2.1. Stability of steady states in a circuit of identical oscillators.....	16
2.2. Stability of steady states in a circuit of real oscillators	19
3. NUMERICAL ANALYSIS OF A RING OF SEVEN UNIDIRECTIONALLY COUPLED DUFFING OSCILLATORS	23
3.1. Numerical results	25
3.2. FFT analysis	45
4. ANALYSIS OF AN EXPERIMENTAL CIRCUIT OF SEVEN UNIDIRECTIONALLY COUPLED DUFFING OSCILLATORS	48
4.1. Structure and parameters of the experimental rig.....	48
4.2. Mathematical description	55
4.3. Experimental investigations	60
4.4. FFT analysis of the electrical circuit	69
5. NUMERICAL ANALYSIS OF A DUFFING OSCILLATOR WITH A TIME DELAY LOOP	72
5.1. Numerical results	73
5.2. FFT analysis of the studied system.....	80
6. ANALYSIS OF THE RESULTS AND CONCLUSIONS	81
BIBLIOGRAPHY	95

CHAPTER 1

INTRODUCTION

A growing interest in the theory of nonlinear dynamical systems has aroused in the last few years. Applications of nonlinear dynamics can be observed in many different fields of science such as physics, chemistry, biology, economics, engineering sciences.

One of the most exciting and fastest growing sectors of nonlinear dynamics is the theory of bifurcation and chaos. According to this theory, dynamical systems, in which there are rapid changes in stability solutions – bifurcation – or irregular, sensitive to initial conditions solutions – chaos, are analyzed.

The reason for observation of chaotic behavior in dynamical systems is their property, which consists in exponential propagation of initially close trajectories in the phase space [1].

The first discovery of chaotic behavior was presented by Jacques Salomon Hadamard, who published his thesis in 1898 [2], describing the balls moving without friction on the surface of negative curvature. Hadamard proved that all trajectories would be unstable under those conditions – they would be exponentially apart from each other.

In the late nineteenth and early twentieth century, the French mathematician Henri Poincaré dealt with the problem of orbits of three mutually attracting celestial bodies [3] (e.g., a star and two planets). Recognizing that the behavior of orbits depends on starting points, Poincaré was able to show very complicated orbits – now called chaotic orbits. Further, remarkable works on chaotic systems were presented by G. Birkhoff in 1920 [4], M.L. Cartwright in 1952 [5], S. Smale in 1961 [6] and Russian mathematicians, especially A.N. Kolmogorov [7,8] and his colleagues.

In 1963, Edward Lorenz proposed and examined the first autonomous chaotic system of three coupled nonlinear differential equations modeling the thermal convection in the atmosphere [9]. He proved that for a certain set of parameters, the system behaved in a chaotic manner – the graph of variables in the phase space demonstrated a strange attractor, now referred to as the Lorenz attractor.

Thirteen years later (1976) Otto Eberhard Rössler presented even a simpler system of three coupled nonlinear differential equations [10]. For some parameters, the trajectory

starting from the initial point located on the surface goes into a set called the Rössler strange attractor.

In 1999, Guanrong Chen and Tetsushi Ueta presented a simple three-dimensional autonomous system [11], where they observed a new chaotic attractor, which had features of the Lorenz and Rössler attractors.

In the next few years, more and more researchers and scientists dealt with the issue of chaos. The reason for this is the fact that the phenomenon of chaos is observed in many areas of life and science. An example of this, some works from the area of biology [12,13,14], chemistry [15,16,17], economics [18,19,20], physics [21,22,23] can be quoted.

The phenomenon of chaos in mechanical and electrical systems has been also well known and analyzed for many years. Numerous authors of papers describing physical systems use the Duffing equation [24-28] to model different types of nonlinear phenomena or the Van der Pol equation [29-34], which is used to describe self-excited systems.

The development of scientific papers on deterministic chaos has led to progress in the description of transition scenarios to chaotic motion [45-50,52,53]. In addition, new research issues such as the control of chaos [35-39] and the synchronization of chaos [40-44] have been observed.

1.1. Scenarios of a transition to chaos

The first scenario of a transition from periodic to chaotic behavior was presented by L.D.Landau in 1944 [45] and four years later (1948) by E.A.Hopf [46], independently. The Landau-Hopf scenario assumed that during a transition of the control parameter that characterized the analyzed system, for example the critical value of the Reynolds number (R), which is a parameter characterizing the fluid flow, the steady flow loses its stability. During an increase in the Reynolds number, some consecutive, new disproportionate frequencies appear (Fig.1.1).

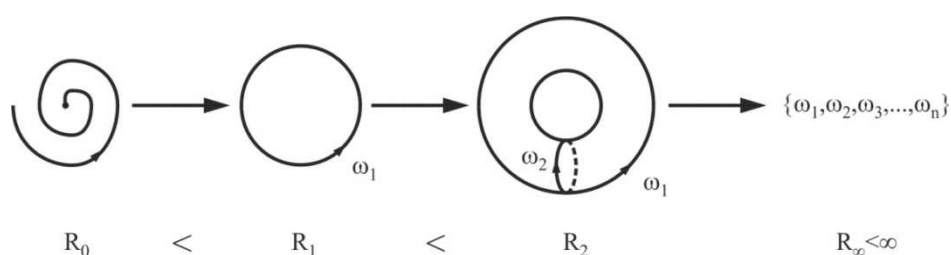


Fig.1.1. Scheme of the Landau-Hopf scenario.

For $R \rightarrow \infty$, the velocity of the generation of a new frequency increases, which leads to an appearance of a wide continuous frequency range characteristic of chaotic behavior. A solution to the Landau-Hopf scenario can be expressed by the formula:

$$y(\rho, t) = \sum_{n=1}^{\infty} A_n(\rho) e^{im(\omega t + \delta)}$$

where: $\omega = \{\omega_1, \omega_2, \dots, \omega_n\}; n \rightarrow \infty; R \rightarrow \infty$.

Another similar scenario of a transition to chaos is the Newhouse-Ruelle-Takens scenario [47]. It refers to the Landau-Hopf scenario and corrects it. In 1971, Ruelle and Takens proved [48] that an infinite series of Hopf bifurcations was not required in order to achieve the stabilization of the system. They presented a system, which just after the third Hopf bifurcations reached the orbit, might lose its stability and transform into a strange chaotic attractor (a more detailed description of the NRT scenario will be discussed later in this study).

Another scenario of a transition to chaos was suggested by M.J. Feigenbaum in 1978 [49,50]. According to this approach, the way of a transition to chaos can be realized by a series of period doubling bifurcations. An example is a simple, one-dimensional logistic map:

$$y_{n+1} = 4\lambda r(1 - y_n), \quad 0 < y < 1,$$

where λ is the control parameter. Feigenbaum discovered that the factor of the difference between successive approximations in place of the bifurcation has a constant value:

$$\lim_{n \rightarrow \infty} \delta_n = \lim_{n \rightarrow \infty} \frac{\lambda_{n+1} - \lambda_n}{\lambda_{n+2} - \lambda_{n+1}} = 4,6692016 \dots$$

Thus, he obtained a fixed factor of convergence, which was also found in the Lorenz model and in the Henon map [51]. The discovery of this constant is an important contribution to the

explanation of more complex behavior of the chaotic system. Therefore, this convergence factor is called the Feigenbaum constant.

Another well-known way to chaos is the Pomeau and Manneville scenario [52,53], which was demonstrated in 1980. It manifests with a transition to chaotic behavior through a sudden jump-type solution during the time evolution of the system. This effect is called intermittency, i.e., a transition between the two types of behavior – the periodic-like and chaotic behavior. Analyzing the Lorenz system, they observed that despite of the chaotic behavior, the trajectory got in the neighborhood of the fixed point, where it could stay for a very long time. A movement to the environment of the fixed point is seemingly at random. The reason for the occurrence of intermittency in the Lorenz system is saddle-node bifurcation, which leads to the formation of stable and unstable fixed points.

Current studies often refer to the above-mentioned scenarios in the analysis of complex dynamical systems.

In the following years, extensive research has led to an emergence of new discoveries in scenarios of a transition to chaos. One of the most interesting and currently studied phenomena in nonlinear dynamics is an existence of a stable three-dimensional torus (3D torus).

1.2. 3D torus

Initially, it was thought that the existence of a 3D torus was unlikely (according to the theory of NRT). However, numerical studies by C.Grebogi, E.Ott, J.A.Yorke [54,55], Battelino [56] and experimental studies by J.P.Gollub, S.V.Benson [57], P.S.Linsay, A.W.Cumming [58], R.Alaggio, G.Regia [59] have confirmed the presence of a stable 3D torus in the phase space of dynamical systems, in contrary to the NRT theory. Further convincing evidence for the existence of a 3D torus was presented in works by U.Feudel, W.Jansen, J.Kurths [60], V.S.Anishchenko [61], U.Feudel [62], J.Yang [63]. In their studies, a 3D torus appeared during a transition to chaos and bifurcations following the scheme: 2D torus→3D torus→2D torus→chaos. The occurrence of a 3D torus is related to the fact that the perturbations that affect these attractors are not generic due to the symmetry of the system (according to the NRT theory, a 3D torus is unstable when subjected to some general perturbations).

Another way of a transition to chaos containing a 3D torus was demonstrated in studies by M.Lopez and F.Marquesa [64,65]. Using the Navier-Stokes equations, they introduced the so-called “gluing bifurcation” of two 3D tori to a new (non-chaotic) 3D torus.

At the turn of the century, M.A.Matias, E.Sanchez and D.Pazo showed in their works a 3D torus in the ring of unidirectionally coupled Chua oscillators [66] and in the ring of Lorenz oscillators [67,68,69]. They found [66,67] that the third zero Lyapunov exponent appeared as a result of the symmetric Hopf bifurcation. Then, we observe an additional rotational degree of freedom, which corresponds to a simultaneous shift to the neighboring oscillator and an advance in time by a period divided by N (N is a number of oscillators in the ring). This leads to the third frequency in the torus and to the high-dimensionality of the chaotic attractor. They found that the spatio-temporal symmetry allowed one to obtain a stable three-dimensional attractor in a finite range of the control parameter. In [68] a different way of a transition to chaos, which is carried out according to the scheme: 2D torus→3D torus→high-dimensional chaos, is presented.

Also, scientists from China presented a study in which they observed a stable 3D torus. For example, Q.Bi [70] analyzed two parametrically coupled Van der Pol oscillators. He presented two ways of bifurcation periodic solutions:

1. Periodic solution as a result of generalized static bifurcation leads to a quasi-periodic solution.
2. Periodic solution as a result of the Hopf bifurcation leads to a stable 3D torus.

With a further increase in the control parameter, the solutions in both cases lead to chaotic behavior.

On the other hand, the research conducted by W.Wu, Z.Chen, Z.Yuan [71] presented an autonomous system of four first-order equations, which showed a rich dynamical behavior. With an increase in the control parameter, the system evolves from a 3D torus, through a series of periodic, quasi-periodic, chaotic behavior and then proceeds to a hyper-chaotic solution, ending in a periodic solution.

The phenomenon of a 3D torus is increasingly recognized and observed in the analysis of dynamical systems.

The present Subsection is closely related to previous Subsection 1.1 because the presence of a 3D torus is noticeable by a transition to chaotic behavior. Currently, there are many works that describe different scenarios of a transition to chaos containing a 3D torus. In this thesis, one of these scenarios is presented.

1.3. Ring of coupled oscillators – a rotating wave

In the cases of series one-way coupled oscillators in a ring, an occurrence of the phenomenon of the so-called rotating wave (RW) should be mentioned. The appearance of the rotating wave is associated with a loss of stability of the system.

Already in 1952, A.M.Turing [72] started the study of linear instabilities in rings of uniform systems. In later years, the phenomenon of the RW was observed in numerical [73,74] and experimental [75] studies.

In 1997, A.Matias, V.Perez-Munuzuri, M.N.Lorenzo, I.P.Marino and V.Perez-Villar [76] studied a system of four unidirectionally coupled Chua oscillators. The system retained symmetry – each of the oscillators had the same parameters. They found that the formation of the rotating wave occurred due to a loss of stability of the system. The stability loss of the system was a result of the Hopf bifurcation. They also found that a similar mechanism of a loss of stability occurred in the ring of Lorenz oscillators. As a result, they found that the source of an occurrence of the RW in the rings of unidirectionally coupled nonlinear oscillators was the symmetry of that configuration.

A detailed study on an occurrence of the rotating wave in rings of unidirectionally coupled Lorenz oscillators was presented by E.Sanchez, D.Pazo, M.A.Matias [77] in 2006. They studied a system of three coupled oscillators, in which they observed an occurrence of both the periodic (PRW) and chaotic (CRW) rotating wave. In the range of the PRW, the largest Lyapunov exponent is equal to zero and other exponents are negative. The CRW range is divided into two areas due to the Lyapunov exponents: the first one was characterized by the positive largest Lyapunov exponent, two zero and a rest of the negative Lyapunov exponents, whereas in the second area, the two largest Lyapunov exponents had positive values, the next one was equal to zero and the others were negative exponents. For the PRW and the CRW, they observed a characteristic phase shift between each of the oscillators. The graphs of time waveforms for the next, adjacent oscillators are phase-shifted by $2\pi/N$ (where N is a number of oscillators).

In 2010, P.Perlikowski *et al.* [78] presented the complex dynamics in a ring of unidirectionally coupled Duffing oscillators. In one part of the work, the behavior of three unidirectionally coupled Duffing oscillators is described. With an increase in the coupling parameter, the presence of the PRW, the quasi-periodic rotating wave (QRW) and the CRW can be observed. Similarly to papers [76,77], the PRW occurs as a result of the Hopf

bifurcation, the QRW arises from the Neimark-Sacker bifurcation (a 2D torus appears). A further increase in the coupling parameter causes a transition to chaotic behavior – the CRW arises. For the PRW, the resulting waveforms for timing graphs are shifted in phase with each other by a fixed value. However, the Neimark-Sacker bifurcation introduced a small symmetry break into the system – a value of the phase shift for the next oscillators was slightly different.

It should be noted that these works describe systems of identical oscillators, which can be realized only in numerical simulations. However, a number of papers describing the behavior of a real circuit, in which each oscillator has slightly different parameters (mismatch of parameters) is significantly smaller [79,80,81]. Therefore, identical rings of oscillators and real rings of slightly non-identical oscillators are examined in this dissertation.

1.4. Systems with time delay

The phenomenon of time delay is one of the most important issues that occur during the analysis of dynamical systems. The research conducted to this point suggests that the dynamics of a system incorporating time delay can be very complicated and can have a number of interesting features. In addition, it is demonstrated that time delay in dynamical systems is one of the most effective methods of chaos control (or anti-control), because time delay can be easily controlled and implemented in real applications.

Already in 1970's it was shown that introducing time delay to the simplest, one-dimensional oscillator could lead to very complicated, chaotic behavior (Mackey and Glass [82], Farmer [83], Lu and He [84]). In the subsequent years, A.Maccari [85] presented an effect of time delay and feedback gain on the peak amplitude of the fundamental resonance in the nonlinear Van der Pol oscillator. He showed that choosing the appropriate value of time delay and feedback gain could reduce the peak amplitude and suppress the quasi-periodic motion.

In 2002, P.Yu, Y.Yuan, J.Xu [86] presented a nonlinear oscillator with time delay introduced for the linear and non-linear part of the equation in the feedback loop. By changing the value of time delay, they observed a rich dynamical behavior of the system. They showed a presence of periodic, quasi-periodic and chaotic motion. They concluded that the feedback value of the nonlinear part had to be different from zero to obtain a chaotic solution. Furthermore, they noted that only the positive feedback value caused bifurcation from one

state to another. They suggested that a positive feedback was necessary in order to obtain a chaotic solution.

In 2003, J.Xu and K.W.Chung [87] presented a Van der Pol-Duffing oscillator with time delay introduced for the linear and non-linear part of the equation in the feedback loop. They got two ways of a transition to solve the chaotic solution – through a period-doubling bifurcation and a torus decay bifurcation. They have recognized that time delay plays a very important role in analyzing the behavior of dynamical systems. A proper selection of time delay suppresses effectively vibrations. They have found that time delay can be used as a simple “switch” to control the behavior of the system. The use of time delay allows one also to generate chaotic solutions.

In this dissertation, a nonlinear Duffing oscillator with time delay introduced in the feedback loop is examined, and in particular, a scenario of a transition to chaotic solution.

1.5. Subject of the work – oscillators under analysis

The subject of this study is an analysis of the classical Duffing oscillator in two configurations:

1. as a closed ring of unidirectionally coupling oscillators (Fig.1.2).
2. as a system with time delay (Fig.1.3).

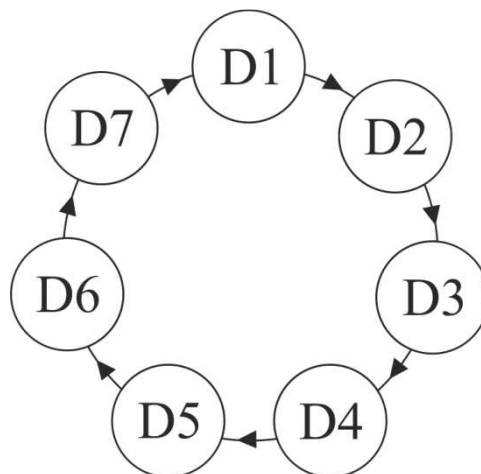


Fig.1.2. Ring of seven, unidirectionally coupled nonlinear Duffing oscillators.

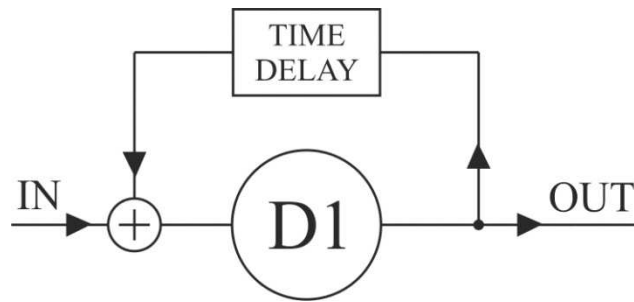


Fig.1.3. Duffing oscillator with time delay.

A nonlinear damped Duffing oscillator (without force) is described by the equation:

$$\ddot{u} + c\dot{u} + au + bu^3 = 0 \tag{1.1}$$

where: a, b, c are parameters. If the parameter a is a positive number, we are talking about the so-called single-well Duffing oscillator (one position of equilibrium). Otherwise ($a < 0$), we have to deal with the so-called double-well Duffing oscillator (three possible positions of equilibrium). In this work, a single-well version ($a > 0$) has been subjected to analysis.

Using the Duffing equation, many mechanical and physical systems and processes can be modeled, for example:

- mathematical and physical (inverted) pendulum [24] (Fig. 1.4),

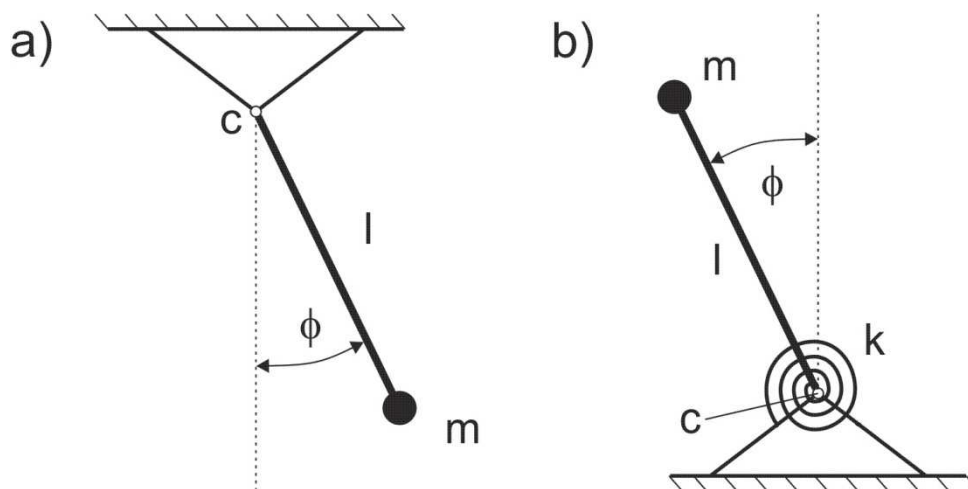


Fig.1.4. Mathematical (a) and physical (inverted) (b) pendulum.

- vibrations of the buckled beam under the action of axial force [25, 26] (Fig. 1.5),

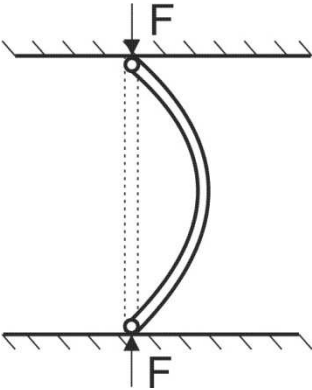


Fig.1.5. Buckled beam under the action of axial force.

- oscillator with a nonlinear spring – a Duffing oscillator [27] (Fig. 1.6),

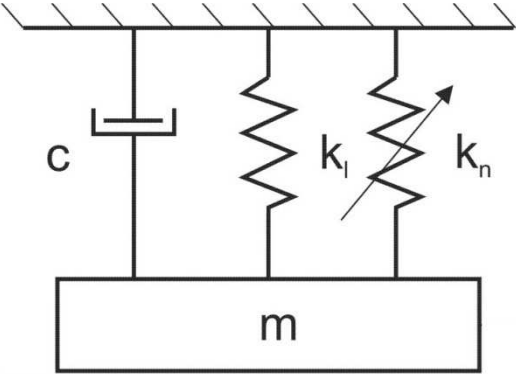


Fig.1.6. Oscillator with a nonlinear spring – a Duffing oscillator.

- RLC circuits with nonlinear inductors [28] (Fig. 1.7).

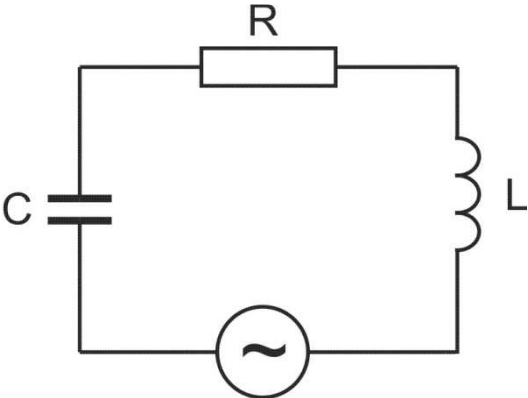


Fig.1.7. RLC circuit with nonlinear inductors.

Coupled oscillators in a ring can be described by following general equation:

$$\ddot{u}_j + c\dot{u}_j + au_j + bu_j^3 = \sigma(u_{j-1} - u_j) \quad (1.2)$$

where:

σ - coefficient of the unidirectionally coupling, $j=1, \dots, N$.

For the purpose of the numerical and experimental analysis, the number $N=7$ of oscillators was adopted, because a wide and interesting from the scientific point of view spectrum of dynamic behavior of the analyzed system was observed for this value.

On the other hand, a single Duffing oscillator with time delay is described the following equation:

$$\ddot{u}(t) + c\dot{u}(t) + au(t) + bu(t)^3 = p[u(t - \tau) - u(t)] \quad (1.3)$$

where:

τ – time delay parameter,

p – delay gain.

1.6. Aims and thesis

The main aim of this dissertation is to show a dynamical analogy between a ring of unidirectionally coupled oscillators and systems with time delay, mainly in the context of similarity of bifurcation scenarios leading from steady-state through periodic motion to hyper-chaos. A particular emphasis is placed on an experimental verification of the numerical results and an identification of the mechanism of destabilization of the steady-state and periodic solution as a result of an increase in the coupling parameter or a magnitude of time delay. Furthermore, the aim of this dissertation also includes an explanation of the mechanism of formation and stabilization of a 3D torus.

Specific objectives of the work:

1. Numerical modeling of nonlinear Duffing oscillators unidirectionally coupled in a ring (Eq. (1.2)) and single Duffing oscillators with a time delay loop (Eq. (1.3)).
2. Stability analysis of stationary states of the investigated array of oscillators as a function of the increasing coupling parameter.
3. Analysis of the results and the solutions observed in the numerical analysis, in particular the expected three-frequency quasi-periodic solution.
4. Design and construction of the experimental ring, optimized on the basis of the numerical simulations.
5. Experimental confirmation of the numerical results and observations.
6. Description of the mechanism of vibration excitation in closed arrays of unidirectionally coupled oscillators.
7. Identification of the stabilization mechanism of the three-frequency torus.
8. Introduction of a feedback with time delay for the analyzed oscillator.
9. Numerical identification of analogies and differences between the ring of unidirectionally coupled oscillators and the system with time delay.
10. Compilation of the results, conclusions and a text of the dissertation.

Work thesis:

A three-frequency quasi-periodic solution in the ring of unidirectionally coupled oscillators can occur and there are many analogies between the dynamic behavior of such systems and oscillators with a delayed feedback.

CHAPTER 2

RING OF SEVEN UNIDIRECTIONALLY COUPLED NONLINEAR DUFFING OSCILLATORS – STABILITY ANALYSIS OF STATIONARY STATES

To analyze the steady states (critical points) of unidirectionally coupled Duffing oscillators in a ring (1.2), a conversion of variables i.e., $x = u, y = \dot{u}$, was applied. Also, a small difference in the parameters of individual oscillators (mismatch of parameters), inevitable in real systems, was taken into account. As a result, the obtained system of first order differential equations takes the general form:

$$\begin{aligned}\dot{x}_j &= y_j \\ \dot{y}_j &= -cy_j - ax_j - bx_j^3 + \sigma(\kappa_{zj}x_{j-1} - \kappa_{yj}x_j)\end{aligned}\quad (2.1)$$

where $j = 1, \dots, 7$. The coefficients κ_{zj} and κ_{yj} model a possible mismatch of coupling terms in the real circuit. For identical items, we have nominal values of parameters: $a_j = a, b_j = b, c_j = c$ and $\kappa_{zj} = \kappa_{yj} = 1$. The overall coupling coefficient σ is considered as the control parameter. When node systems (2.1) are uncoupled ($\sigma = 0$), then the solution to Eq. (2.1) tends to a stable fixed point $U(0,0)$, i.e., $x_j = 0, y_j = 0$, in the phase space due to the presence of damping ($c > 0$) and a lack of forcing. Then, free damped vibrations (oscillation death) can be observed. The coupled oscillators also have only one critical point $U(0, \dots, 0)$ in the fourteen-dimensional phase space of system (2.1). In order to evaluate its stability, such an analysis for the linearized system around the critical point is performed.

In the case of identical coupled oscillators, Eq. (2.1) can be written in the following matrix form:

$$\dot{u}_j = Au_j + B(u_j) + Ku_{j-1}\quad (2.2)$$

where:

$$u_j \in \mathbf{R}^2 \quad (j = 1, 2, \dots, N),$$

A – Jacobi matrix of the linear part,

$B(u_j)$ – matrix of the nonlinear part,

$K: \mathbf{R}^2 \rightarrow \mathbf{R}^2$ – output function (coupling matrix) of each oscillator variables that is used in the coupling.

Thus, individual vectors and matrices in the Eq. (2.2) are described by following formulas:

$$u_j = \begin{pmatrix} x_j \\ y_j \end{pmatrix} \quad \dot{u}_j = \begin{pmatrix} \dot{x}_j \\ \dot{y}_j \end{pmatrix} \quad u_{j-1} = \begin{pmatrix} x_{j-1} \\ y_{j-1} \end{pmatrix}$$

$$A = \begin{bmatrix} 0 & 1 \\ -(a + \sigma) & -c \end{bmatrix} \quad B(u_j) = \begin{bmatrix} 0 & 0 \\ -x_j^3 & 0 \end{bmatrix} \quad K = \begin{bmatrix} 0 & 0 \\ \sigma & 0 \end{bmatrix}$$

2.1. Stability of steady states in a circuit of identical oscillators

Using [78] in order to analyze the stability of stationary states, the ring of seven nonlinear Duffing oscillators can be represented in the notation of a block matrix:

$$\dot{\mathbf{u}} = (\mathbf{I} \otimes A)\mathbf{u} + \mathbf{D}(\mathbf{u}) + (\mathbf{G} \otimes K)\mathbf{u} \quad (2.1.1)$$

where \otimes is a direct (Kronecker) product of two matrices, $\mathbf{u} = [u_1, u_2, u_3, u_4, u_5, u_6, u_7]^T$, $\mathbf{D}(\mathbf{u}) = \text{diag}[B(u_1), \dots, B(u_7)]$, \mathbf{I} is the 7×7 identity matrix, \mathbf{G} is the 7×7 connectivity matrix representing the topology of connections between the ring nodes. For the unidirectional ring structure, the matrix \mathbf{G} has the following structure:

$$\mathbf{G} = \begin{bmatrix} 0 & 0 & 0 & 0 & 0 & 0 & 1 \\ 1 & 0 & 0 & 0 & 0 & 0 & 0 \\ 0 & 1 & 0 & 0 & 0 & 0 & 0 \\ 0 & 0 & 1 & 0 & 0 & 0 & 0 \\ 0 & 0 & 0 & 1 & 0 & 0 & 0 \\ 0 & 0 & 0 & 0 & 1 & 0 & 0 \\ 0 & 0 & 0 & 0 & 0 & 1 & 0 \end{bmatrix}$$

Equation (2.1.1) has a symmetric equilibrium point $\mathbf{u} = [0, 0, 0, 0, 0, 0, 0]^T$.

By linearization of Eq. (2.1.1), we obtain a variational equation of the form:

$$\delta \dot{\mathbf{u}} = [\mathbf{I} \otimes \mathbf{A} + \mathbf{G} \otimes \mathbf{K}] \delta \mathbf{u} \quad (2.1.2)$$

where: $\delta \mathbf{u} = [\delta u_1, \delta u_2, \delta u_3, \delta u_4, \delta u_5, \delta u_6, \delta u_7]^T$.

After diagonalization of variational Eq. (2.1.2) seven independent equations appear [88,89]:

$$\delta \dot{u}_j = (A + \gamma_j K) \delta u_j, \quad j = 1, \dots, 7, \quad (2.1.3)$$

where δu_j are variational coordinates and γ_j are eigenvalues of the connectivity matrix G , which can be expressed as:

$$\gamma_j = e^{i2\pi j/7}, \quad j = 1, \dots, 7. \quad (2.1.4)$$

After some transformations, the stability analysis reduces to the characteristic equation:

$$\theta(\lambda, j) := \det(\lambda \mathbf{I} - \mathbf{A} - \gamma_j \mathbf{K}) = 0, \quad j = 1, \dots, 7. \quad (2.1.5)$$

Substituting Eq. (2.1.4) into Eq. (2.1.5), we obtain:

$$\theta(\lambda, j) := \det(\lambda \mathbf{I} - \mathbf{A} - e^{i2\pi j/7} \mathbf{K}) = 0, \quad j = 1, \dots, 7. \quad (2.1.6)$$

Solving Eq. (2.1.6), the eigenvalues of the Jacobi matrix can be expressed by the formulas:

$$\lambda_{1,2}(j) = -\frac{c}{2} \pm \sqrt{\left(\frac{c}{2}\right)^2 - a - \sigma(1 - e^{\frac{i2\pi j}{7}})}, \quad j = 1, \dots, 7. \quad (2.1.7)$$

For the analyzed, ideal system (with the same parameters in all subsystems) of seven unidirectionally coupled nonlinear Duffing oscillators, the dimensionless parameters are as follows: $c = 0.03162$; $a = 1$; and σ is the control parameter of bifurcation. A detailed description of these parameters is given in Chapter 4.

The calculations of the matrix eigenvalues (Fig. 2.1.1, 2.1.2, 2.2.1, 2.2.2) were performed with Wolfram Mathematica 8 and the graphs were drawn up in OriginPro 8.

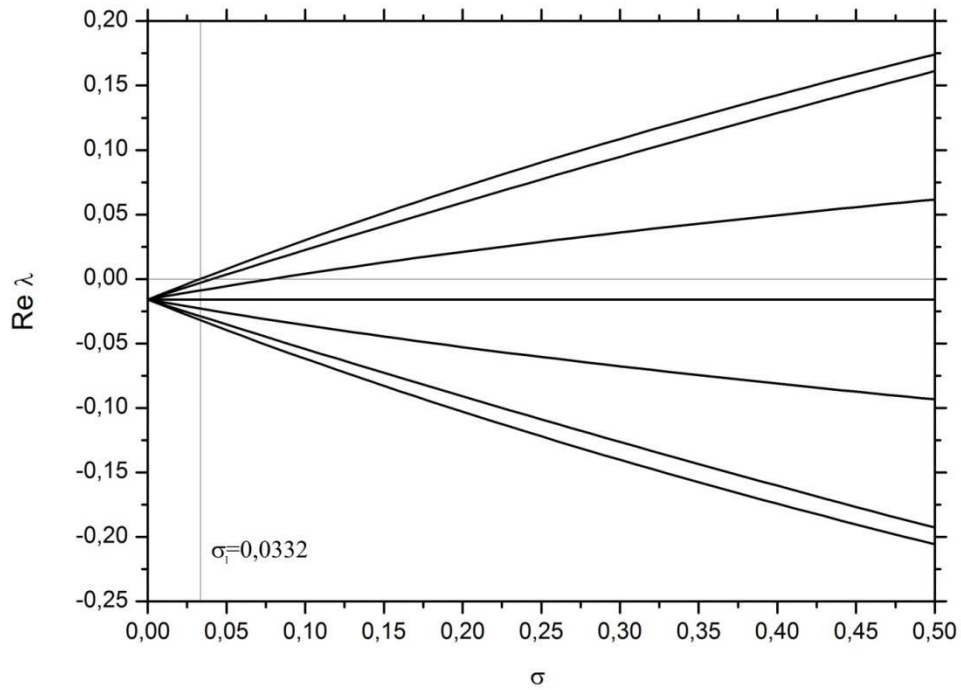


Fig. 2.1.1. Graph of the real eigenvalues $Re \lambda$ of linearized system (2.1.2) versus the coupling parameter σ for a ring of seven identical Duffing oscillators.

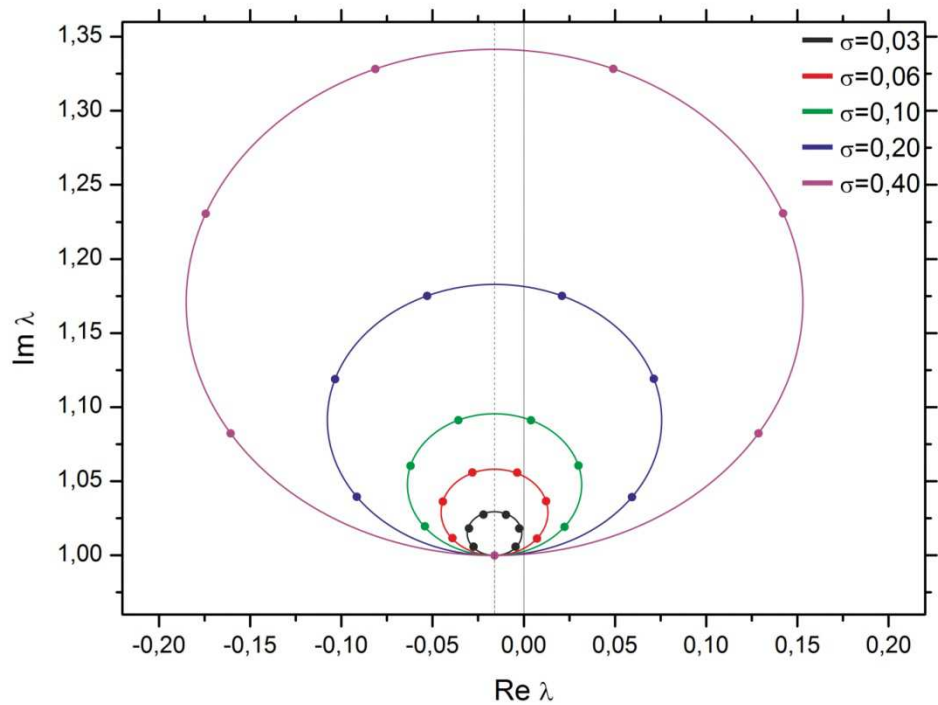


Fig. 2.1.2. Eigenvalues of linearized system (2.1.2) on the complex plane (the positive imaginary parts $Im \lambda$ versus the real parts $Re \lambda$) for a ring of seven identical Duffing oscillators with different values of the coupling parameter σ .

In Fig. 2.1.1 a dependence of the real eigenvalues $Re \lambda$ of linearized system (2.1.2) as a function of the coupling parameter σ for a ring of seven identical Duffing oscillators is shown. In this graph, the critical value of the coupling parameter, for which the first real eigenvalue changes its sign to positive, amounts to $\sigma = 0.0332$. This means that there is a supercritical Hopf bifurcation – a transition of the system from the critical point to the limit cycle occurs. The graph shows the curves representing fourteen $Re \lambda$, however, only seven of them are visible because each curve is drawn twice. The same values of real parts overlap the following pairs of oscillators: $j = 1$ and $j = 6$, $j = 2$ and $j = 5$, $j = 3$ and $j = 4$. For the oscillator $j = 7$, the values of real parts are fixed and the same for the positive and negative real part.

In Fig. 2.1.2, eigenvalues of linearized system (2.1.2) on the complex plane for five different values of the coupling parameter (σ : 0.03; 0.06; 0.10; 0.20; 0.40 are depicted. Only positive values of the imaginary parts are drawn in order to illustrate better the results. Negative values of the imaginary part are a symmetric reflection with respect to the $Im \lambda = 0$ points shown in the described graph. In Fig. 2.1.2, a constant value for each of the parameter σ can be seen. Drawing a vertical broken line through this constant value, the symmetry of the remaining points with respect to this line can be observed. Combining the received points for each adopted value of the parameter, we obtain a characteristic ellipse.

2.2. Stability of steady states in a circuit of real oscillators

In next Chapters (3 and 4), a real system in which there is no perfect symmetry between the oscillators is examined. Values of the parameters c and a and a value of the dimensionless coupling between oscillators - κ_{zj} , κ_{yj} - are different for each of the oscillator. Therefore, a stability analysis was also performed for the real system. The real parameters have been reduced to a dimensionless form (a transition to the dimensionless form and all the indications and explanations of variables – see Chapter 4) yielding:

$$D1: c_1 = 0.031667; a_1 = 1.0000; \kappa_{z1} = 0.987; \kappa_{y1} = 0.984,$$

$$D2: c_2 = 0.031379; a_2 = 1.0065; \kappa_{z2} = 0.993; \kappa_{y2} = 0.992,$$

$$D3: c_3 = 0.031213; a_3 = 1.0148; \kappa_{z3} = 1.003; \kappa_{y3} = 1.004,$$

$$D4: c_4 = 0.031533; a_4 = 0.9948; \kappa_{z4} = 0.982; \kappa_{y4} = 0.982,$$

$$D5: c_5 = 0.032047; a_5 = 1.0393; \kappa_{z5} = 1.021; \kappa_{y5} = 1.023,$$

$$D6: c_6 = 0.031829; a_6 = 1.0137; \kappa_{z6} = 0.995; \kappa_{y6} = 0.998,$$

D7: $c_7 = 0.031490$; $a_7 = 0.9953$; $\kappa z_7 = 0.976$; $\kappa y_7 = 0.976$.

Using Eq. (2.1.2) for the ring of seven real nonlinear Duffing oscillators, we have:

$$\delta \dot{\mathbf{u}} = [\mathbf{I} \otimes A_j + \mathbf{G} \otimes K_j] \delta \mathbf{u}, \quad j = 1, \dots, 7, \quad (2.2.1)$$

where:

$$A_j = \begin{bmatrix} 0 & 1 \\ -(a_j + \sigma * \kappa y_j) & -c_j \end{bmatrix}$$

$$K_j = \begin{bmatrix} 0 & 0 \\ \sigma * \kappa z_j & 0 \end{bmatrix}$$

In calculation of the eigenvalues of Eq. (2.2.1), the following graphs were obtained:

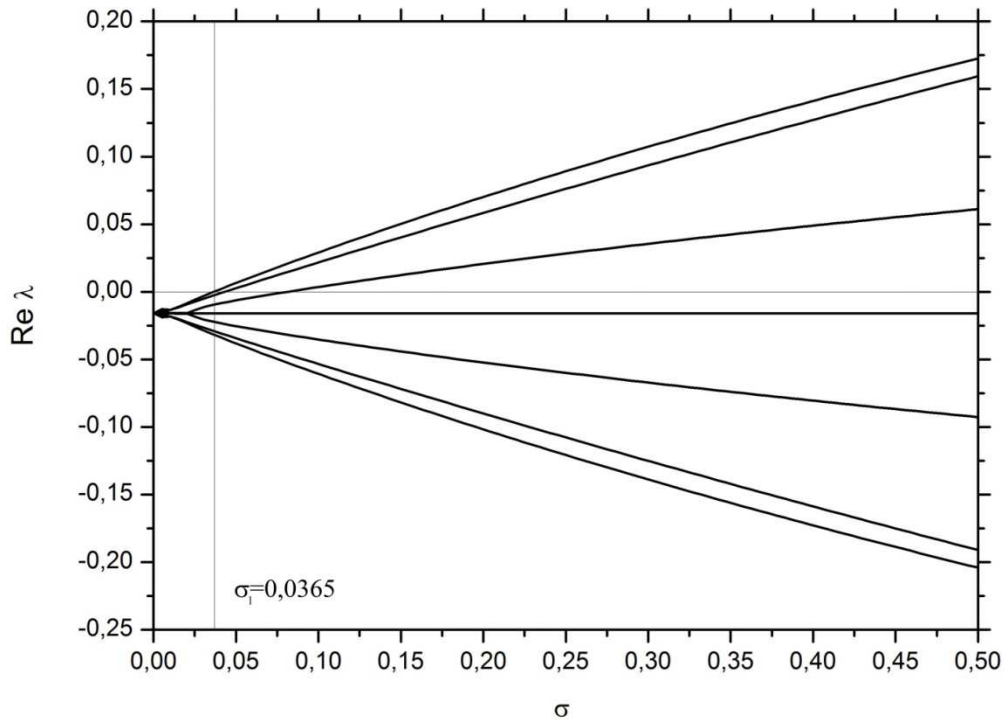


Fig. 2.2.1. Graph of the real eigenvalues $Re \lambda$ of linearized system (2.2.1) versus the coupling parameter σ for a ring of seven real Duffing oscillators.

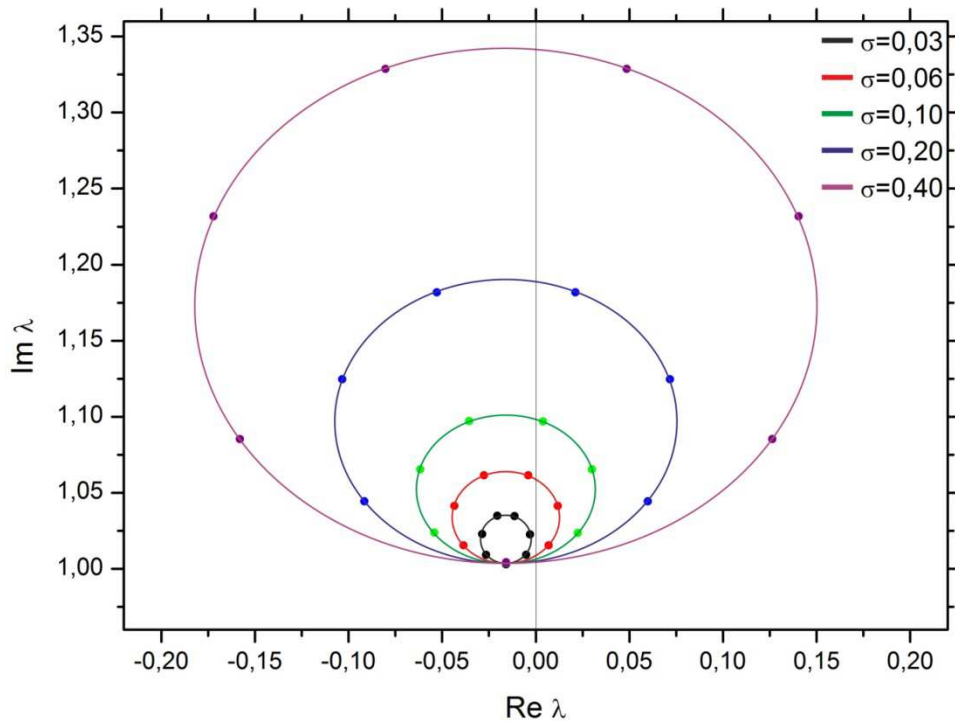


Fig. 2.2.2. Eigenvalues of linearized system (2.2.1) on the complex plane (the positive imaginary parts $Im \lambda$ versus the real parts $Re \lambda$) for a ring of seven real Duffing oscillators with different values of the coupling parameter σ .

In Fig. 2.2.1, a dependence of the real eigenvalues $Re \lambda$ of linearized system (2.2.1) as a function of the coupling parameter σ for a ring of seven real Duffing oscillators is shown. As a result of the occurrence of two different parameters in the coupling term for real oscillators (κ_{zj} , κ_{yj} – detailed explanation in Chapter 4), the expressions $\sigma^* \kappa_{zj}$ and $\sigma^* \kappa_{yj}$ were introduced into the matrices A_j and K_j (Eq. (2.2.1)). This makes it possible to compare Fig. 2.2.1 with Fig. 2.1.1 (σ), and take into account different coupling parameters for each of the oscillators (κ_{zj} , κ_{yj}). In contrast to the identical system (Fig. 2.1.1), the critical value of the coupling parameter, for which one of the real part changes to a positive sign, is $\sigma = 0.0365$. For this value, the Hopf bifurcation occurs – a transition from the critical point to the limit cycle takes place. Similarly, as shown in Fig. 2.1.1, only seven curves can be seen because for pairs of oscillators $j = 1$ and $j = 6$, $j = 2$ and $j = 5$, $j = 3$ and $j = 4$, we get the same values of real parts. For the oscillator $j = 7$, the values of the real parts are fixed and the same for the positive and negative real part.

In Fig. 2.2.2, eigenvalues of linearized system (2.2.1) on the complex plane for five different values of the coupling parameter (σ : 0.3; 0.06; 0.10; 0.20; 0.40) are demonstrated by

analogy to Fig. 2.1.2. Negative values of the imaginary part are also a symmetric reflection with respect to the $Im \lambda = 0$ points shown on the described graph. One can also see almost constant value of each of the parameter σ – for each σ , this value is slightly different. The values of these differences are not larger than 0.001. Therefore, despite a slight symmetry breaking, we obtain a characteristic ellipse combining the remaining points for each of the parameter σ .

CHAPTER 3

NUMERICAL ANALYSIS OF A RING OF SEVEN UNIDIRECTIONALLY COUPLED DUFFING OSCILLATORS

This chapter presents results of the numerical analysis of a ring of seven identical and also real, unidirectionally coupled, nonlinear Duffing oscillators (Eq. (2.1)). In both cases, an impact of changes in a value of the coupling coefficient on the dynamics of the test system was analyzed. In addition, a comparison of the results of the numerical simulations for identical and real oscillators was performed.

The obtained results are represented by:

- bifurcation diagrams (Figs. 3.1.1, 3.1.3),
- phase portraits (Figs. 3.1.7, 3.1.9, 3.1.11, 3.1.13, 3.1.15, 3.1.17, 3.1.19, 3.1.21, 3.1.23, 3.1.25, 3.1.27),
- Poincaré maps (Figs. 3.1.8, 3.1.10, 3.1.12, 3.1.14, 3.1.16, 3.1.18, 3.1.20, 3.1.22, 3.1.24, 3.1.26, 3.1.28),
- Lyapunov exponents graphs (3.1.2, 3.1.4-3.1.6),
- FFT spectrum analysis (3.1.29-3.1.37).

According to Eq. (2.1), a full description of the ring of seven identical, unidirectionally coupled, nonlinear Duffing oscillators can be represented by fourteen first-order differential equations:

$$\begin{aligned}\dot{x}_1 &= y_1 \\ \dot{y}_1 &= -cy_1 - ax_1 - bx_1^3 + \sigma(x_7 - x_1) \\ \dot{x}_2 &= y_2 \\ \dot{y}_2 &= -cy_2 - ax_2 - bx_2^3 + \sigma(x_1 - x_2) \\ \dot{x}_3 &= y_3 \\ \dot{y}_3 &= -cy_3 - ax_3 - bx_3^3 + \sigma(x_2 - x_3) \\ \dot{x}_4 &= y_4 \\ \dot{y}_4 &= -cy_4 - ax_4 - bx_4^3 + \sigma(x_3 - x_4) \\ \dot{x}_5 &= y_5 \\ \dot{y}_5 &= -cy_5 - ax_5 - bx_5^3 + \sigma(x_4 - x_5)\end{aligned}\tag{3.1}$$

$$\begin{aligned}
\dot{x}_6 &= y_6 \\
\dot{y}_6 &= -cy_6 - ax_6 - bx_6^3 + \sigma(x_5 - x_6) \\
\dot{x}_7 &= y_7 \\
\dot{y}_7 &= -cy_7 - ax_7 - bx_7^3 + \sigma(x_6 - x_7)
\end{aligned}$$

where the parameters are:

$$c = 0.03162; \quad a = 1.00; \quad b = 10;$$

and $\sigma = Rs*k$ is a bifurcation parameter, where: $Rs \in <0 \div 99900> [\Omega]$, $k = 0.00001 [1/\Omega]$.

Parameter values were selected in such a way as to correspond to the values of elements (resistors and capacitors) of the identical electrical system (see Chapter 4).

The circuit of seven real, unidirectionally coupled, nonlinear Duffing oscillators can be represented by the following equations:

$$\begin{aligned}
\dot{x}_1 &= y_1 \\
\dot{y}_1 &= -c_1y_1 - a_1x_1 - b_1x_1^3 + \sigma(\kappa_{z1}x_7 - \kappa_{y1}x_1) \\
\dot{x}_2 &= y_2 \\
\dot{y}_2 &= -c_2y_2 - a_2x_2 - b_2x_2^3 + \sigma(\kappa_{z2}x_1 - \kappa_{y2}x_2) \\
\dot{x}_3 &= y_3 \\
\dot{y}_3 &= -c_3y_3 - a_3x_3 - b_3x_3^3 + \sigma(\kappa_{z3}x_2 - \kappa_{y3}x_3) \\
\dot{x}_4 &= y_4 \\
\dot{y}_4 &= -c_4y_4 - a_4x_4 - b_4x_4^3 + \sigma(\kappa_{z4}x_3 - \kappa_{y4}x_4) \\
\dot{x}_5 &= y_5 \\
\dot{y}_5 &= -c_5y_5 - a_5x_5 - b_5x_5^3 + \sigma(\kappa_{z5}x_4 - \kappa_{y5}x_5) \\
\dot{x}_6 &= y_6 \\
\dot{y}_6 &= -c_6y_6 - a_6x_6 - b_6x_6^3 + \sigma(\kappa_{z6}x_5 - \kappa_{y6}x_6) \\
\dot{x}_7 &= y_7 \\
\dot{y}_7 &= -c_7y_7 - a_7x_7 - b_7x_7^3 + \sigma(\kappa_{z7}x_6 - \kappa_{y7}x_7)
\end{aligned} \tag{3.2}$$

where the values of each parameter are:

$$c_1 = 0.031667; \quad a_1 = 1.0000; \quad b_1 = 9.940;$$

$$\begin{aligned}
c_2 &= 0.031379; & a_2 &= 1.0065; & b_2 &= 10.015; \\
c_3 &= 0.031213; & a_3 &= 1.0148; & b_3 &= 10.107; \\
c_4 &= 0.031533; & a_4 &= 0.9948; & b_4 &= 9.898; \\
c_5 &= 0.032047; & a_5 &= 1.0393; & b_5 &= 10.320; \\
c_6 &= 0.031829; & a_6 &= 1.0137; & b_6 &= 10.056; \\
c_7 &= 0.031490; & a_7 &= 0.9953; & b_7 &= 9.853;
\end{aligned}$$

$$\begin{aligned}
\kappa z_1 &= 0.987; & \kappa y_1 &= 0.984; \\
\kappa z_2 &= 0.993; & \kappa y_2 &= 0.992, \\
\kappa z_3 &= 1.003; & \kappa y_3 &= 1.004, \\
\kappa z_4 &= 0.982; & \kappa y_4 &= 0.982, \\
\kappa z_5 &= 1.021; & \kappa y_5 &= 1.023, \\
\kappa z_6 &= 0.995; & \kappa y_6 &= 0.998, \\
\kappa z_7 &= 0.976; & \kappa y_7 &= 0.976.
\end{aligned}$$

The above dimensionless parameters correspond to the values of elements (resistors and capacitors) of the real electrical circuit (see Chapter 4).

3.1. Numerical results

All bifurcation diagrams, phase portraits and Poincaré maps were made with the Borland-Delphi software, whereas Lyapunov exponents were calculated using the C++ software. These results are presented below.

I hereby wish to thank my colleagues from the Division of Dynamics, Lodz University of Technology – Dr. Przemysław Perlikowski and Dr. Artur Dąbrowski for their assistance in the implementation of the programs for the purposes of this dissertation.

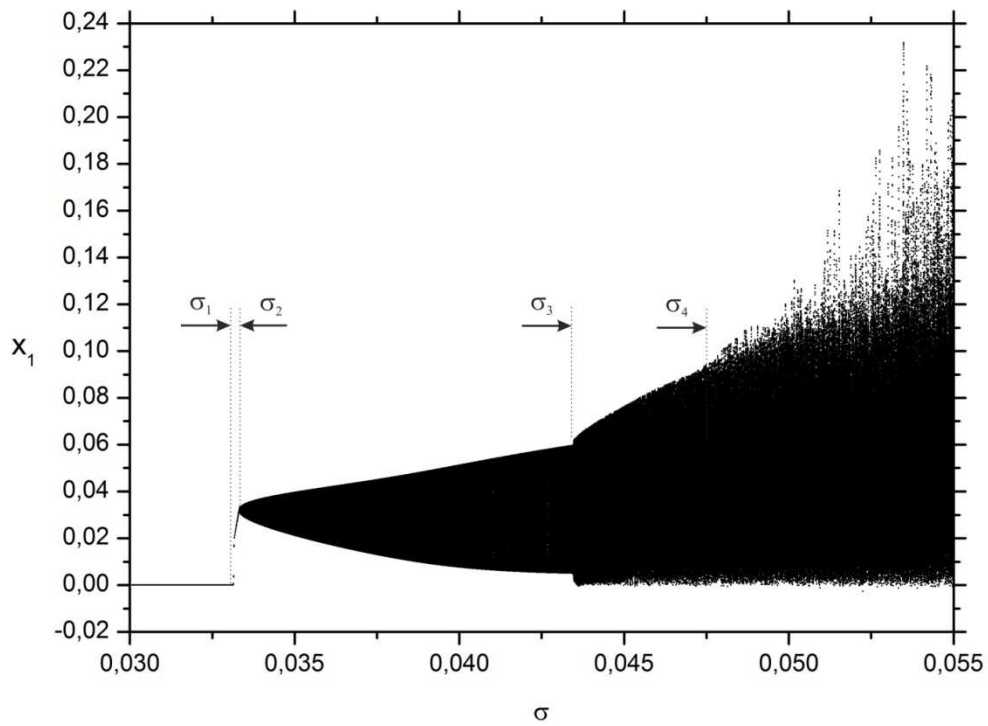


Fig. 3.1.1. Bifurcation diagram of the variable x_1 versus the coupling parameter σ for a circuit of seven identical Duffing oscillators (Eq. (3.1)).

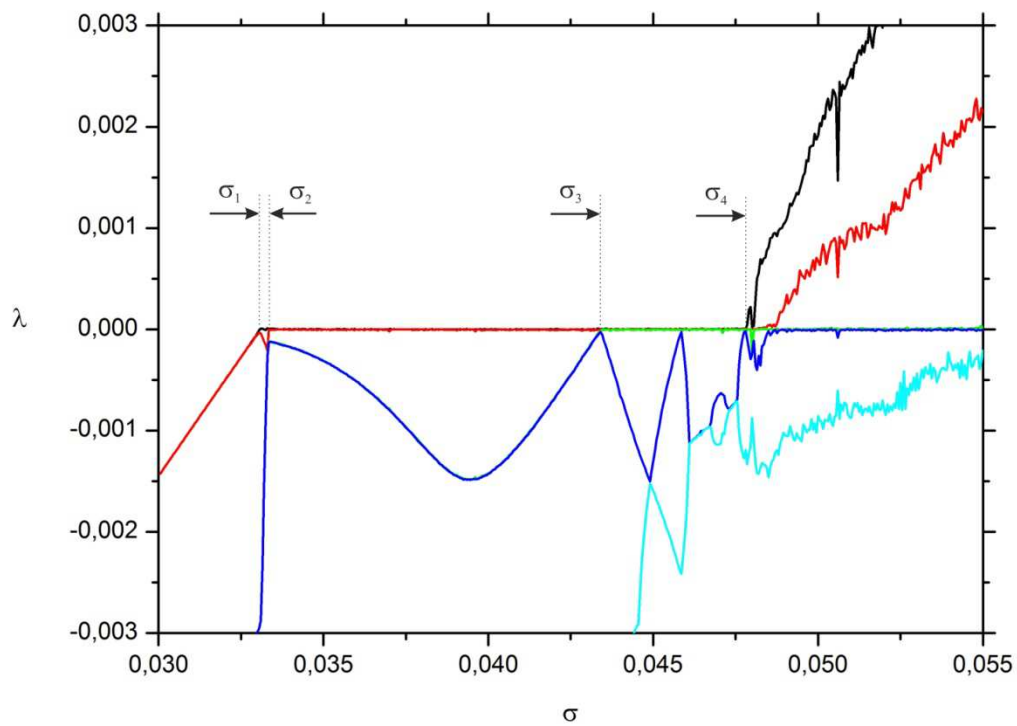


Fig. 3.1.2. Graph of the five largest Lyapunov exponents λ versus the coupling parameter σ for a circuit of seven identical Duffing oscillators (Eq. (3.1)).

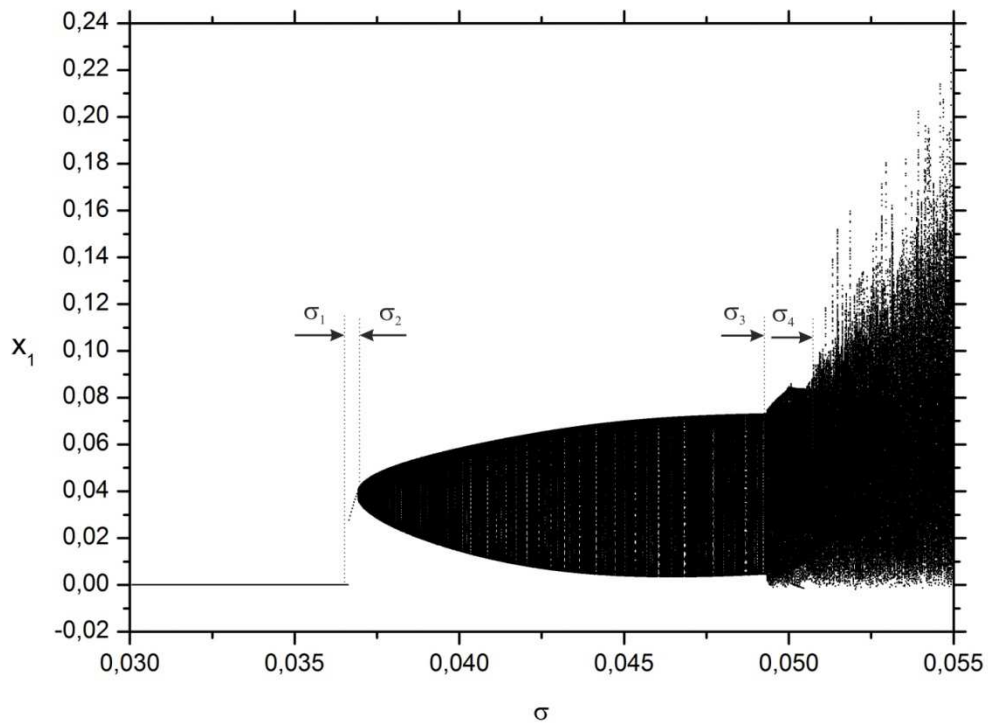


Fig. 3.1.3. Bifurcation diagram of the variable x_1 versus the coupling parameter σ for a circuit of seven real Duffing oscillators (Eq. (3.2)).

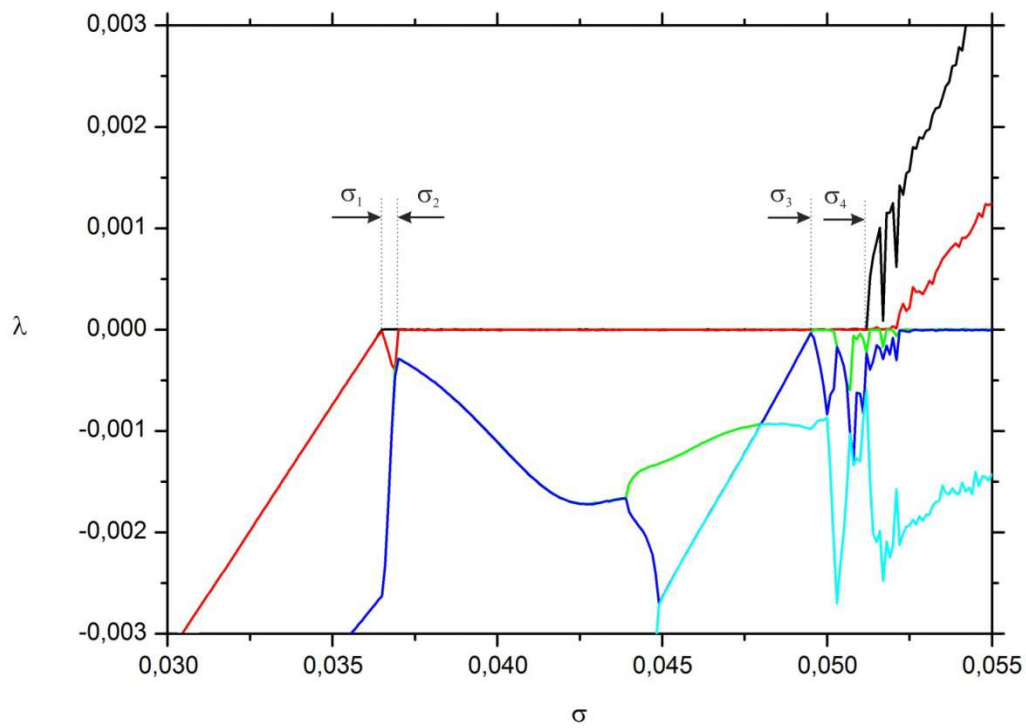


Fig. 3.1.4. Graph of the five largest Lyapunov exponents λ versus the coupling parameter σ for a circuit of seven real Duffing oscillators (Eq. (3.2)).

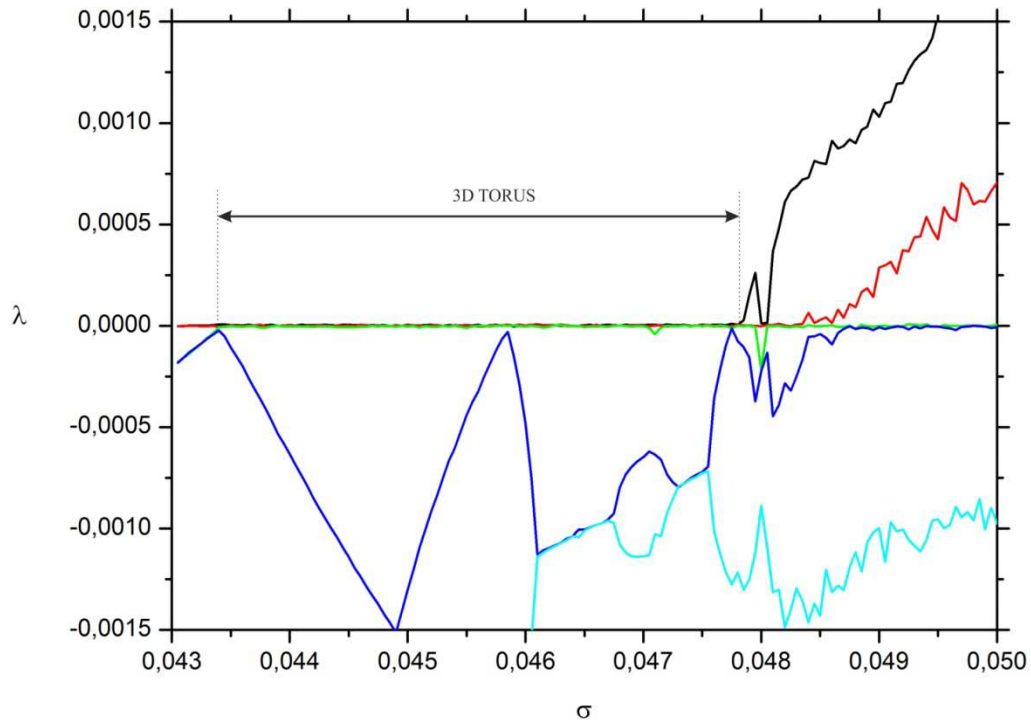


Fig. 3.1.5. Detailed graph of the largest Lyapunov exponents λ versus the coupling parameter σ for a circuit of seven identical Duffing oscillators (Eq. (3.1)).

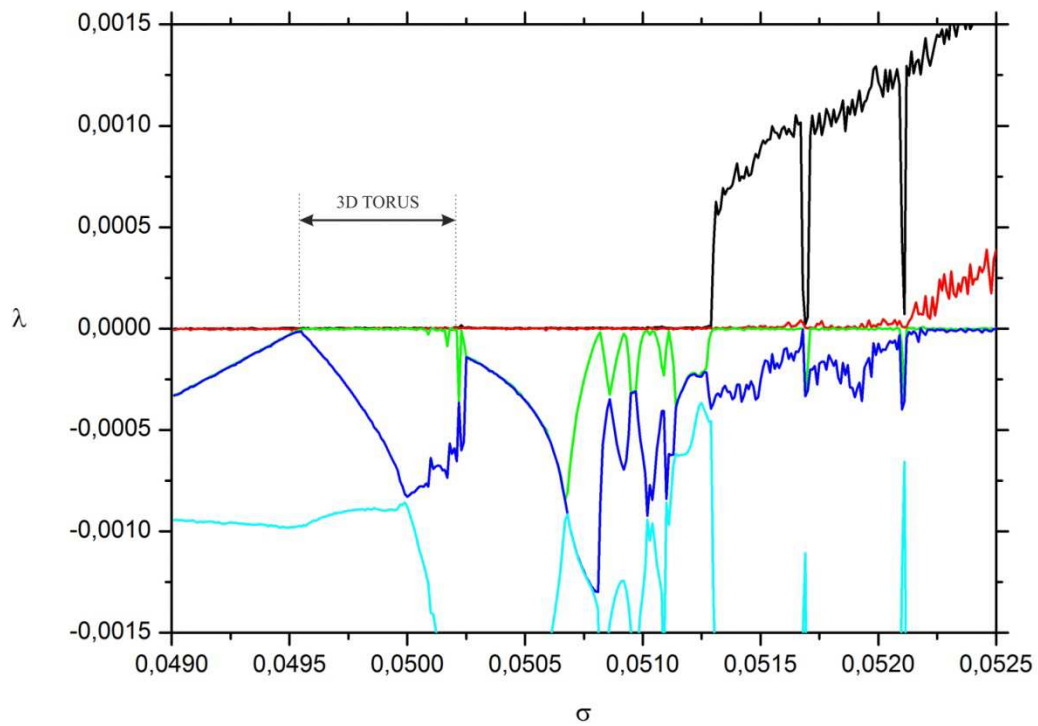


Fig. 3.1.6. Detailed graph of the largest Lyapunov exponents λ versus the coupling parameter σ for a circuit of seven real Duffing oscillators (Eq. (3.2)).

After analyzing the bifurcation diagram (Fig. 3.1.1) and the graph of largest Lyapunov exponents (Fig. 3.1.2) for a circuit of seven identical Duffing oscillators, it can be concluded that the first Hopf bifurcation occurs for the parameter $\sigma_1 = 0.0332$. As a result, the first frequency of oscillation appears and a transition from the stable equilibrium position to the limit cycle is observed in the test system under consideration. Then, all oscillators in the ring start to vibrate harmonically and a *periodic rotating wave* (PRW - see Subsection 1.3) is formed. The largest Lyapunov exponent is equal to zero. Such a harmonic solution takes place in a small range of the coupling coefficient – $\sigma \in \langle 0.0332 \div 0.0336 \rangle$, i.e., between σ_1 and σ_2 in Fig. 3.1.2. For $\sigma > 0.0336$, the second disproportionate frequency appears as a result of the next Hopf-type bifurcation. In this interval, two largest Lyapunov exponents are equal to zero. The transition of the system from a periodic to quasi-periodic solution leads to the appearance of a 2D torus, which dominates in a wide range of the coupling parameter - $\sigma \in \langle 0.0337 \div 0.0435 \rangle$. A further increase in the coupling parameter, over the value σ_3 , causes an emergence of the subsequent, third Hopf-type bifurcation. The third disproportionate frequency appears and three largest Lyapunov exponents have values equal to zero, i.e., a transition from the 2D torus to a three-frequency solution – a 3D torus (Fig. 3.1.5) – takes place. The range of the 3D torus occurrence is $\sigma \in \langle 0.0436 \div 0.0477 \rangle$. In addition, for the coupling parameter $\sigma = 0.0458$, a period-doubling bifurcation in the 3D torus appears. For $\sigma_4 = 0.0477$, the largest Lyapunov exponent reaches a positive value and the system becomes to behave chaotically. Chaos appears on the 2D torus, because the next two largest Lyapunov exponents are equal to zero. Chaotic behavior occurs for the coupling parameter $\sigma \in \langle 0.0478 \div 0.0486 \rangle$. For the coupling parameter $\sigma > 0.0486$, the second largest Lyapunov exponent reaches a positive value and a transition from chaotic to hyper-chaotic behavior is observed. Hyper-chaotic behavior also occurs on the 2D torus, because the next two largest Lyapunov exponents are equal to zero.

Comparing the bifurcation diagram (Fig. 3.1.3) and the graph of largest Lyapunov exponents (Fig. 3.1.4) for a circuit of seven real Duffing oscillators with the bifurcation diagram (Fig. 3.1.1) and the graph of largest Lyapunov exponents (Fig. 3.1.2) for a circuit of seven identical Duffing oscillators, it can be seen that the first Hopf bifurcation occurs for the coupling parameter value slightly larger than for the identical system. The first frequency of oscillation occurs for the coupling parameter $\sigma_1 = 0.0365$. Similarly to the identical system, the largest Lyapunov exponent is equal to zero, so one can observe a periodic solution. Periodic motion also occurs in a narrow range of the coupling parameter -

$\sigma \in \langle 0.0365 \div 0.0370 \rangle$. An increase in the coupling parameter over $\sigma_2 = 0.0371$ leads to the second Hopf-type bifurcation. A second disproportionate frequency appears and the two largest Lyapunov exponents are equal to zero. Similarly to the identical system, as a result of the system transition from the periodic solution in the quasi-periodic one, a 2D torus appears. The 2D torus occurs for the coupling parameter $\sigma \in \langle 0.0371 \div 0.0495 \rangle$. For $\sigma_3 = 0.0496$, the third disproportionate frequency appears, as a result of the third Hopf-type bifurcation. The three largest Lyapunov exponents assume the value of zero, which means that the three-frequency solution (a 3D torus in Fig. 3.1.6) is stable. However, in contrast to the ideal system, a 3D torus does not occur until the system reaches a chaotic solution. The three-frequency solution exists in the range of the coupling parameter $\sigma \in \langle 0.0496 \div 0.0502 \rangle$. A further increase in the coupling parameter leads to a reverse Hopf bifurcation and a sequence of period-doubling bifurcations in the range $\sigma \in \langle 0.0508 \div 0.0512 \rangle$. They are period-doubling bifurcations of the 2D torus, because the value of the third largest Lyapunov exponent is negative. For $\sigma_4 = 0.0513$, the largest Lyapunov exponent reaches a positive value. Then, a transition from the quasi-periodic solution to the chaotic one takes place. As for the ideal system, this is a chaotic behavior on the 2D torus, because values of two consecutive Lyapunov exponents are equal to zero. A further increase in the coupling parameter leads to an increase in the value of the second largest Lyapunov exponent. This exponent reaches a positive value for $\sigma > 0.0521$, resulting in a transition from chaotic to hyper-chaotic behavior.

For each of the solutions, i.e., the fixed point, the limit cycle, the 2D torus, the 3D torus, the period-doubling (the real system) and chaotic behavior (hyper-chaotic), phase portraits and Poincaré maps (Fig. 3.1.7 – 3.1.26) were generated. In addition, an FFT spectrum analysis was performed for each of the solution (Fig. 3.1.27 – 3.1.35).

Graphs for the following values of the coupling parameter σ : 0.0330; 0.0332; 0.0430; 0.0440; 0.0500 were prepared for a circuit of seven identical Duffing oscillators.

The following values of the coupling parameter σ : 0.0360; 0.0368; 0.0490; 0.0500; 0.0540 were selected for a circuit of seven real Duffing oscillators.

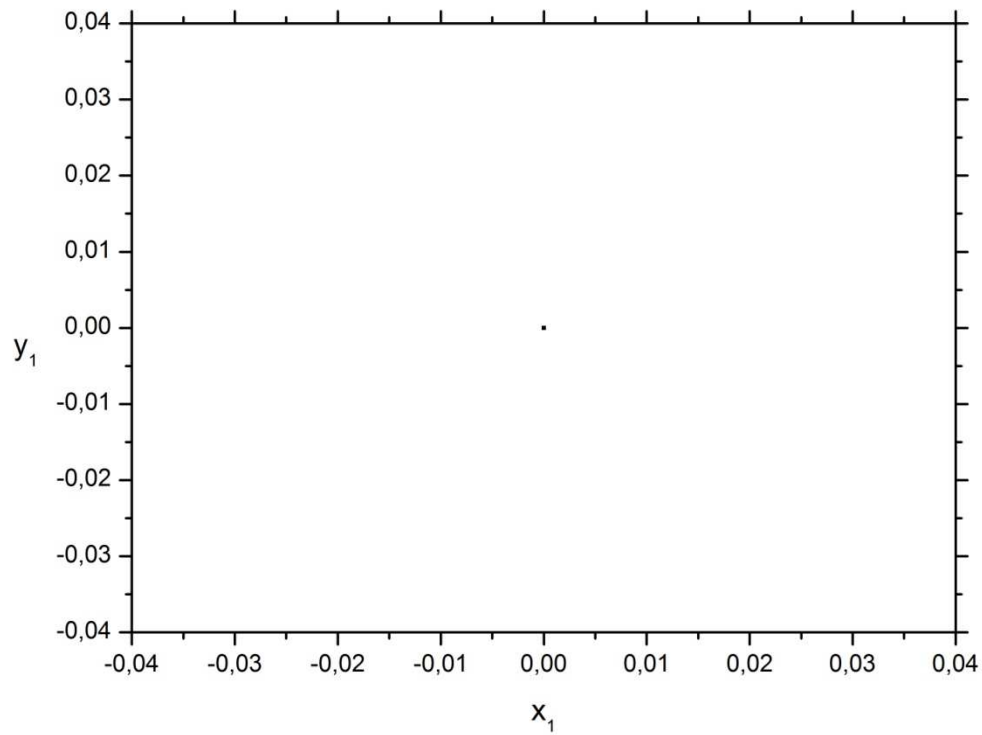


Fig. 3.1.7. Phase portrait for the coupling parameter $\sigma=0.0330$ – a circuit of seven identical Duffing oscillators.

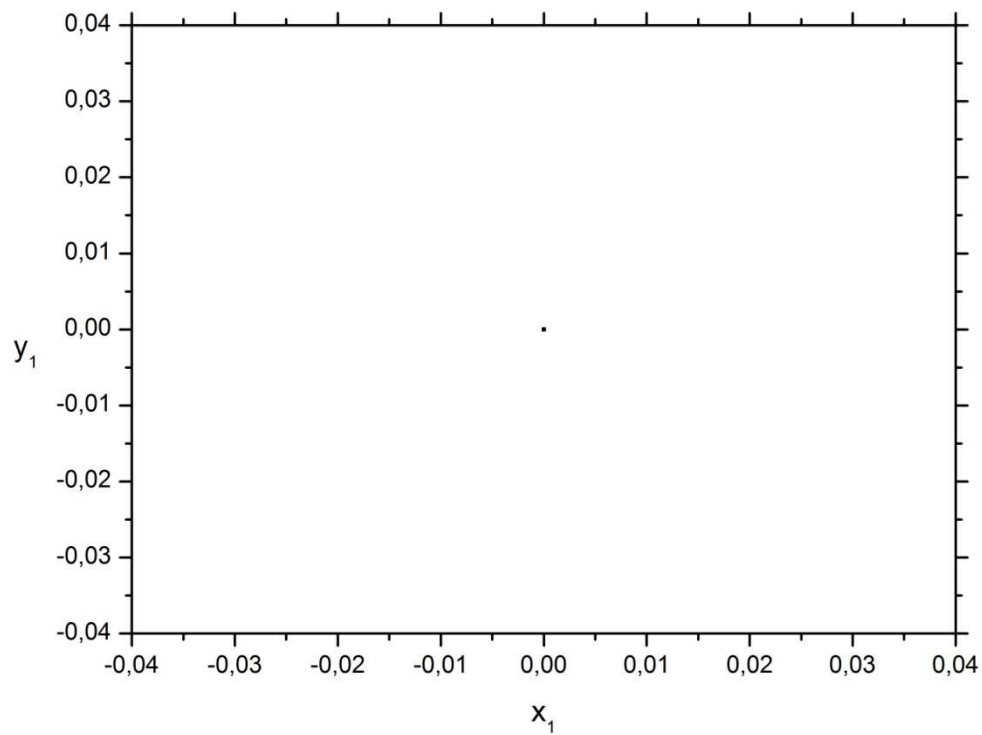


Fig. 3.1.8. Phase portrait for the coupling parameter $\sigma=0.0360$ – a circuit of seven real Duffing oscillators.

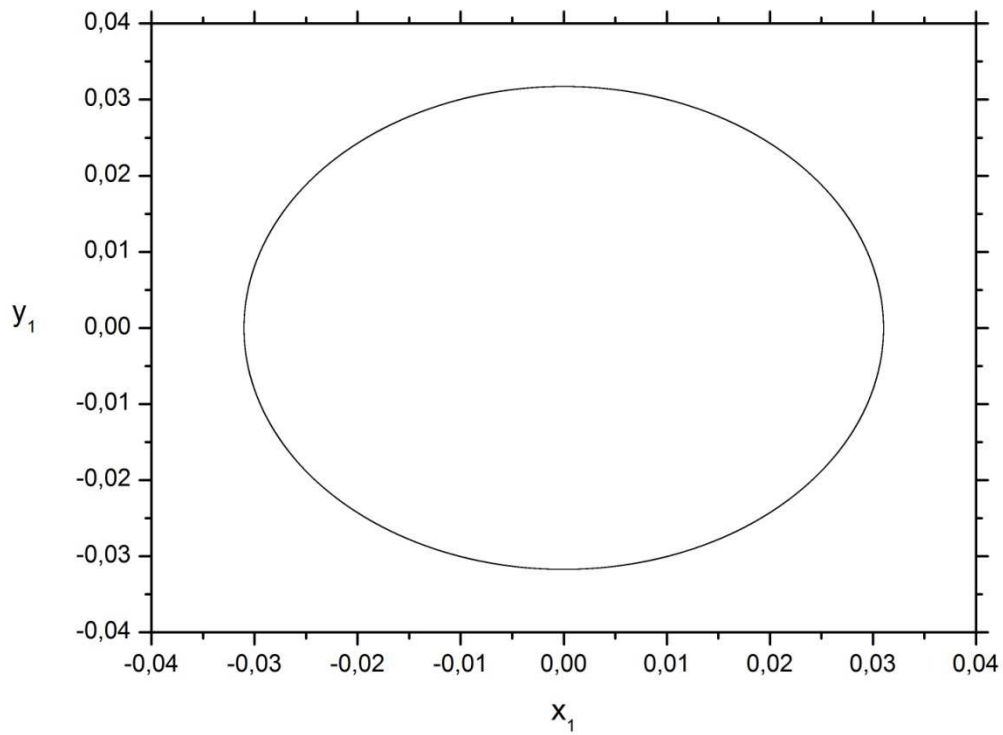


Fig. 3.1.9. Phase portrait for the coupling parameter $\sigma=0.0332$ – a circuit of seven identical Duffing oscillators.

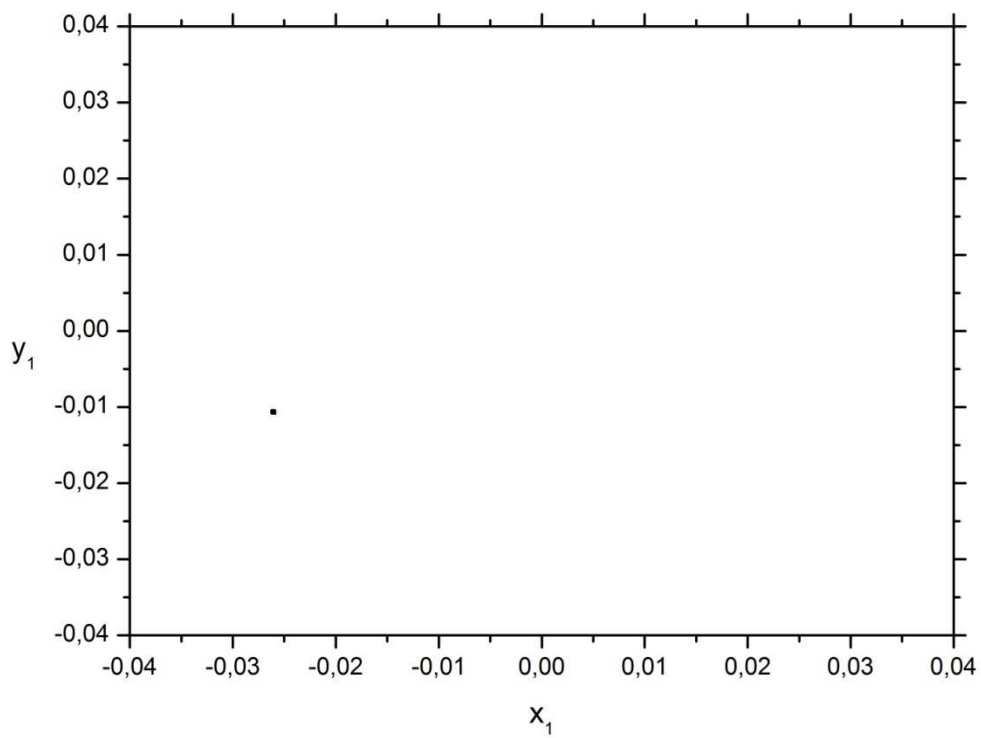


Fig. 3.1.10. Poincaré map for the coupling parameter $\sigma=0.0332$ – a circuit of seven identical Duffing oscillators.

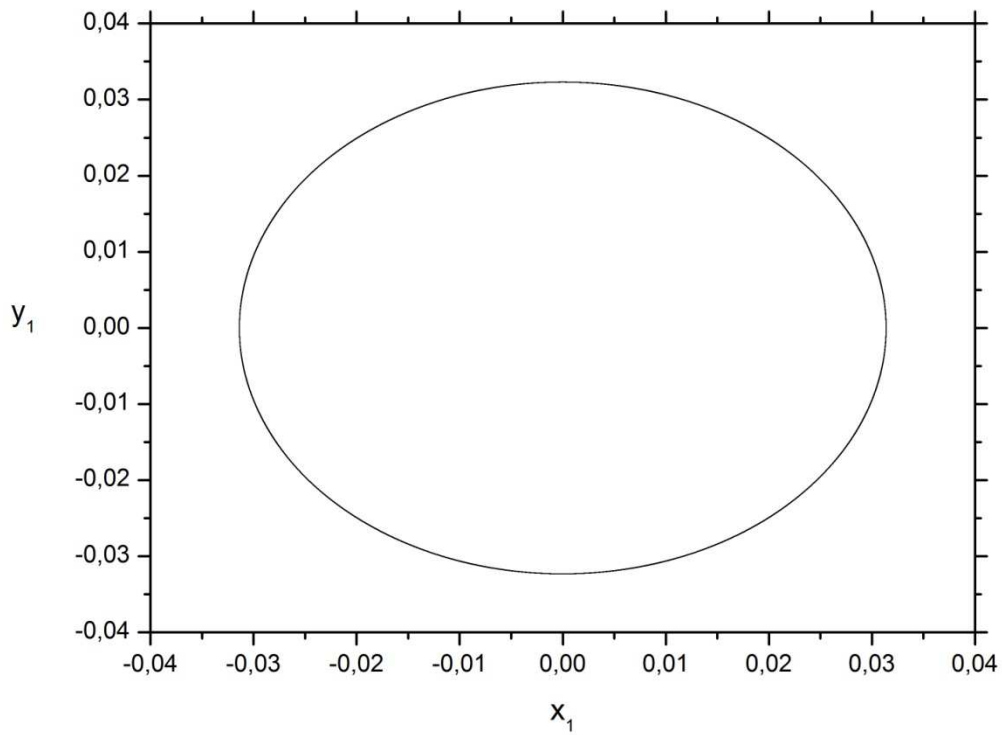


Fig. 3.1.11. Phase portrait for the coupling parameter $\sigma=0.0368$ – a circuit of seven real Duffing oscillators.

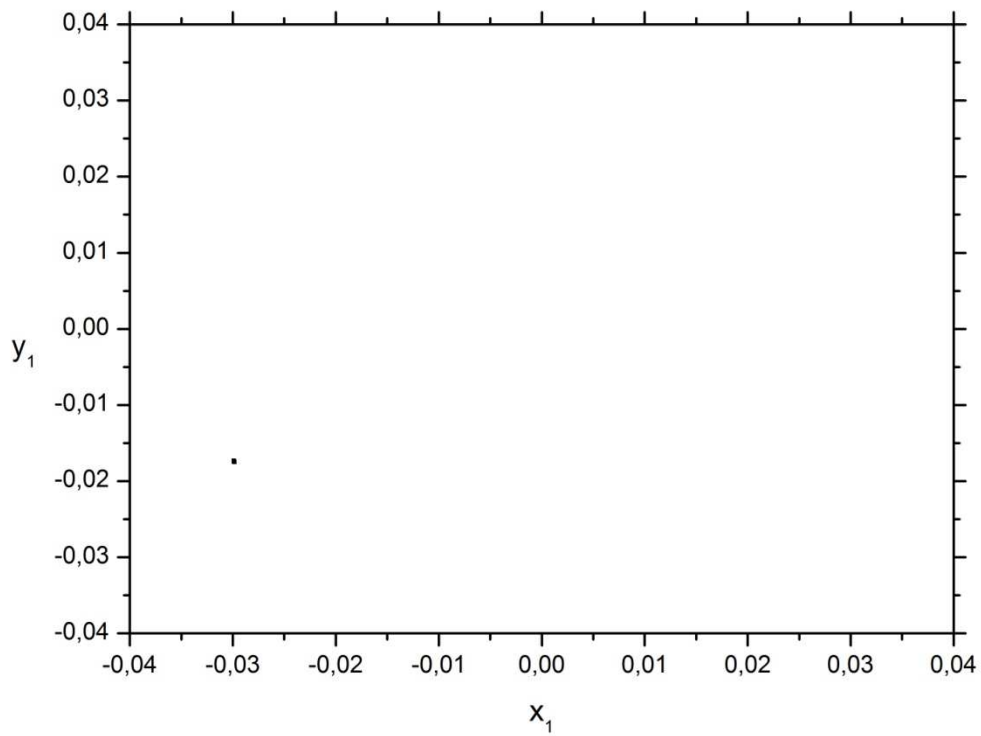


Fig. 3.1.12. Poincaré map for the coupling parameter $\sigma=0.0368$ – a circuit of seven real Duffing oscillators.

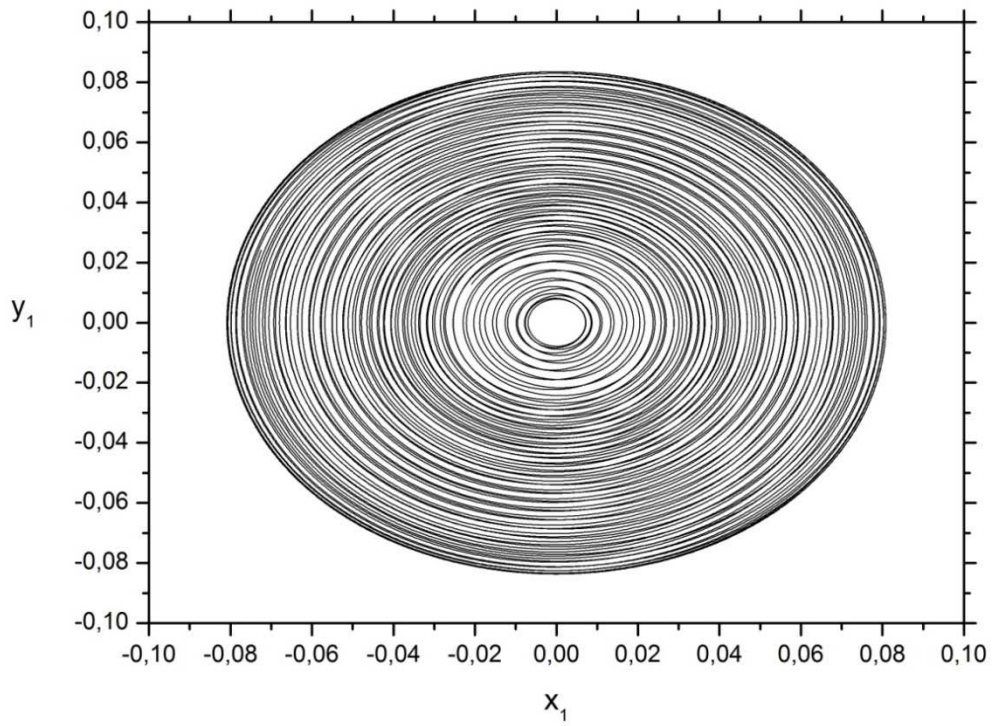


Fig. 3.1.13. Phase portrait for the coupling parameter $\sigma=0.0430$ – a circuit of seven identical Duffing oscillators.

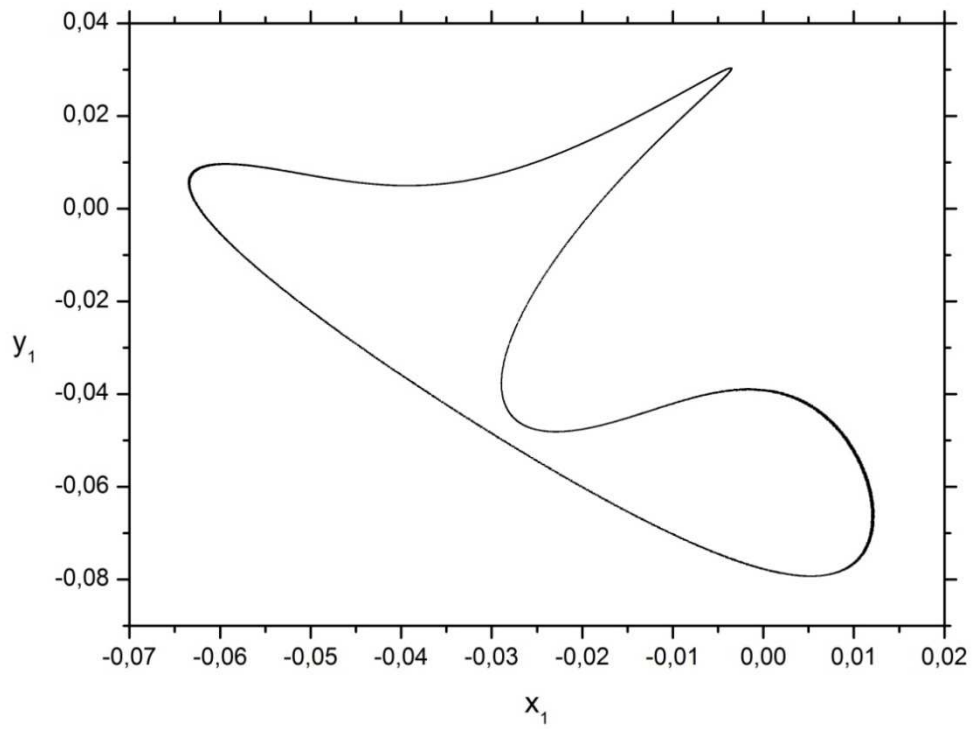


Fig. 3.1.14. Poincaré map for the coupling parameter $\sigma=0.0430$ – a circuit of seven identical Duffing oscillators.

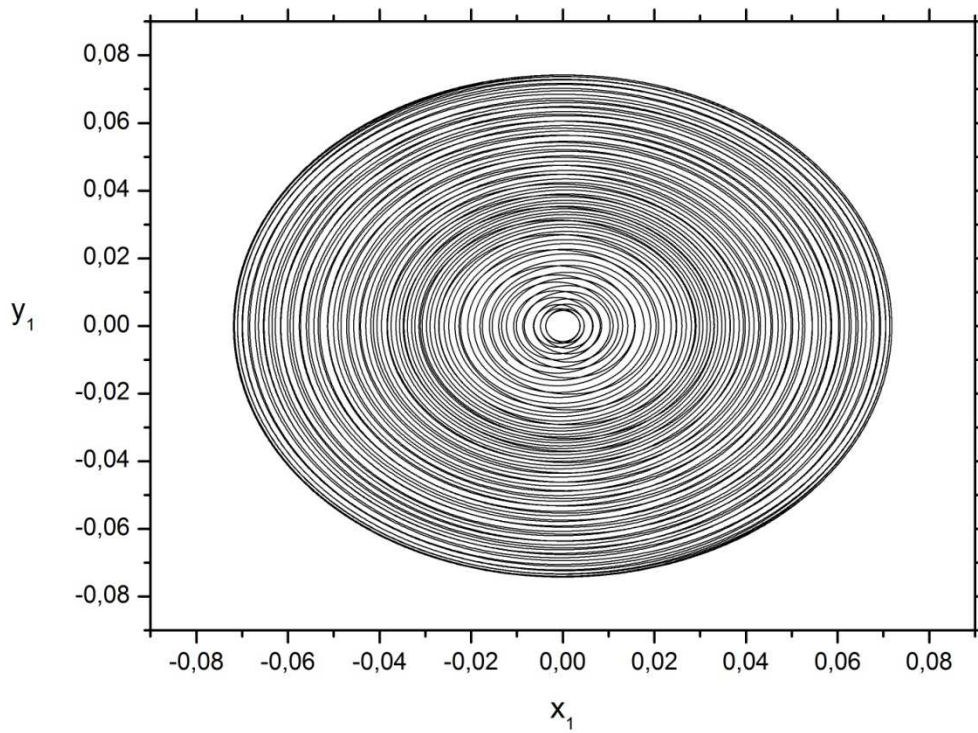


Fig. 3.1.15. Phase portrait for the coupling parameter $\sigma=0.0490$ – a circuit of seven real Duffing oscillators.

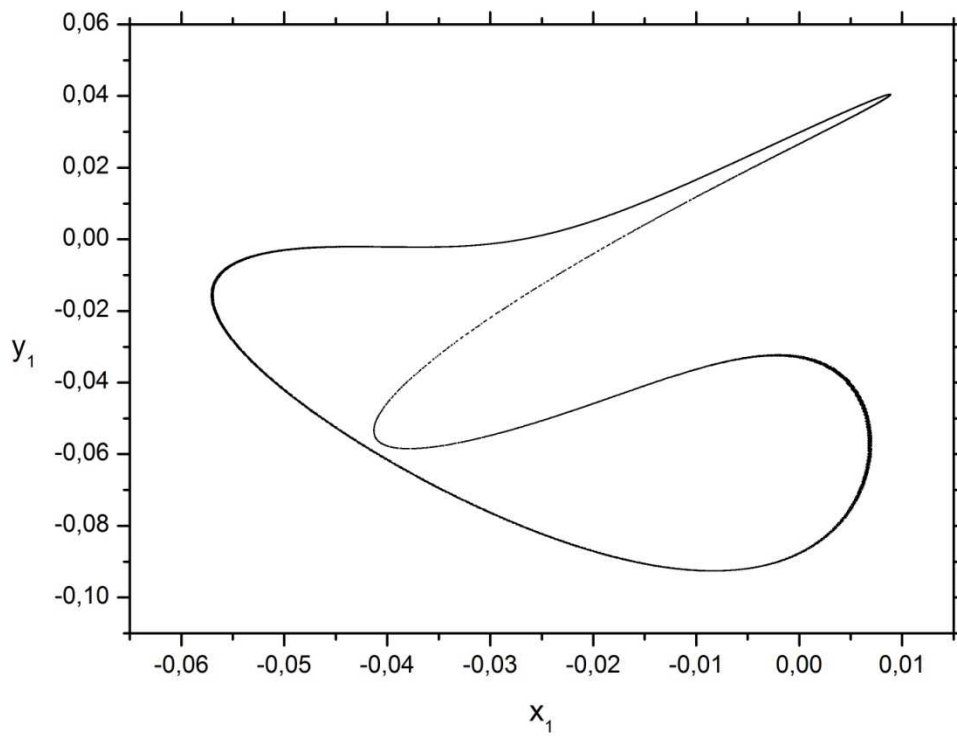


Fig. 3.1.16. Poincaré map for the coupling parameter $\sigma=0.0490$ – a circuit of seven real Duffing oscillators.

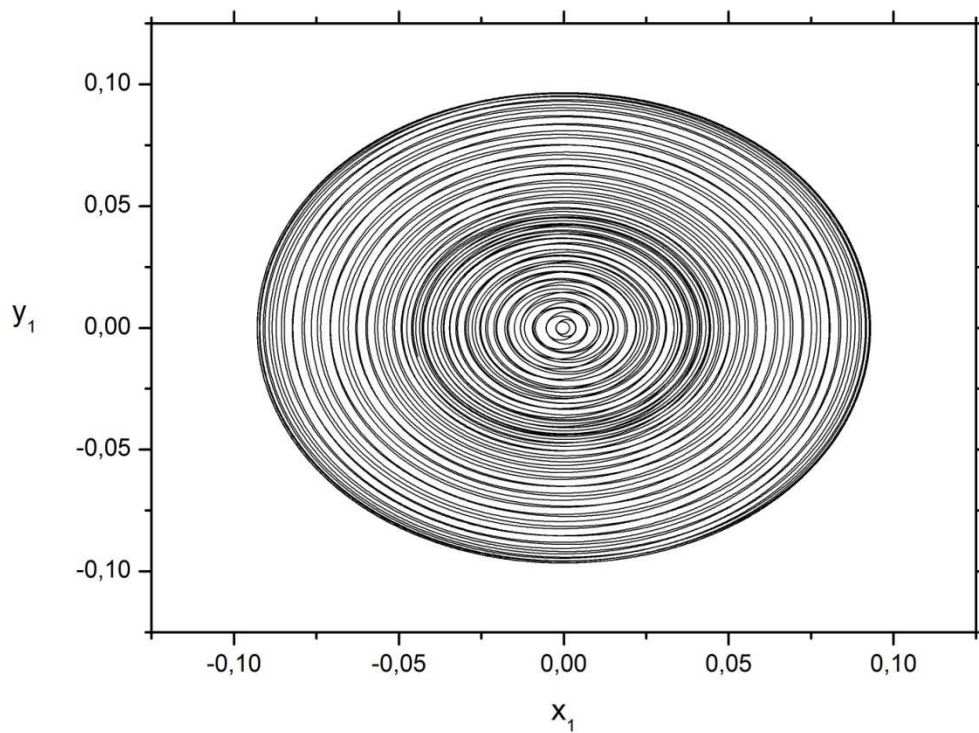


Fig. 3.1.17. Phase portrait for the coupling parameter $\sigma=0.0440$ – a circuit of seven identical Duffing oscillators.

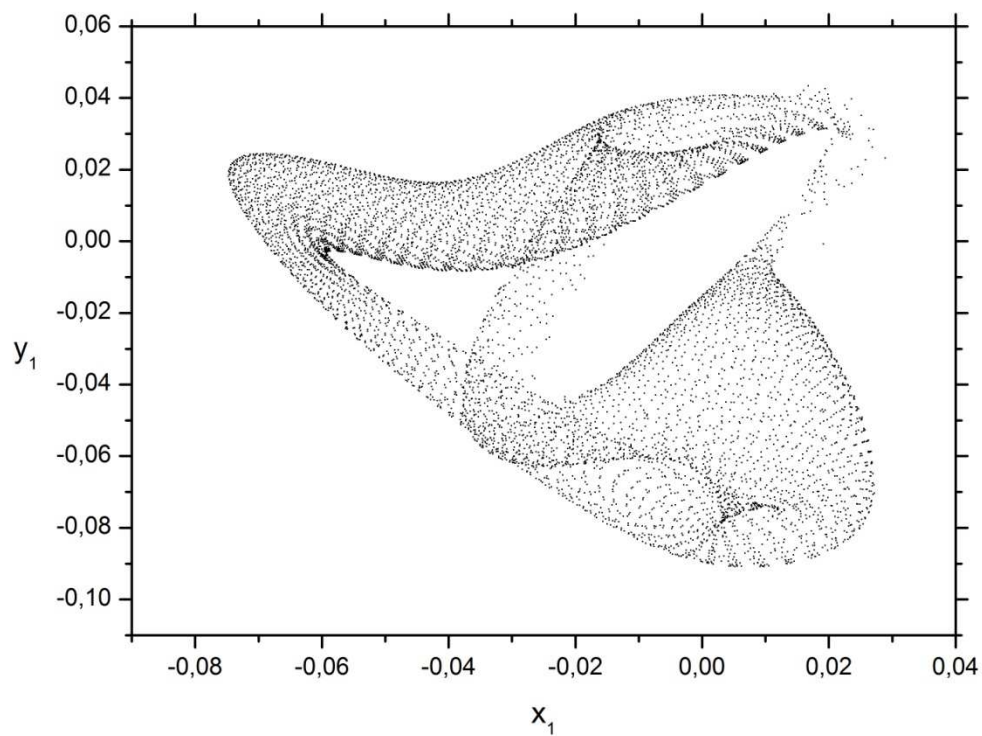


Fig. 3.1.18. Poincaré map for the coupling parameter $\sigma=0.0440$ – a circuit of seven identical Duffing oscillators.

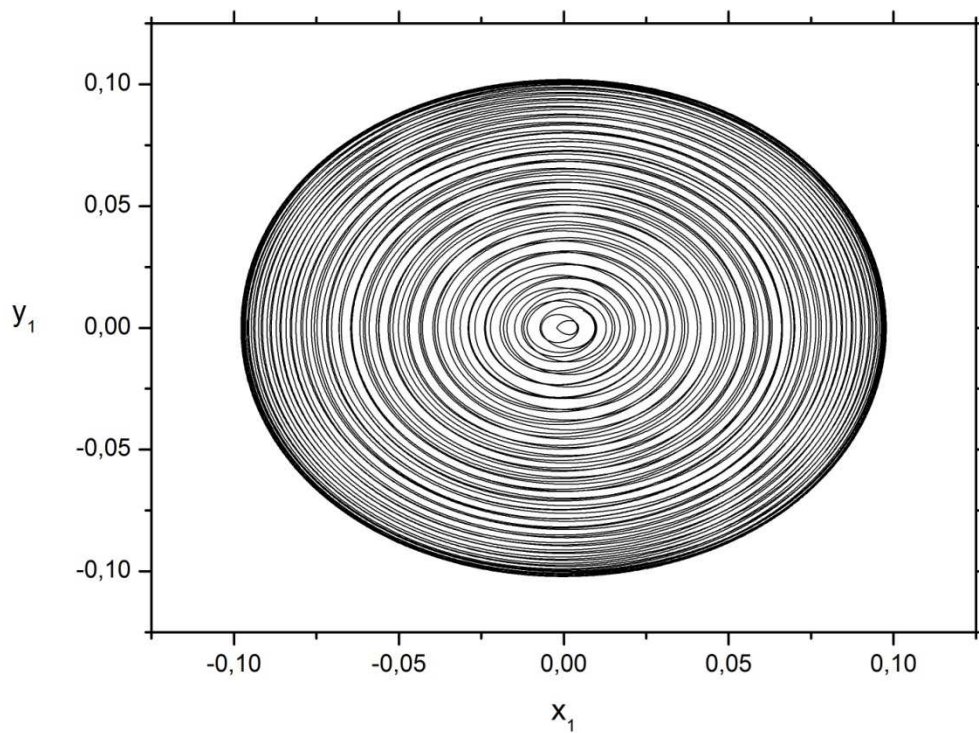


Fig. 3.1.19. Phase portrait for the coupling parameter $\sigma=0.0500$ – a circuit of seven real Duffing oscillators.

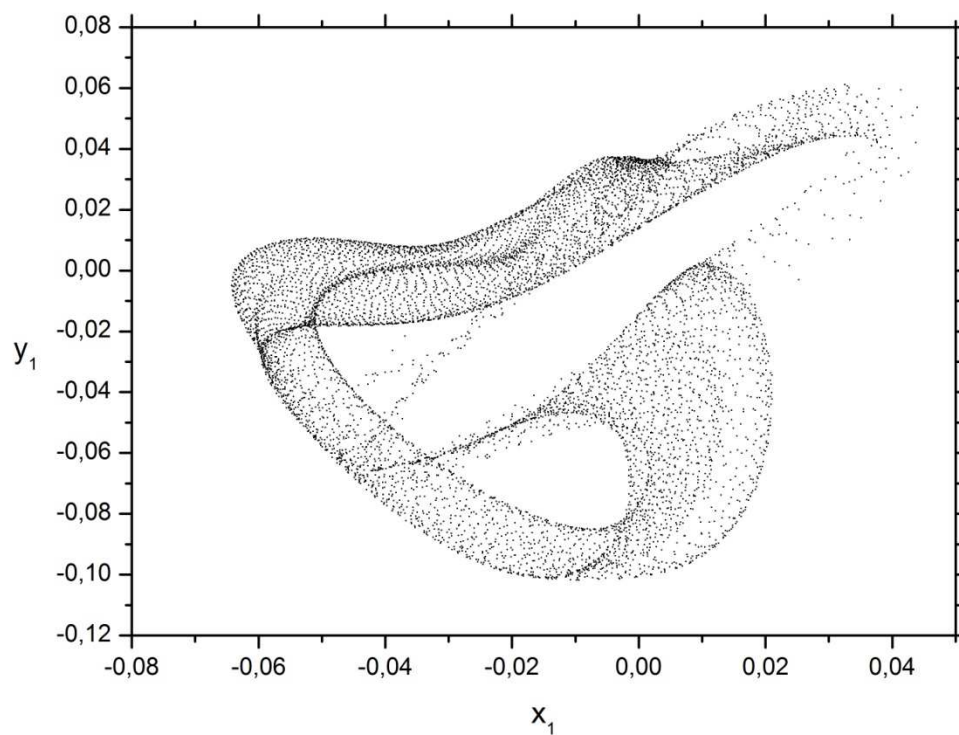


Fig. 3.1.20. Poincaré map for the coupling parameter $\sigma=0.0500$ – a circuit of seven real Duffing oscillators.

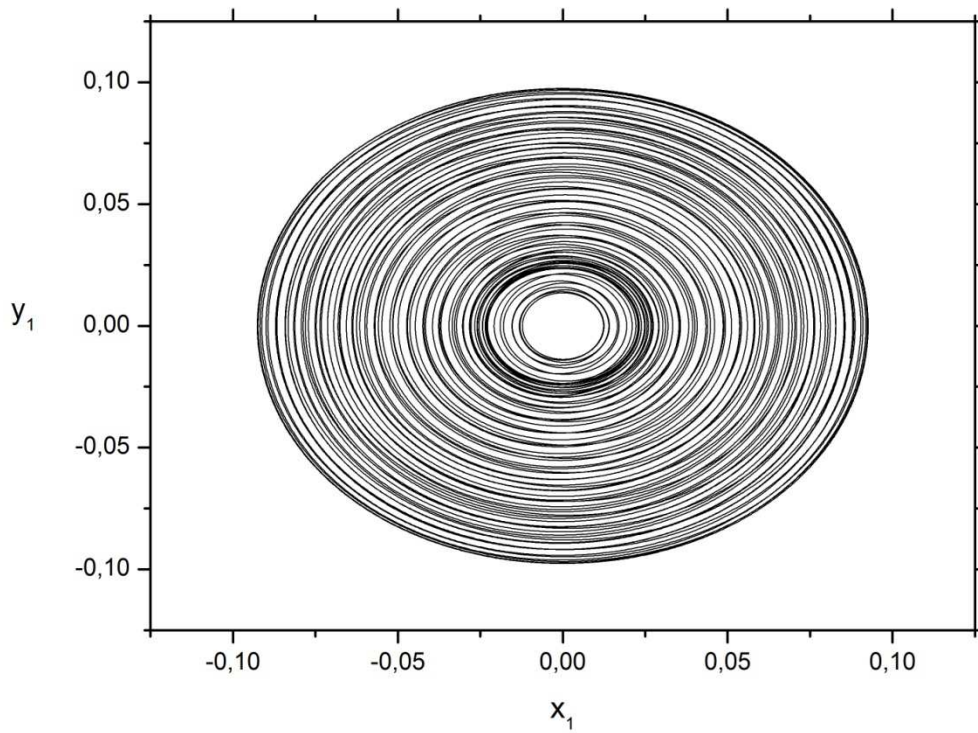


Fig. 3.1.21. Phase portrait for the coupling parameter $\sigma=0.0505$ – a circuit of seven real Duffing oscillators.

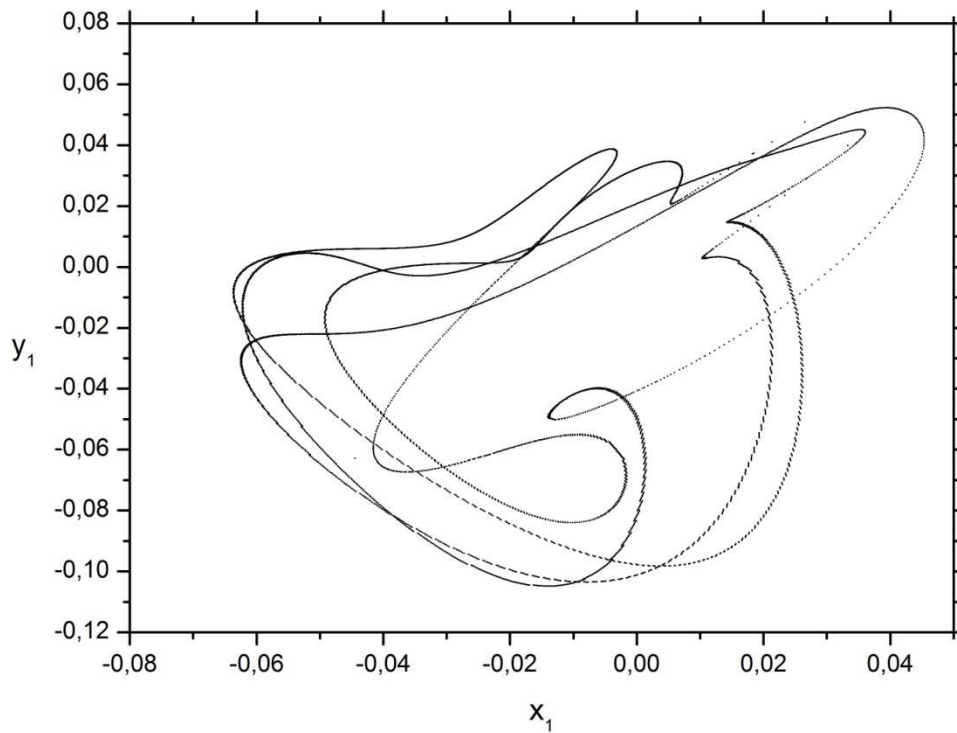


Fig. 3.1.22. Poincaré map for the coupling parameter $\sigma=0.0505$ – a circuit of seven real Duffing oscillators.

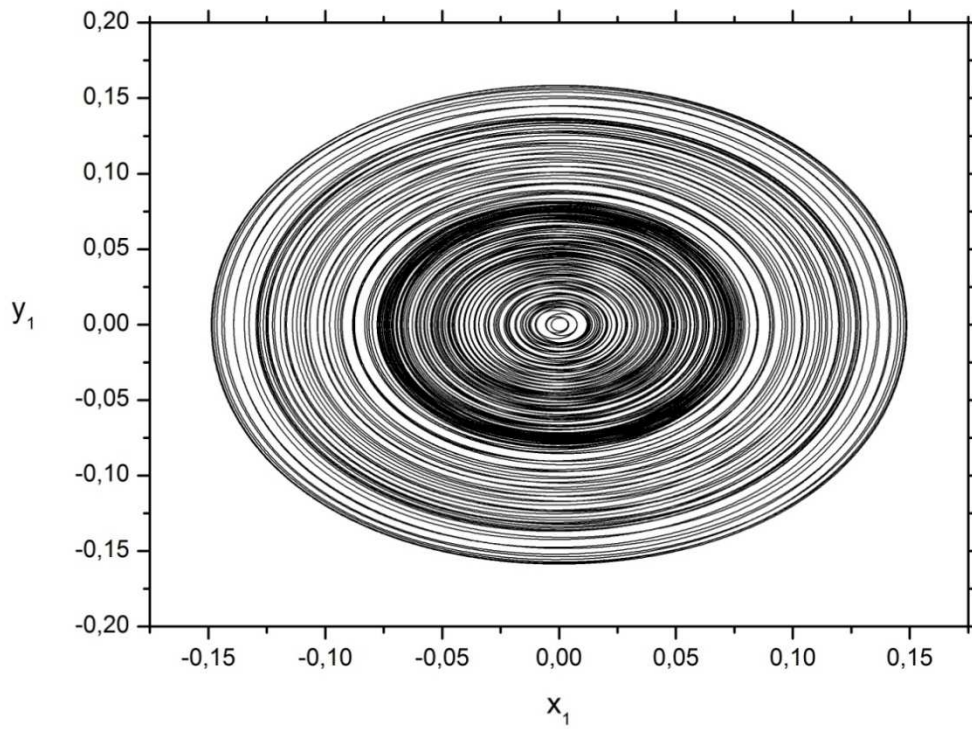


Fig. 3.1.23. Phase portrait for the coupling parameter $\sigma=0.0500$ – a circuit of seven identical Duffing oscillators.

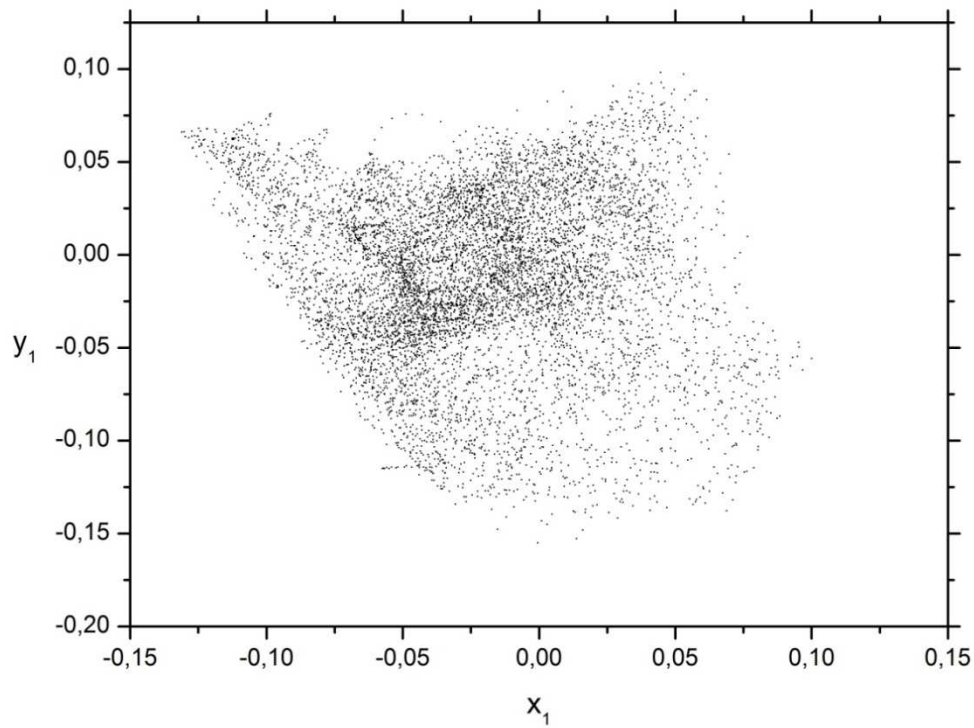


Fig. 3.1.24. Poincaré map for the coupling parameter $\sigma=0.0500$ – a circuit of seven identical Duffing oscillators.

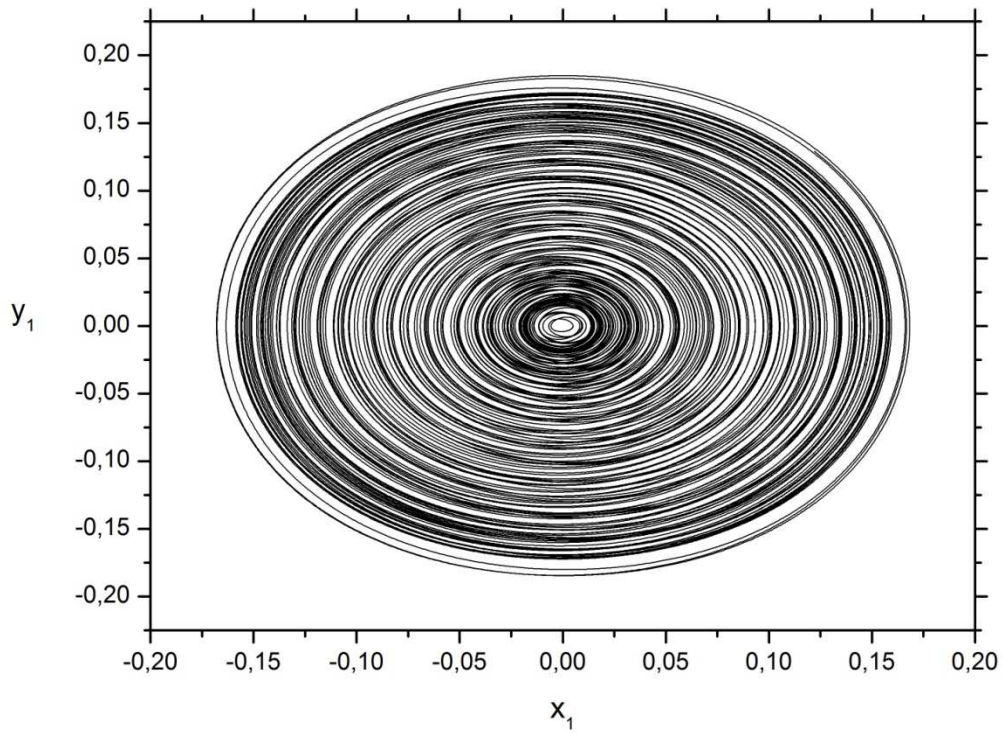


Fig. 3.1.25. Phase portrait for the coupling parameter $\sigma=0.0540$ – a circuit of seven real Duffing oscillators.

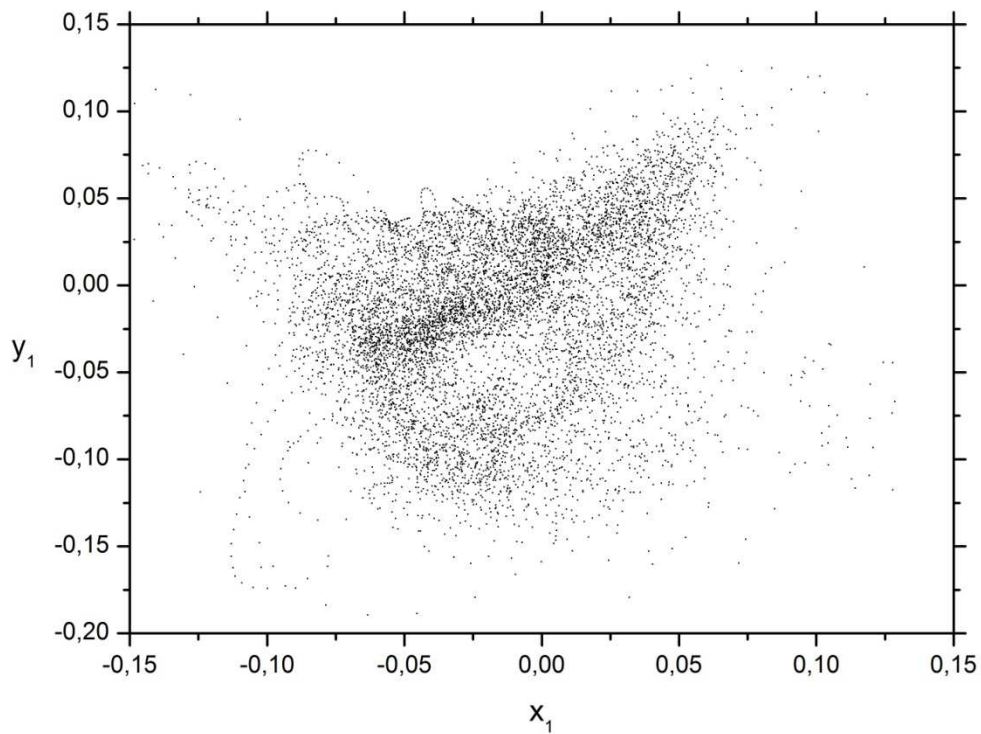


Fig. 3.1.26. Poincaré map for the coupling parameter $\sigma=0.0540$ – a circuit of seven real Duffing oscillators.

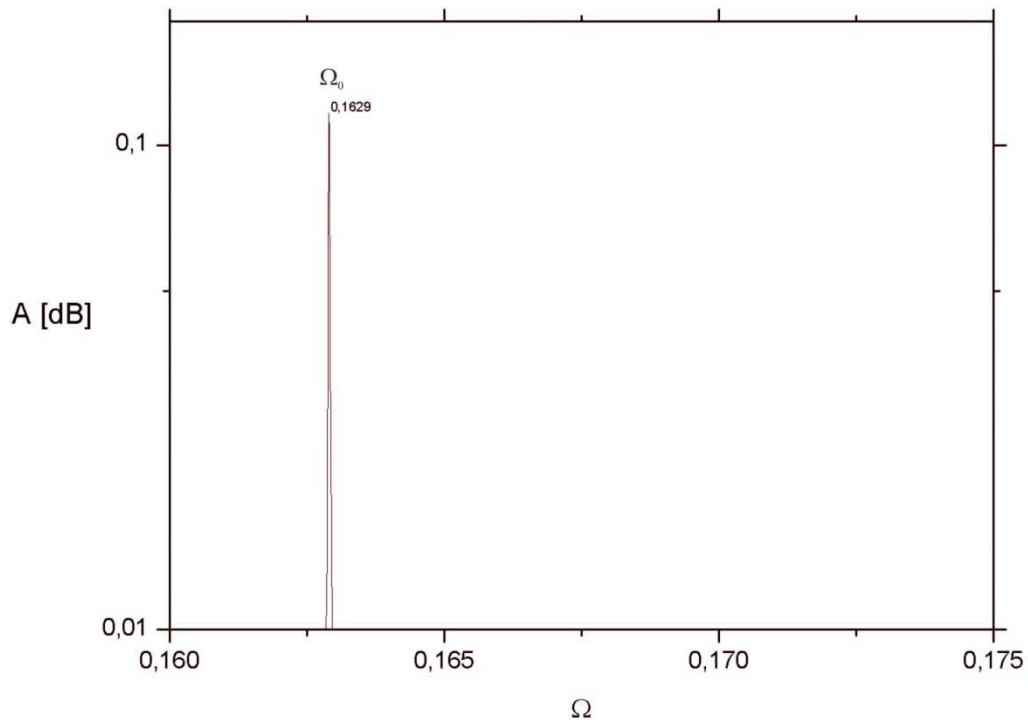


Fig. 3.1.27. FFT spectrum analysis for the coupling parameter $\sigma=0.0332$ – a circuit of seven identical Duffing oscillators.

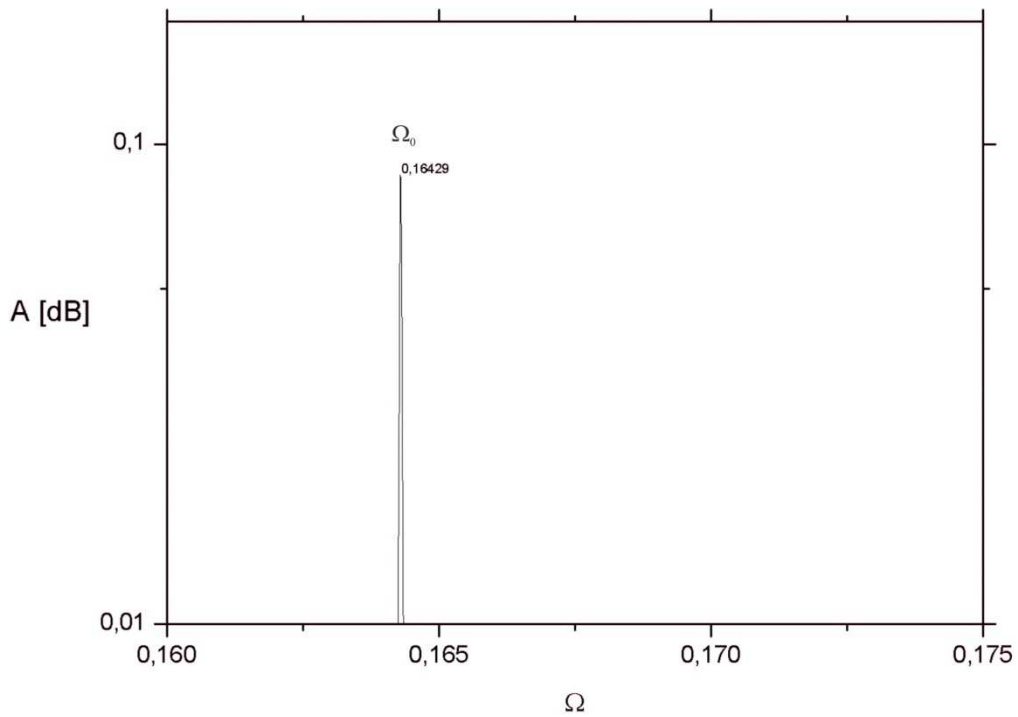


Fig. 3.1.28. FFT spectrum analysis for the coupling parameter $\sigma=0.0368$ – a circuit of seven real Duffing oscillators.

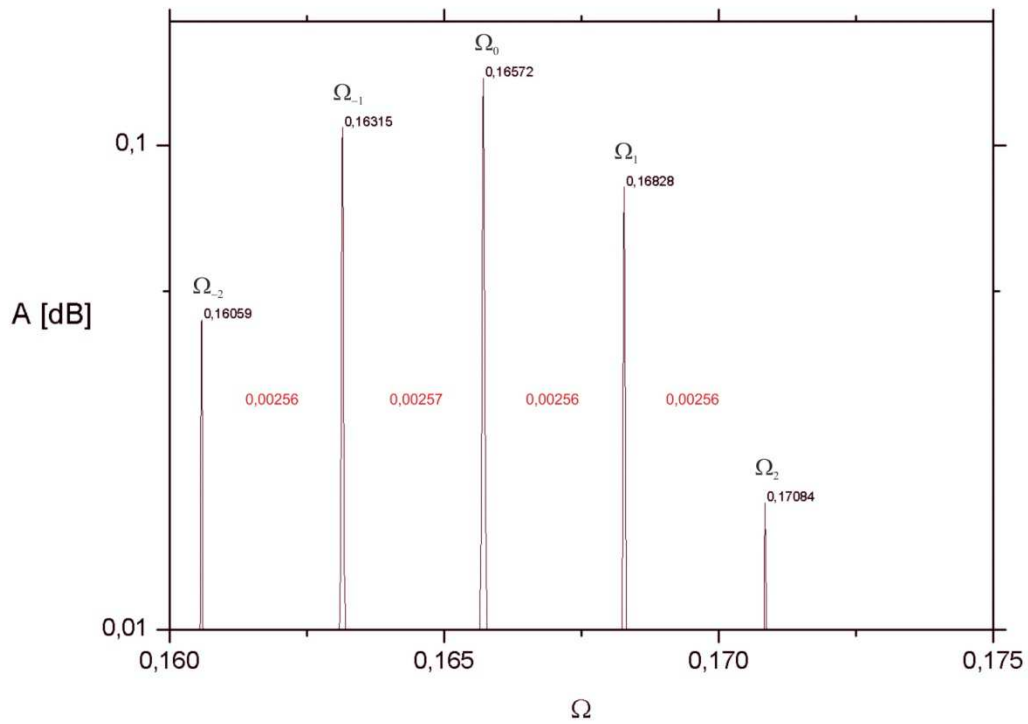


Fig. 3.1.29. FFT spectrum analysis for the coupling parameter $\sigma=0.0430$ – a circuit of seven identical Duffing oscillators.

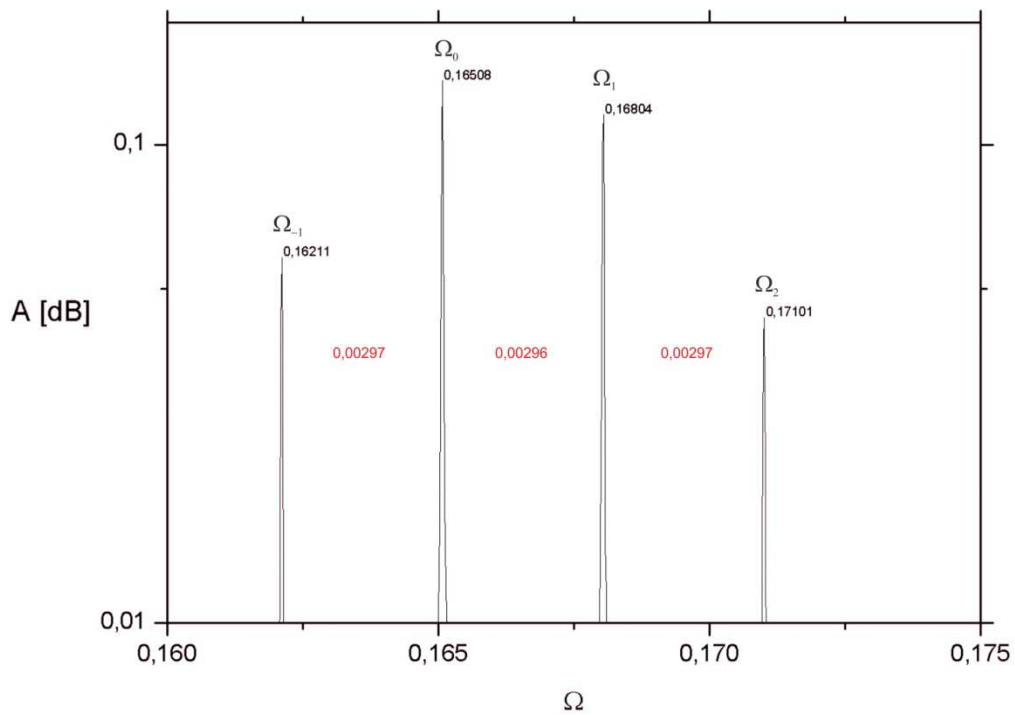


Fig. 3.1.30. FFT spectrum analysis for the coupling parameter $\sigma=0.0490$ – a circuit of seven real Duffing oscillators.

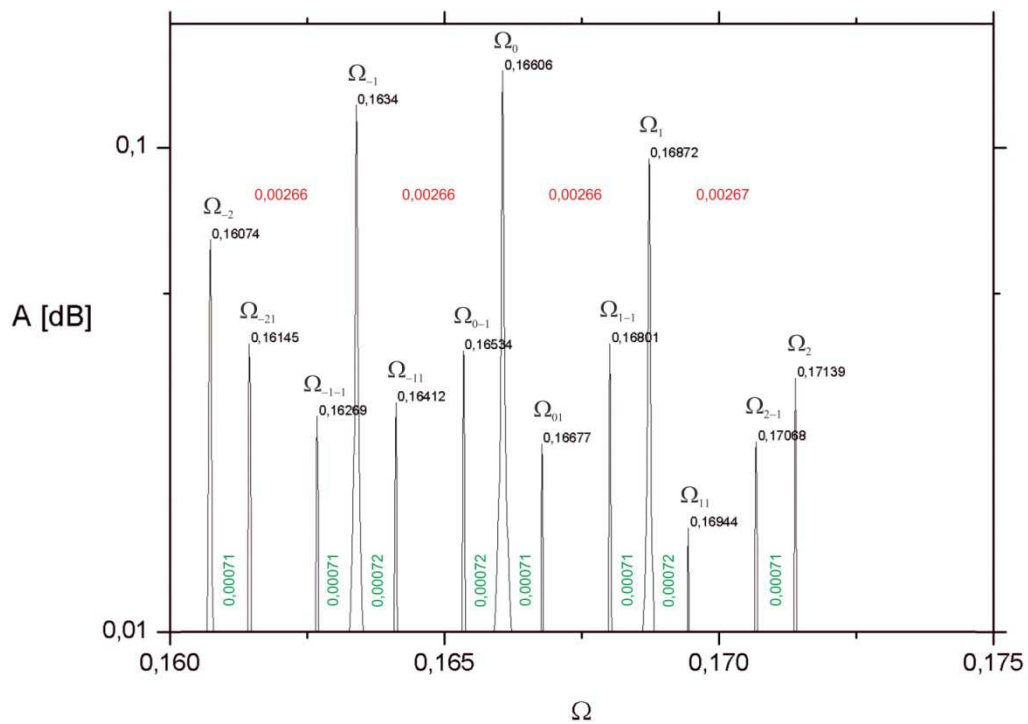


Fig. 3.1.31. FFT spectrum analysis for the coupling parameter $\sigma=0.0440$ – a circuit of seven identical Duffing oscillators.

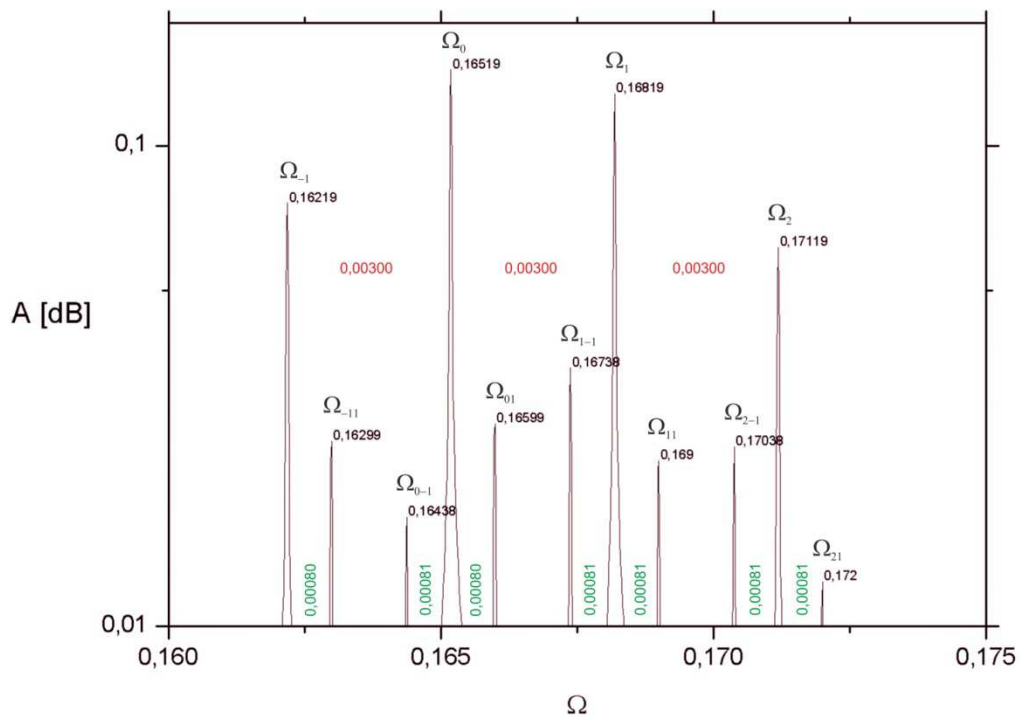


Fig. 3.1.32. FFT spectrum analysis for the coupling parameter $\sigma=0.0500$ – a circuit of seven real Duffing oscillators.

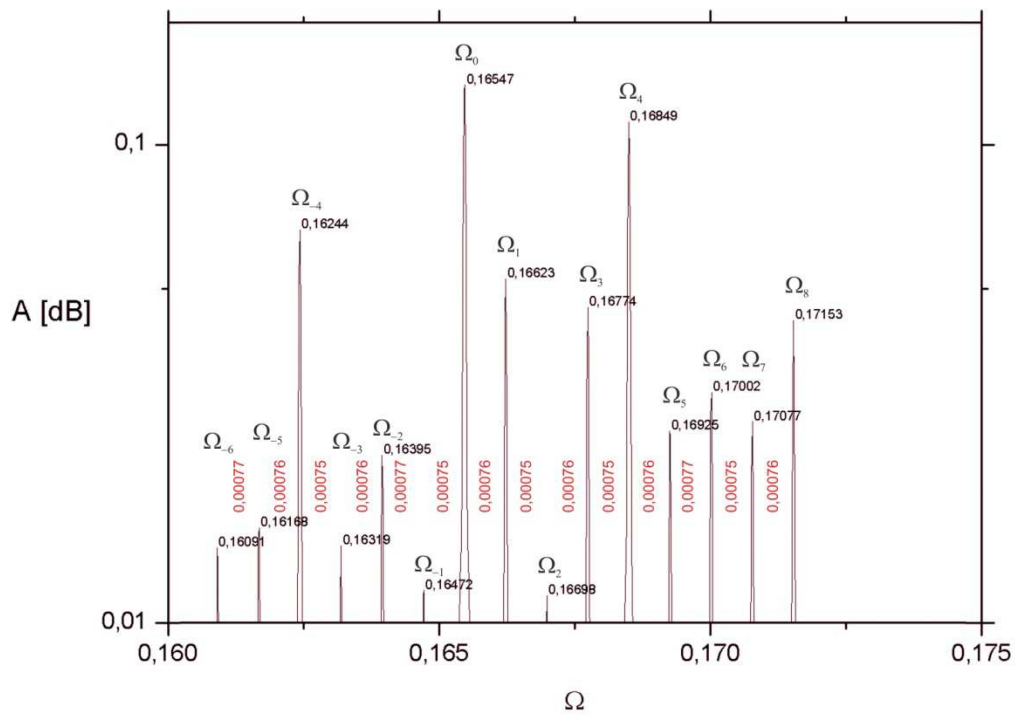


Fig. 3.1.33. FFT spectrum analysis for the coupling parameter $\sigma=0.0505$ – a circuit of seven real Duffing oscillators.

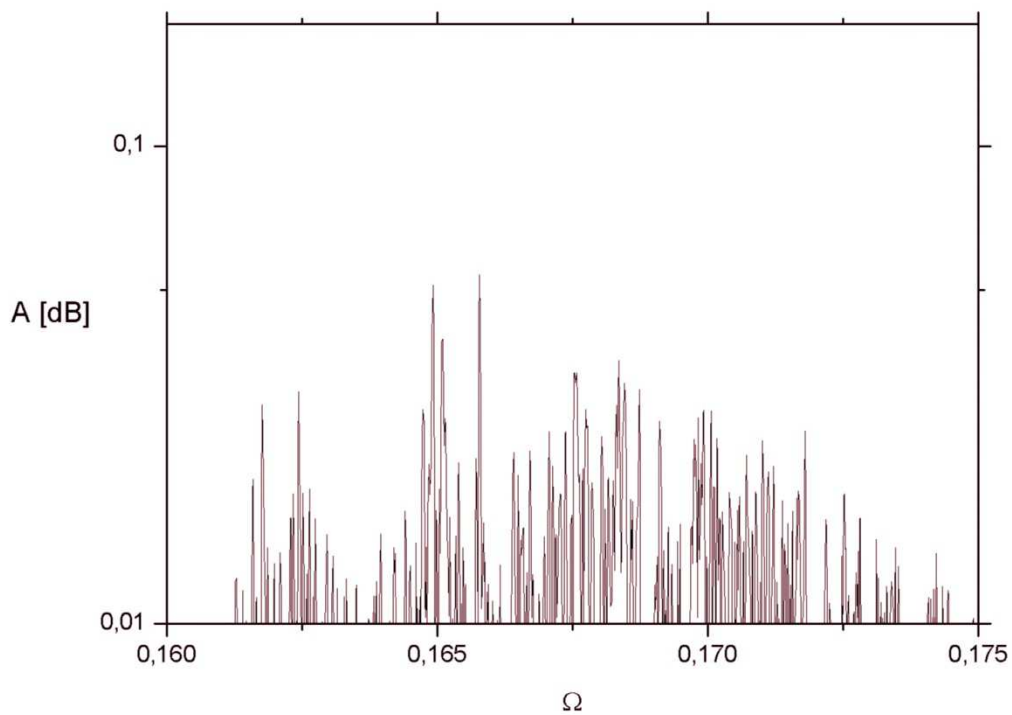


Fig. 3.1.34. FFT spectrum analysis for the coupling parameter $\sigma=0.0500$ – a circuit of seven identical Duffing oscillators.

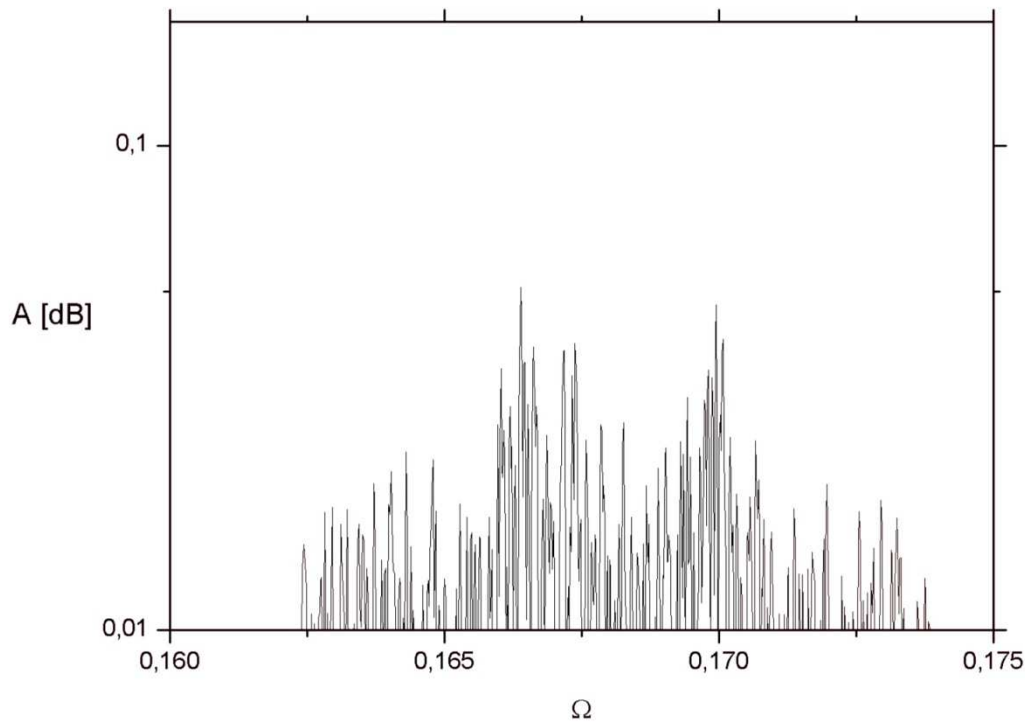


Fig. 3.1.35. FFT spectrum analysis for the coupling parameter $\sigma=0.0540$ – a circuit of seven real Duffing oscillators.

3.2. FFT analysis

To use a concept of the dimensionless frequency Ω , all the frequencies on the FFT spectrum analysis graphs (Fig. 3.1.27-3.1.35) were divided by the value ω_0 – the fundamental frequency characterizing the ideal circuit (see Chapter 4).

Comparing the spectrum of the signal for a circuit of seven identical Duffing oscillators with the spectrum of the signal for a circuit of seven real Duffing oscillators, identical solutions for the corresponding areas of the bifurcation of the two systems – periodic solutions, the 2D torus, the 3D torus, the chaotic solution – can be seen practically. A small difference in the values of the received frequencies, resulting from a difference in parameters between the identical and real system, is observed. With an increase in the coupling parameter σ , the value of the frequency rises.

The periodic solution is represented by a single, main frequency Ω_0 , which is the result of the first Hopf bifurcation (Fig. 3.1.27, 3.1.28). The emergence of the second

disproportionate frequency (the second Hopf bifurcation) causes an appearance of next frequencies around the main frequency (Fig. 3.1.29, 3.1.30). Analyzing the newly formed peaks, one can see that the offset between all received peaks and the main peak is constant or is a multiplication of this constant (for all the analyzed solutions, a ≈ 0.00002 difference is related to the sampling frequency of the signal). As a result, the first frequency is characterized by the peak Ω_0 and the second, disproportionate to the first frequency, is associated with a fixed value (marked in red on the graphs) of other peaks shifted with respect to the peak Ω_0 :

$$\Omega_n = \Omega_0 + n\beta_1 \quad (3.2.1)$$

where:

β_1 (≈ 0.00002) – constant offset between the peaks,

n – number of the analyzed frequency.

For example, using Fig. 3.1.29 and formula (3.2.1), the frequency marked by Ω_2 is:

$$\Omega_2 = \Omega_0 + 2\beta_1 = 0.16572 + 2 * 0.00256 = 0.17084$$

As a result of the third Hopf-type bifurcation, the third frequency Ω_{nm} appears, which is disproportionate to the two previous ones (Ω_0 and Ω_n). Newly formed peaks are also characterized by a constant offset relative to the peaks of the first and second frequency (the value marked in green on the graphs). The third disproportionate frequency can be described by the equation:

$$\Omega_{nm} = \Omega_n + m\beta_2 \quad (3.2.2)$$

where:

β_2 (≈ 0.00002) - constant offset between the peaks,

n, m - number of the analyzed frequency.

Using formula (3.2.2), the frequency Ω_{21} of Fig. 3.1.32 can be calculated as follows:

$$\Omega_{21} = \Omega_2 + \beta_2 = \Omega_0 + 2\beta_1 + \beta_2 = 0.16519 + 2 * 0.00300 + 0.00081 = 0.172$$

For the circuit of seven real Duffing oscillators, a series of period-doubling bifurcations of the 2D torus (Fig. 3.1.21, 3.1.22) can be seen, which is not present in the case of identical oscillators. In Fig. 3.1.33, newly formed peaks that divide the distance between the peaks representing the quasi-periodic solution (2D torus), for example, peaks Ω_0 and Ω_4 at equal distances, are shown. The distance between peaks Ω_0 and Ω_4 is divided by the value of Ω_2 , and then the distance between peaks Ω_0 and Ω_2 is divided by the value of Ω_1 . In such a way, a series of two period-doubling bifurcations of the 2D torus is manifested on the frequency diagram. To calculate the value of a selected frequency, formula (3.2.1) should be used. Calculating the frequency Ω_1 , we obtain:

$$\Omega_1 = \Omega_0 + \beta_1 = 0.16547 + 0.00076 = 0.16623$$

For chaotic (hyper-chaotic) solutions (Fig. 3.1.34, 3.1.35), it is difficult to present a description of the dominant frequencies as well as the relationships between them. The resulting frequency spectrum is continuous. Therefore, the spectral signal analysis with a detailed identification of the peak values was impossible to carry out in this case.

CHAPTER 4

ANALYSIS OF AN EXPERIMENTAL CIRCUIT OF SEVEN UNIDIRECTIONALLY COUPLED DUFFING OSCILLATORS

In this Chapter, a structure of a real circuit, identification of the parameters and experimental confirmation of the numerical investigations for a circuit of seven real, unidirectionally coupled, nonlinear Duffing oscillators is presented.

4.1. Structure and parameters of the experimental rig

For the purposes of an experimental analysis of the real circuit, an electrical system shown in Fig.4.1.2 was built. This system consists of LM358N operational amplifiers, AD663JN multipliers, resistors, capacitors, a 2x10 pin header, jumpers and a power strip. The LM358N operational amplifier is a dual low-power amplifier (Fig. 4.1.1). The voltage of the amplifier is 3 - 32V and the temperature range 0 - +70°C.

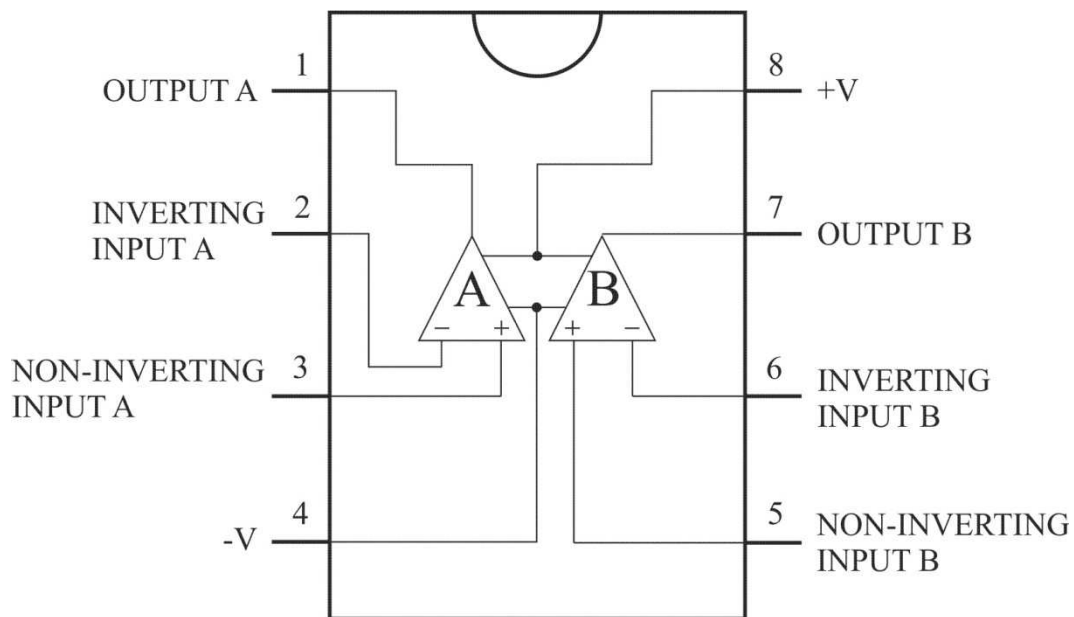


Fig. 4.1.1. Scheme of the LM358N operational amplifier.

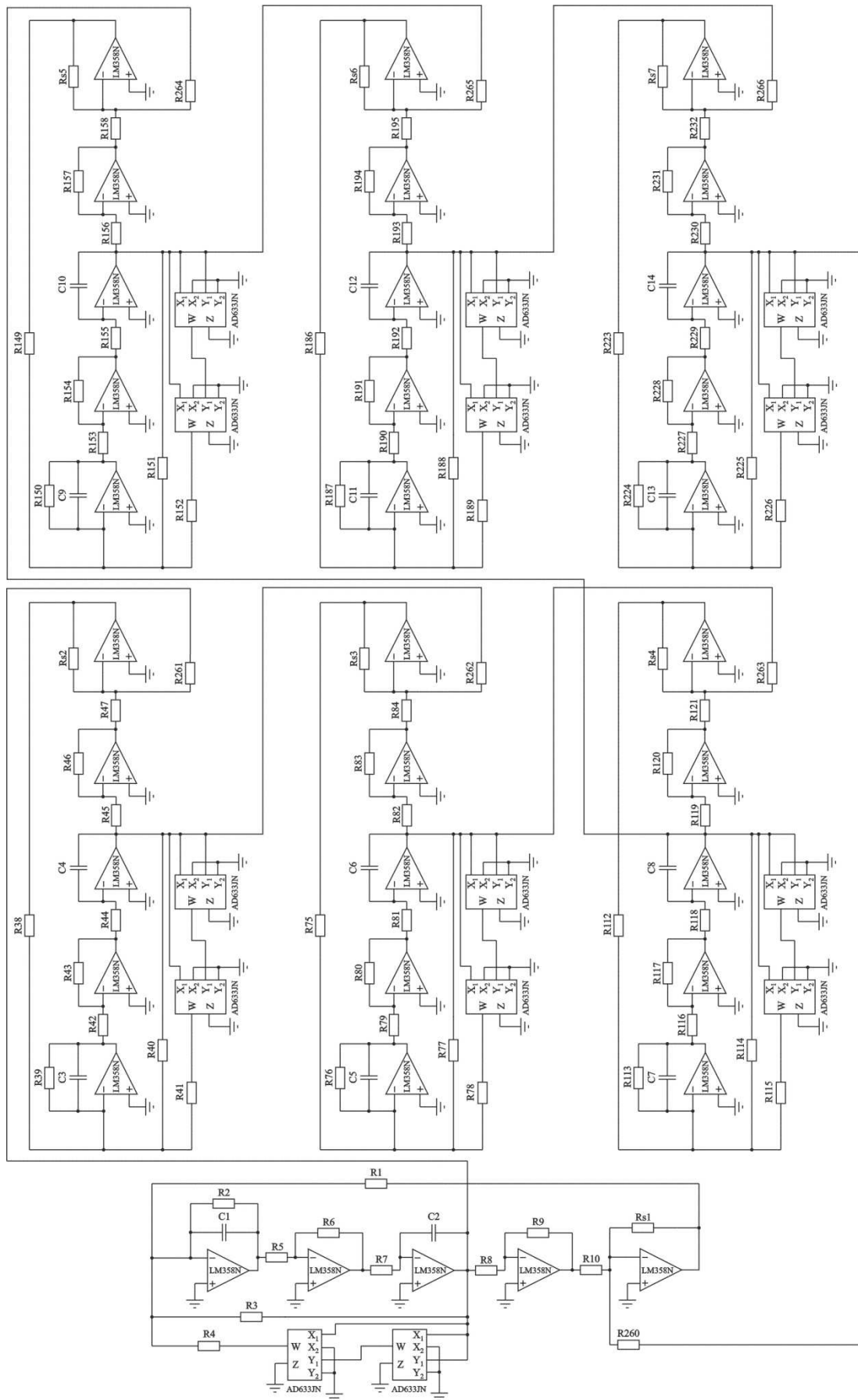


Fig. 4.1.2. Schematic diagram of the electrical circuit of seven real, unidirectionally coupling, nonlinear Duffing oscillators.

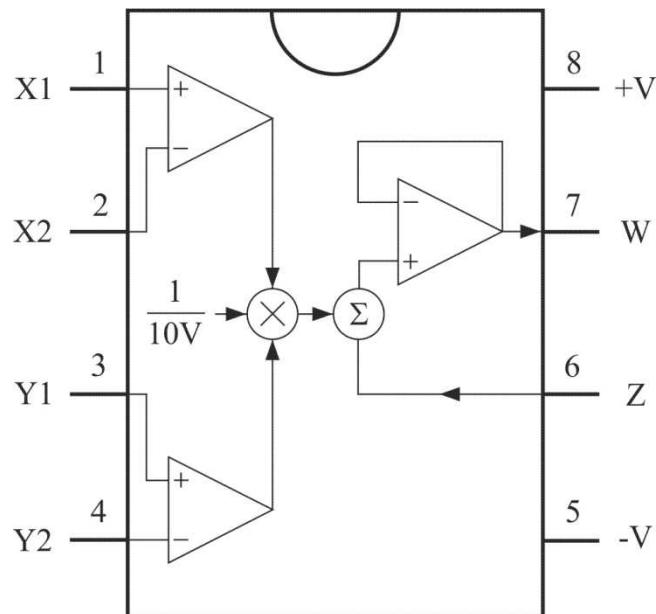


Fig. 4.1.3. Scheme of the AD633JN multiplier.

The AD633JN multiplier voltage (Fig. 4.1.3) is $\pm 8 - \pm 18V$, the temperature range: $0 - +70^{\circ}C$. The multiplier is characterized by a very high accuracy – the maximum multiplication error is 2%. The non-linearity in the system is realized by means of this multiplier:

$$W = \frac{(X_1 - X_2)(Y_1 - Y_2)}{10V} + Z$$

where:

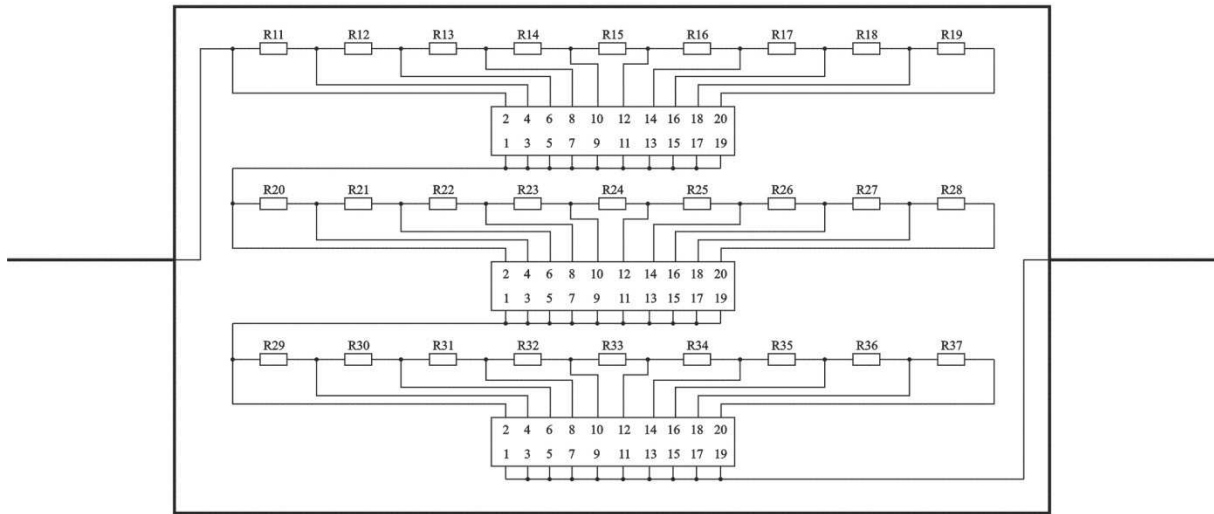
X_1, X_2, Y_1, Y_2 – inputs,

W – output,

Z – input for adding a variety of analog functions.

The $R_{s1} \div R_{s7}$ resistors, visible in Fig. 4.1.2, implement a coupling between the oscillators. They are drawn in a simplified manner. In fact, each of the resistors is composed of a group of resistors, a 2x10 pin header and jumpers by means of which it is possible to set a coupling between adjacent oscillators (see Fig 4.1.4).

Rs1



▪
▪
▪
▪
▪
▪
▪
▪
▪

Rs7

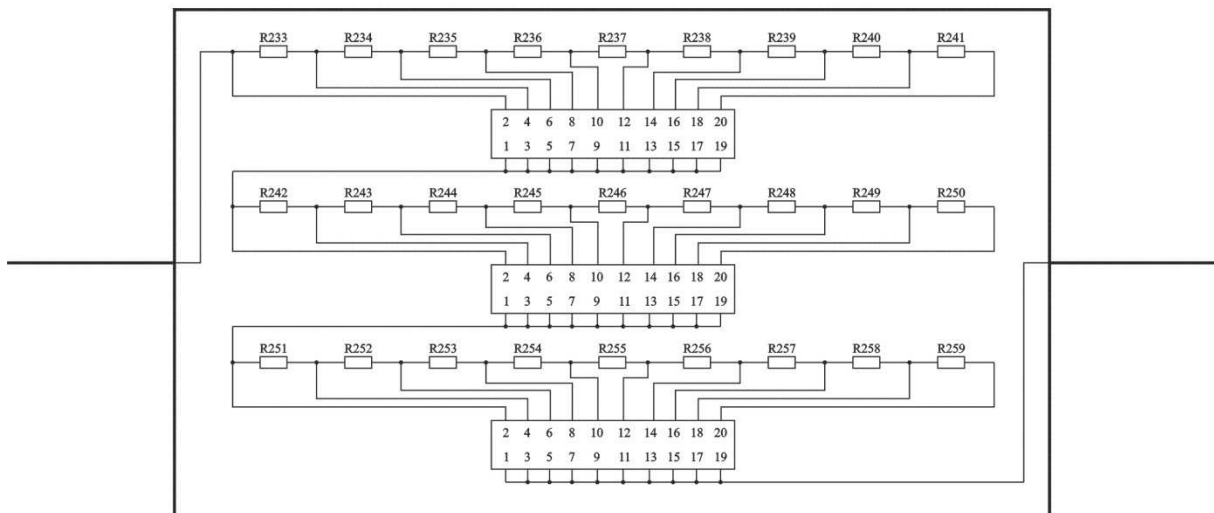


Fig. 4.1.4. Detailed scheme of the Rs1÷Rs7 coupling resistors.

A wiring diagram for all components on the circuit board is shown in Fig. 4.1.5.

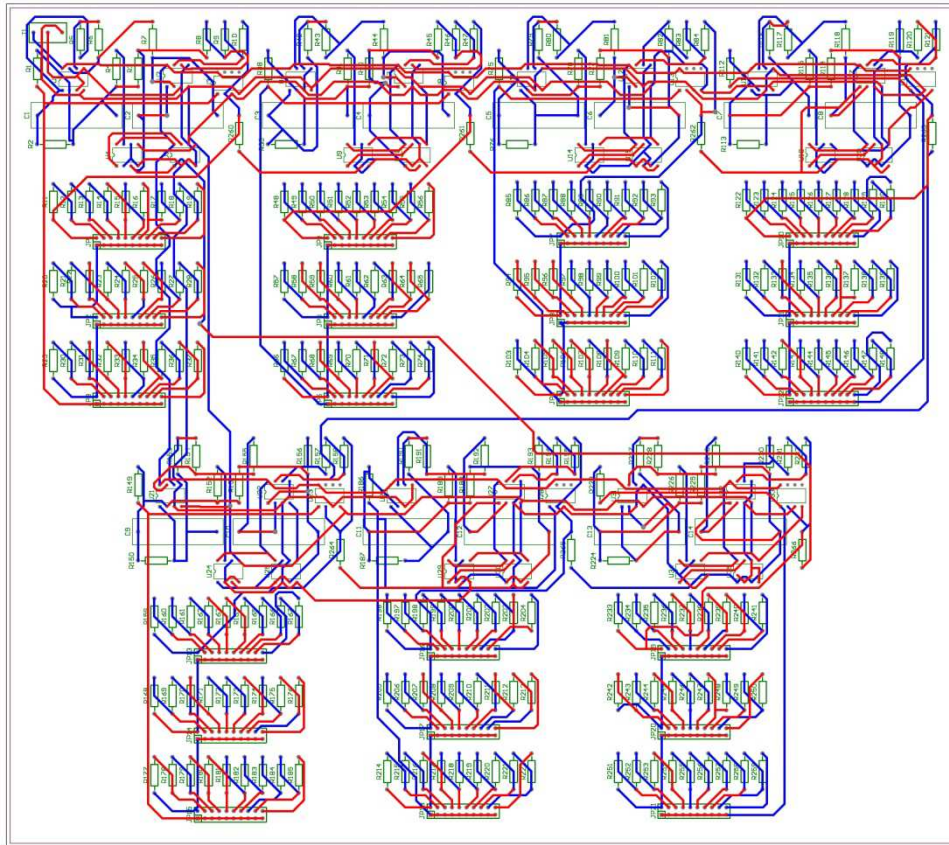


Fig. 4.1.5. Printed circuit board (PCB) – wiring components.

The constructed board is a double-sided PCB, i.e., some paths are routed on the top layer (red paths) and the remaining ones on the bottom layer (blue paths). Nominal values of resistors and capacitors are as follows:

R1, R2, R38, R39, R75, R76, R112, R113, R149, R150, R186, R187, R223, R224 = 1M Ω ;

R3, R5, R6, R8, R9, R40, R42, R43, R45, R46, R77, R79, R80, R82, R83, R114, R116, R117, R119, R120, R151, R153, R154, R156, R157, R188, R190, R191, R193, R194, R225, R227, R228, R230, R231 = 100k Ω ;

R4, R7, R10, R11, R12, R13, R14, R15, R16, R17, R18, R19, R41, R44, R47, R48, R49, R50, R51, R52, R53, R54, R55, R56, R78, R81, R84, R85, R86, R87, R88, R89, R90, R91, R92, R93, R115, R118, R121, R122, R123, R124, R125, R126, R127, R128, R129, R130, R152, R155, R158, R159, R160, R161, R162, R163, R164, R165, R166, R167, R189, R192, R195, R196, R197, R198, R199, R200, R201, R202, R203, R204, R226, R229, R232, R233, R234, R235, R236, R237, R238, R239, R240, R241, R260, R261, R262, R263, R264, R265, R266 = 10k Ω ;

R20, R21, R22, R23, R24, R25, R26, R27, R28, R57, R58, R59, R60, R61, R62, R63, R64, R65, R94, R95, R96, R97, R98, R99, R100, R101, R102, R131, R132, R133, R134, R135, R136, R137,

R138, R139, R168, R169, R170, R171, R172, R173, R174, R175, R176, R205, R206, R207, R208, R209, R210, R211, R212, R213, R242, R243, R244, R245, R246, R247, R248, R249, R250 = 1k Ω ;

R29, R30, R31, R32, R33, R34, R35, R36, R37, R66, R67, R68, R69, R70, R71, R72, R73, R74, R103, R104, R105, R106, R107, R108, R109, R110, R111, R140, R141, R142, R143, R144, R145, R146, R147, R148, R177, R178, R179, R180, R181, R182, R183, R184, R185, R214, R215, R216, R217, R218, R219, R220, R221, R222 = 100 Ω ;

C1, C2, C3, C4, C5, C6, C7, C8, C9, C10, C11, C12, C13, C14 = 10nF.

In the constructed real circuit, it is impossible to select all the elements having identical nominal values like in the ideal circuit. Actual, measured values of resistors and capacitors, in the real electric circuit, are as follows:

D1: R1 = 1006k Ω ; R2 = 1005k Ω ; R3 = 99.4k Ω ; R4 = 10.00k Ω ; R5 = 100.2k Ω ;
R6 = 100.3k Ω ; R7 = 9.98k Ω ; R8 = 100.3k Ω ; R9 = 100.1k Ω ; R10 = 10.02k Ω ;
R11, R12, R13, R14, R15, R16, R17, R18, R19 = 10.02k Ω ;
R20, R21, R22, R23, R24, R25, R26, R27, R28 = 998 Ω ;
R29, R30, R31, R32, R33, R34, R35, R36, R37 = 100.2 Ω ;
C1 = 11.80nF; C2 = 12.06nF;

D2: R38 = 1007k Ω ; R39 = 1004k Ω ; R40 = 99.4k Ω ; R41 = 9.99k Ω ; R42 = 100.4k Ω ;
R43 = 100.2k Ω ; R44 = 10.01k Ω ; R45 = 100.2k Ω ; R46 = 100.2k Ω ; R47 = 10.02k Ω ;
R48, R49, R50, R51, R52, R53, R54, R55, R56 = 10.02k Ω ;
R57, R58, R59, R60, R61, R62, R63, R64, R65 = 998 Ω ;
R66, R67, R68, R69, R70, R71, R72, R73, R74 = 100.2 Ω ;
C3 = 11.92nF; C4 = 11.79nF;

D3: R75 = 1006k Ω ; R76 = 1005k Ω ; R77 = 99.5k Ω ; R78 = 9.99k Ω ; R79 = 100.3k Ω ;
R80 = 100.3k Ω ; R81 = 10.00k Ω ; R82 = 100.0k Ω ; R83 = 100.1k Ω ; R84 = 10.01k Ω ;
R85, R86, R87, R88, R89, R90, R91, R92, R93 = 10.02k Ω ;
R94, R95, R96, R97, R98, R99, R100, R101, R102 = 998 Ω ;
R103, R104, R105, R106, R107, R108, R109, R110, R111 = 100.2 Ω ;
C5 = 11.63nF; C6 = 12.01nF;

D4: R112 = 1007k Ω ; R113 = 1005k Ω ; R114 = 99.5k Ω ; R115 = 10.00k Ω ;
R116 = 100.3k Ω ; R117 = 100.2k Ω ; R118 = 10.01k Ω ; R119 = 100.3k Ω ;
R120 = 100.2k Ω ; R121 = 10.00k Ω ;
R122, R123, R124, R125, R126, R127, R128, R129, R130 = 10.02k Ω ;
R131, R132, R133, R134, R135, R136, R137, R138, R139 = 998 Ω ;
R140, R141, R142, R143, R144, R145, R146, R147, R148 = 100.2 Ω ;
C7 = 11.85nF; C8 = 12.00nF;

D5: R149 = 1007k Ω ; R150 = 1005k Ω ; R151 = 99.2k Ω ; R152 = 9.99k Ω ;
R153 = 100.1k Ω ; R154 = 100.2k Ω ; R155 = 10.02k Ω ; R156 = 100.3k Ω ;
R157 = 100.3k Ω ; R158 = 10.01k Ω ;
R159, R160, R161, R162, R163, R164, R165, R166, R167 = 10.02k Ω ;
R168, R169, R170, R171, R172, R173, R174, R175, R176 = 998 Ω ;
R177, R178, R179, R180, R181, R182, R183, R184, R185 = 100.2 Ω ;
C9 = 11.66nF; C10 = 11.72nF;

D6: R186 = 1007k Ω ; R187 = 1005k Ω ; R188 = 99.1k Ω ; R189 = 9.99k Ω ;
R190 = 100.4k Ω ; R191 = 100.2k Ω ; R192 = 10.02k Ω ; R193 = 100.2k Ω ;
R194 = 100.2k Ω ; R195 = 10.00k Ω ;
R196, R197, R198, R199, R200, R201, R202, R203, R204 = 10.02k Ω ;
R205, R206, R207, R208, R209, R210, R211, R212, R213 = 998 Ω ;
R214, R215, R216, R217, R218, R219, R220, R221, R222 = 100.2 Ω ;
C11 = 11.74nF; C12 = 11.91nF;

D7: R223 = 1006k Ω ; R224 = 1003k Ω ; R225 = 99.1k Ω ; R226 = 10.00k Ω ;
R227 = 100.4k Ω ; R228 = 100.4k Ω ; R229 = 9.99k Ω ; R230 = 100.3k Ω ;
R231 = 100.2k Ω ; R232 = 10.02k Ω ;
R233, R234, R235, R236, R237, R238, R239, R2040, R241 = 10.02k Ω ;
R242, R243, R244, R245, R246, R247, R248, R249, R250 = 998 Ω ;
R251, R252, R253, R254, R255, R256, R257, R258, R259 = 100.2 Ω ;
C13 = 11.89nF; C14 = 12.05nF.

4.2. Mathematical description

A differential equation was derived on the basis of a scheme of the first coupled Duffing oscillator (Fig. 4.2.1).

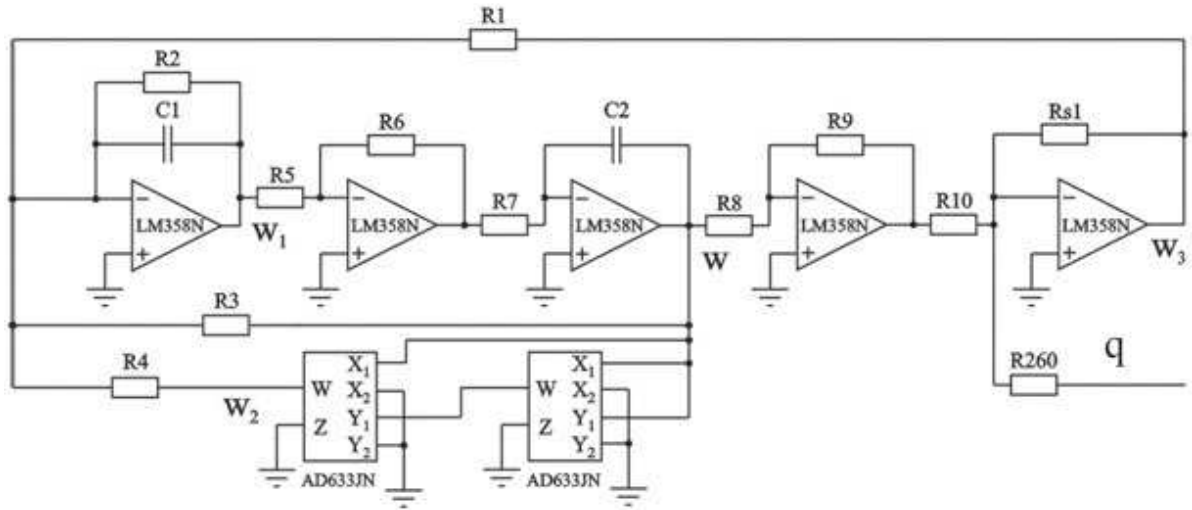


Fig. 4.2.1. Scheme of the first of coupled Duffing oscillators.

For w_1 , the equation is:

$$w_1 = -\frac{1}{R1C1} \int w_3 dt - \frac{1}{R2C1} \int w_1 dt - \frac{1}{R3C1} \int w dt - \frac{1}{R4C1} \int w_2 dt \quad (4.2.1)$$

From the characteristics of the AD633JN multiplier results:

$$w_2 = \frac{w^3}{100} \quad (4.2.2)$$

For w , we can write a relationship:

$$w = -\frac{1}{R7C2} \int \left(-\frac{R6}{R5} w_1\right) dt \quad (4.2.3)$$

After integration of Eq. (4.2.3), we obtain:

$$\dot{w} = \frac{R6}{R7C2R5} w_1 \quad (4.2.4)$$

A transformation of Eq. (4.2.4) yields:

$$w_1 = \frac{R7C2R5}{R6} \dot{w} \quad (4.2.5)$$

For w_3 , we can write a relationship:

$$w_3 = -\frac{Rs1}{R10} \left(-\frac{R9}{R8} w \right) - \frac{Rs1}{R260} q = \frac{Rs1R9}{R10R8} w - \frac{Rs1}{R260} q \quad (4.2.6)$$

Substituting Eqs. (4.2.1), (4.2.2) and (4.2.6) into Eq. (4.2.4), we have:

$$\begin{aligned} \dot{w} = & \frac{R6}{R7C2R5} \left(-\frac{1}{R1C1} \int \left(\frac{Rs1R9}{R10R8} w - \frac{Rs1}{R260} q \right) dt - \frac{1}{R2C1} \int \left(\frac{R7C2R5}{R6} \dot{w} \right) dt \right. \\ & \left. - \frac{1}{R3C1} \int w dt - \frac{1}{R4C1} \int \frac{w^3}{100} dt \right) \end{aligned} \quad (4.2.7)$$

An integration of Eq. (4.2.7) gives:

$$\dot{w} = \frac{R6}{R7C2R5} \left(-\frac{Rs1R9}{R1C1R10R8} w + \frac{Rs1}{R1C1R260} q - \frac{R7C2R5}{R2C1R6} \dot{w} - \frac{1}{R3C1} w - \frac{1}{100R4C1} w^3 \right) \quad (4.2.8)$$

After a transformation of Eq. (4.2.8), a dimensional differential equation was obtained:

$$\begin{aligned} \ddot{w} + \frac{1}{R2C1} \dot{w} + \frac{R6}{R3R5R7C1C2} w + \frac{R6}{100R4R5R7C1C2} w^3 = & \frac{R6Rs1}{R1R5R7R260C1C2} q \\ - \frac{R6R9Rs1}{R1R5R7R8R10C1C2} w \end{aligned} \quad (4.2.9)$$

For the needs of mathematical analysis such as the calculation of Lyapunov exponents, Eq. (4.2.9) has to be written in a dimensionless form after the following transformations:

$$\frac{1}{\omega_0^2} \ddot{w} + \frac{1}{R2C1\omega_0} \frac{1}{\omega_0} \dot{w} + w + \frac{R3}{100R4} w^3 = \frac{R3Rs1}{R1R260} q - \frac{R3R9Rs1}{R1R8R10} w \quad (4.2.10)$$

Dividing Eq. (4.2.10) by $V_0=1V$ [90]:

$$\frac{1}{V_0\omega_0^2} \ddot{w} + \frac{1}{R2C1\omega_0} \frac{1}{V_0\omega_0} \dot{w} + \frac{1}{V_0} w + \frac{R3}{R4} \frac{1}{100V_0} w^3 = \frac{R3Rs1}{R1R260} \frac{1}{V_0} q - \frac{R3R9Rs1}{R1R8R10} \frac{1}{V_0} w \quad (4.2.11)$$

We finally obtain:

$$\ddot{u} + c\dot{u} + au + bu^3 = \sigma_z v - \sigma_y u \quad (4.2.12)$$

where:

$$\omega_0^2 = \frac{R6}{R3R5R7C1C2}$$

$$c = \frac{1}{R2C1\omega_0}$$

$$a = 1$$

$$b = \frac{R3}{R4}$$

$$\sigma_z = \frac{R3Rs1}{R1R260}$$

$$\sigma_y = \frac{R3R9Rs1}{R1R8R10}$$

$$u = \frac{1}{V_0} w$$

$$\dot{u} = \frac{1}{V_0\omega_0} \dot{w}$$

$$\ddot{u} = \frac{1}{V_0\omega_0^2} \ddot{w}$$

$$u^3 = \frac{1}{100[V^2]V_0} w^3$$

$$v = \frac{1}{V_0} q$$

After considering the substitution and the relations between these parameters for the real and ideal circuit, Eq. (4.2.12) can be written in the general (2.1) or detailed ((3.1) and (3.2)) forms which were considered during the numerical analysis.

For the ideal circuit of seven unidirectionally coupled, nonlinear Duffing oscillators, the frequency ω_0 and the remaining dimensionless parameters are as follows:

$$\omega_0^2 = 10000000 [1/s^2]; c = 0.03162; a = 1; b = 10;$$

$$\sigma_z = \sigma_y = \sigma = R_s * k$$

where:

$$k = \frac{R3}{R1R260} = \frac{R3R9}{R1R8R10} = 0,00001 \left[\frac{1}{\Omega} \right]$$

k – according to the nominal values of real parameters;

$$R_s = R_{s1} = R_{s2} = R_{s3} = R_{s4} = R_{s5} = R_{s6} = R_{s7}$$

$$R_s \in \langle 0 \div 99900 \rangle [\Omega]$$

R_s is the resistor controlling the value of the coupling.

For the real circuit, the frequencies ω_0 and the remaining dimensionless parameters are as follows:

$$\omega_{01}^2 = 7090665.05 [1/s^2]; c_1 = 0.031667; a_1 = 1.0000; b_1 = 9.940;$$

$$\omega_{02}^2 = 7137128.00 [1/s^2]; c_2 = 0.031379; a_2 = 1.0065; b_2 = 10.015;$$

$$\omega_{03}^2 = 7195387.66 [1/s^2]; c_3 = 0.031213; a_3 = 1.0148; b_3 = 10.107;$$

$$\omega_{04}^2 = 7053587.10 [1/s^2]; c_4 = 0.031533; a_4 = 0.9948; b_4 = 9.898;$$

$$\omega_{05}^2 = 7369331.41 [1/s^2]; c_5 = 0.032047; a_5 = 1.0393; b_5 = 10.320;$$

$$\omega_{06}^2 = 7188077.88 [1/s^2]; c_6 = 0.031829; a_6 = 1.0137; b_6 = 10.056;$$

$$\omega_{07}^2 = 7057167.34 [1/s^2]; c_7 = 0.031490; a_7 = 0.9953; b_7 = 9.853;$$

$$\sigma_{zj} = \sigma * \frac{kz_j}{k} = R_{sj} * k * \frac{kz_j}{k} = R_{sj} * kz_j; \quad \sigma_{yj} = \sigma * \frac{ky_j}{k} = R_{sj} * k * \frac{ky_j}{k} = R_{sj} * ky_j;$$

where:

$$R_s = R_{s1} = R_{s2} = R_{s3} = R_{s4} = R_{s5} = R_{s6} = R_{s7}$$

$$R_s \in \langle 0 \div 99900 \rangle [\Omega]$$

$$k_{z_1} = 0.00000987 [1/\Omega]; \quad k_{y_1} = 0.00000984 [1/\Omega];$$

$$k_{z_2} = 0.00000993 [1/\Omega]; \quad k_{y_2} = 0.00000992 [1/\Omega];$$

$$k_{z_3} = 0.00001003 [1/\Omega]; \quad k_{y_3} = 0.00001004 [1/\Omega];$$

$$k_{z_4} = 0.00000982 [1/\Omega]; \quad k_{y_4} = 0.00000982 [1/\Omega];$$

$$k_{z_5} = 0.00001021 [1/\Omega]; \quad k_{y_5} = 0.00001023 [1/\Omega];$$

$$k_{z_6} = 0.00000995 [1/\Omega]; \quad k_{y_6} = 0.00000998 [1/\Omega];$$

$$k_{z_7} = 0.00000976 [1/\Omega]; \quad k_{y_7} = 0.00000976 [1/\Omega];$$

Moreover, from the above description of the real circuit parameters, the following relationships between the dimensionless and dimensional parameters of the coupling result:

$$\kappa_{z_j} = k_{z_j}/k; \quad \kappa_{y_j} = k_{y_j}/k.$$

4.3. Experimental investigations

The built circuit (1), an AC (2), a NATIONAL INSTRUMENTS data acquisition card (3), the LabVIEW SignalExpress 2010 software and a notebook (4) were used in the experimental tests (Fig. 4.3.1).

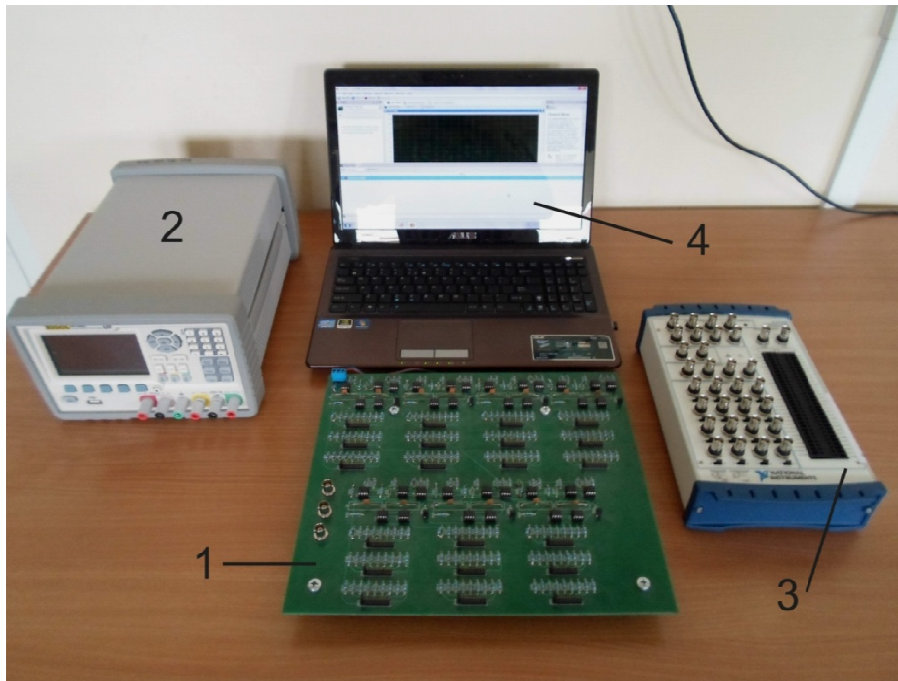


Fig. 4.3.1. Experimental rig.

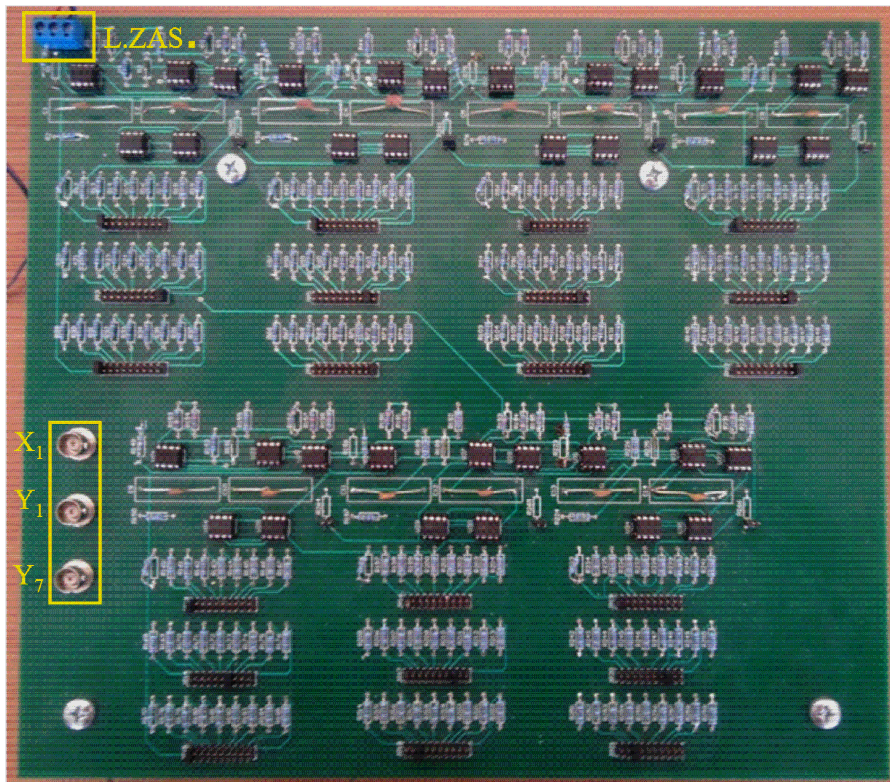


Fig. 4.3.2. Electrical circuit of seven unidirectionally coupled, nonlinear Duffing oscillators.

The test circuit (1) was connected via a power strip (L.ZAS. in Fig. 4.3.2) with an AC RIGOL (2). The value of the supply voltage was equal to $\pm 15V$. The circuit outputs (x_1, y_1, y_7 in Fig. 4.3.2) were connected to a data acquisition card (3). The values of the three recorded signals (x_1, y_1, y_7) were transmitted in real time to a notebook (4), which saved the results through the LabVIEW SignalExpress 2010 software.

The obtained results are presented in the form:

- phase portraits (Figs. 4.3.3, 4.3.4, 4.3.6, 4.3.8, 4.3.10, 4.3.12),
- Poincaré maps (Figs. 4.3.5, 4.3.7, 4.3.9, 4.3.11, 4.3.13),
- FFT spectrum analysis (Figs. 4.3.14-4.3.18).

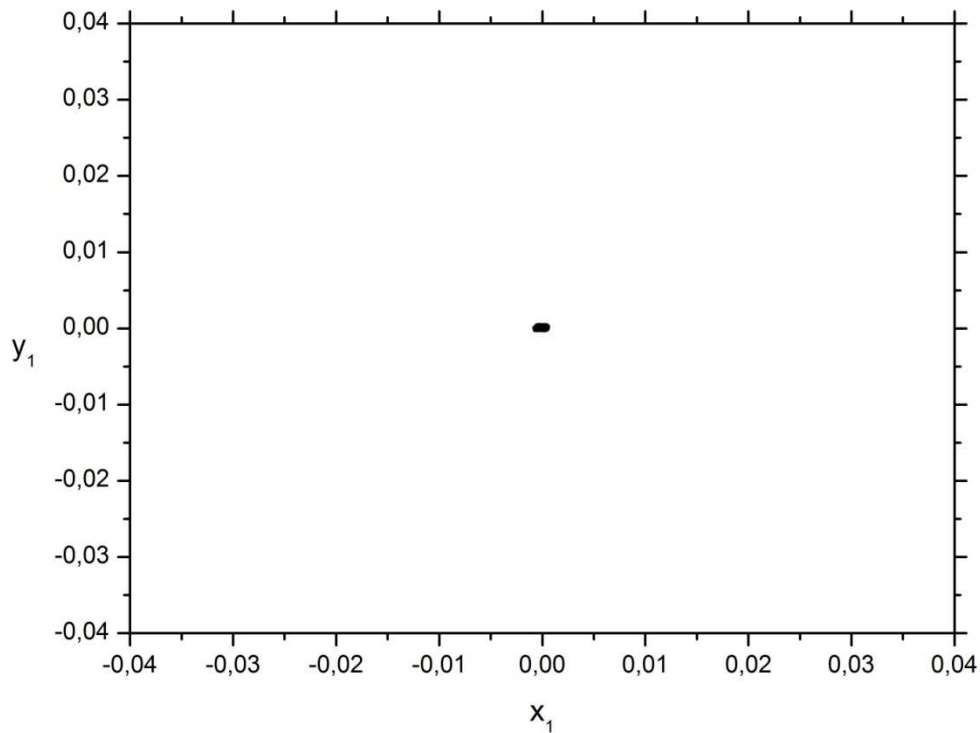


Fig. 4.3.3. Phase portrait for the coupling parameter $\sigma=0.0480$ – a circuit of seven real Duffing oscillators.

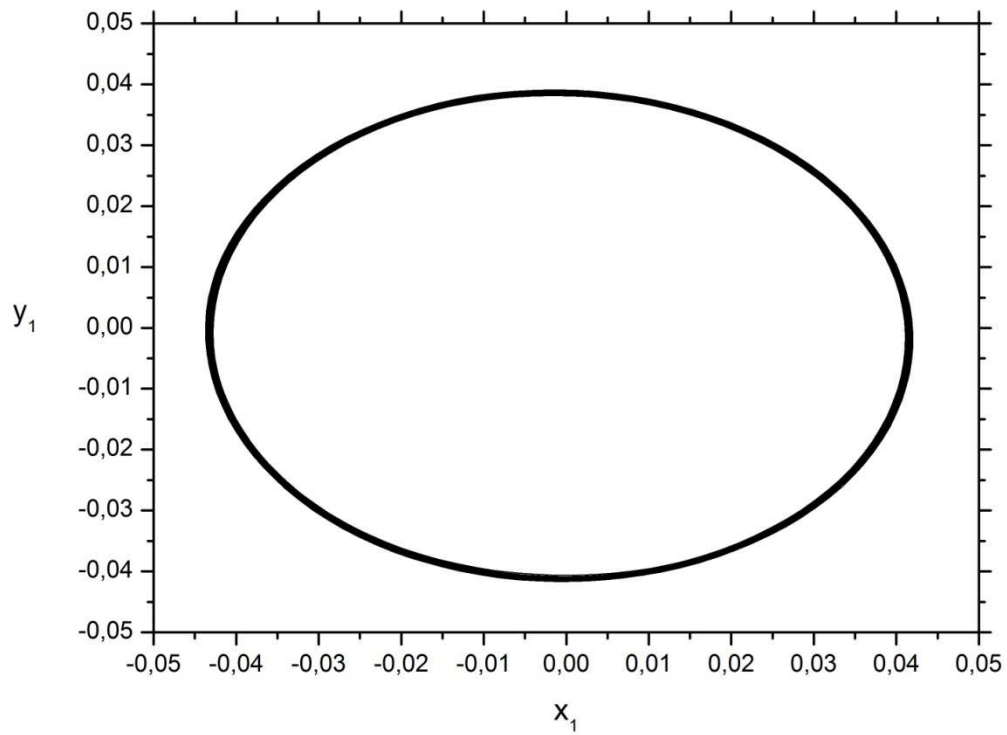


Fig. 4.3.4. Phase portrait for the coupling parameter $\sigma=0.0490$ – a circuit of seven real Duffing oscillators.

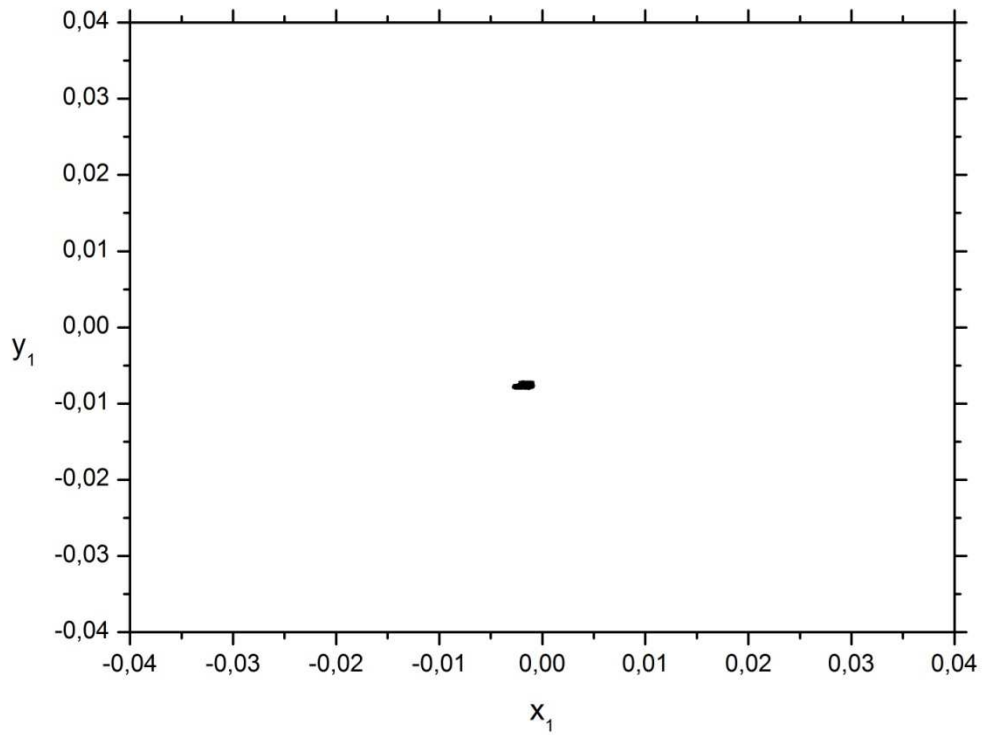


Fig. 4.3.5. Poincaré map for the coupling parameter $\sigma=0.0490$ – a circuit of seven real Duffing oscillators.

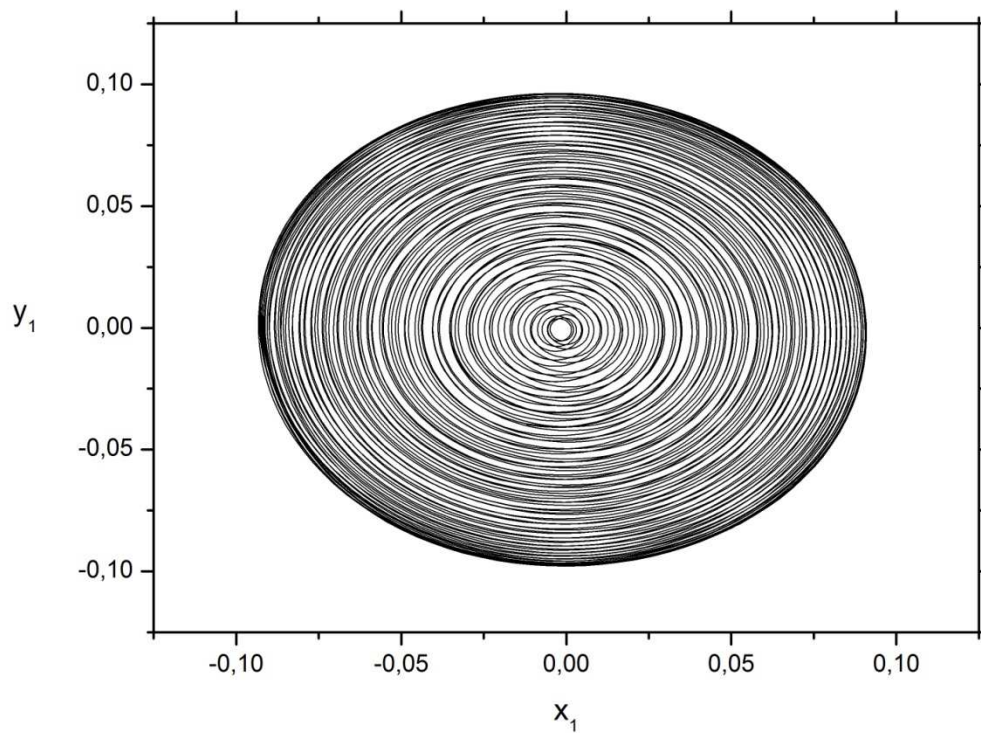


Fig. 4.3.6. Phase portrait for the coupling parameter $\sigma=0.0660$ – a circuit of seven real Duffing oscillators.

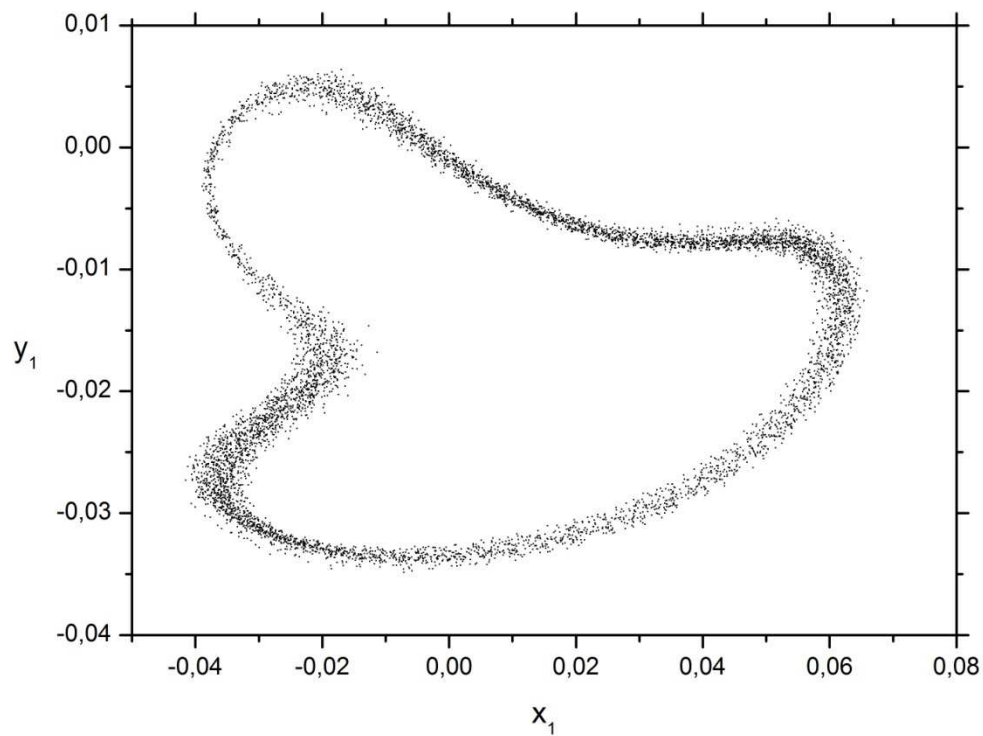


Fig. 4.3.7. Poincaré map for the coupling parameter $\sigma=0.0660$ – a circuit of seven real Duffing oscillators.

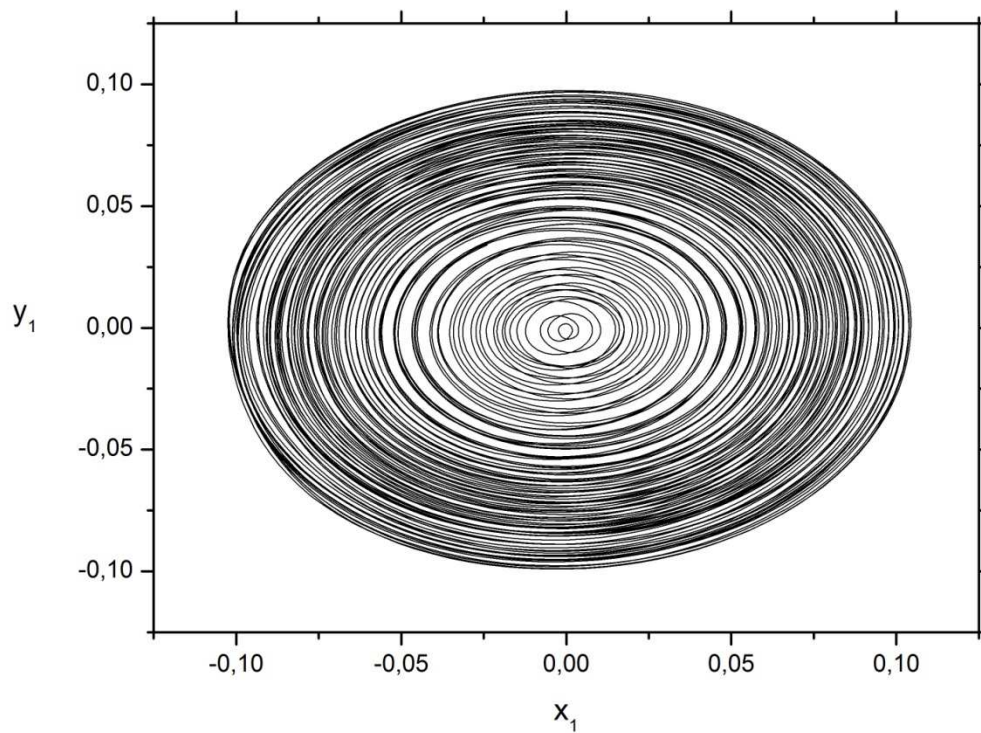


Fig. 4.3.8. Phase portrait for the coupling parameter $\sigma=0.0680$ – a circuit of seven real Duffing oscillators.

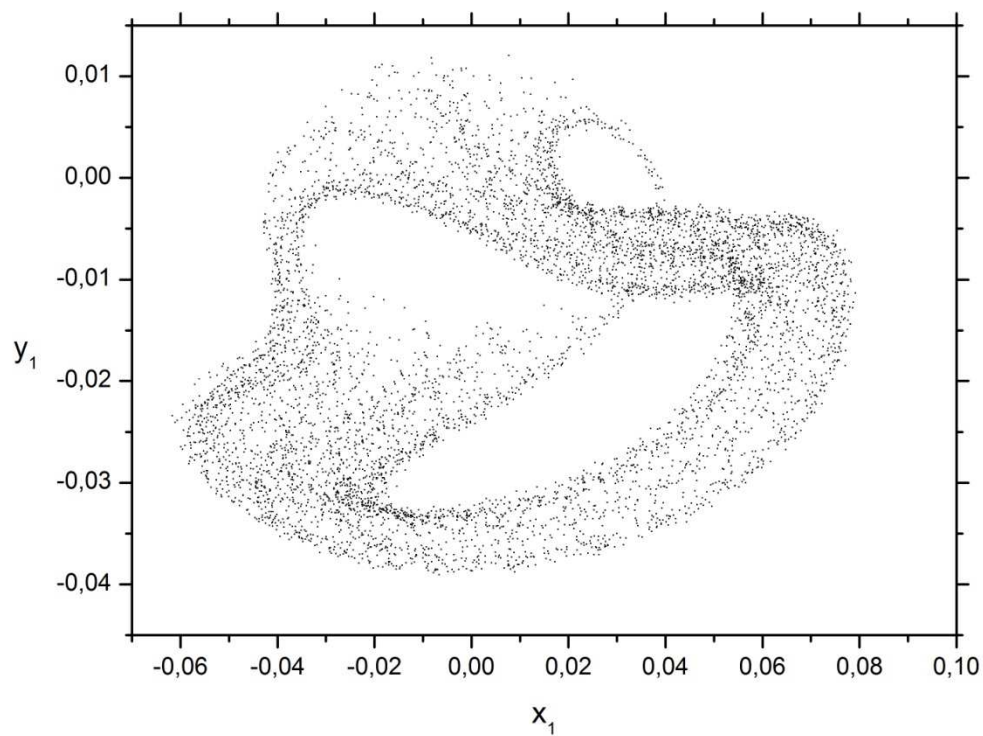


Fig. 4.3.9. Poincaré map for the coupling parameter $\sigma=0.0680$ – a circuit of seven real Duffing oscillators.

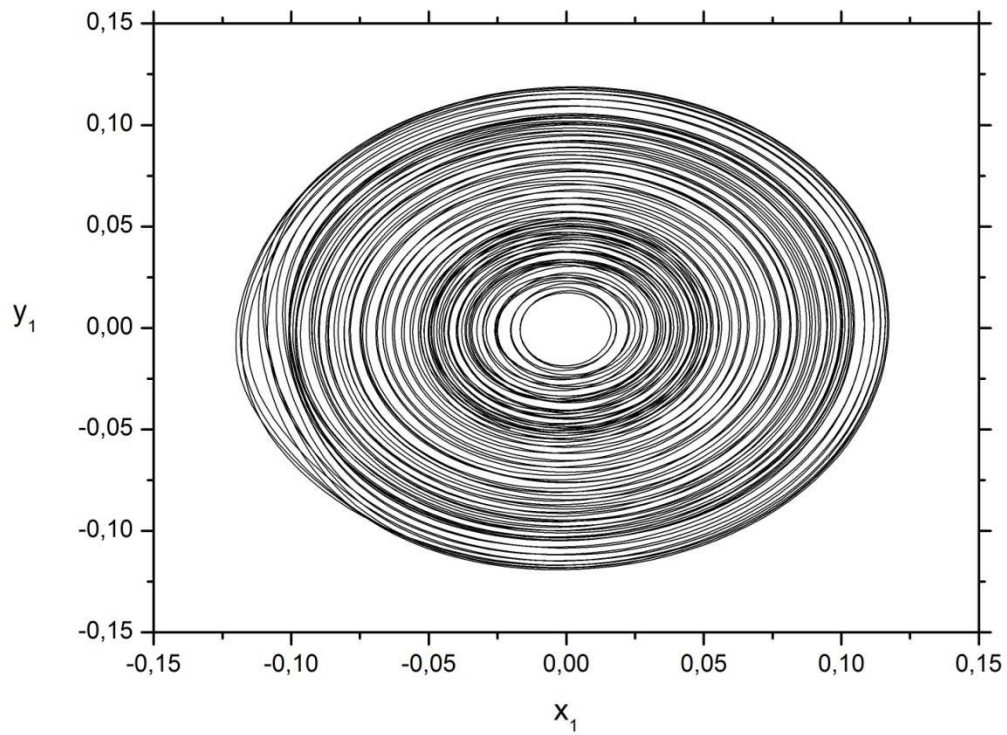


Fig. 4.3.10. Phase portrait for the coupling parameter $\sigma=0.0700$ – a circuit of seven real Duffing oscillators.

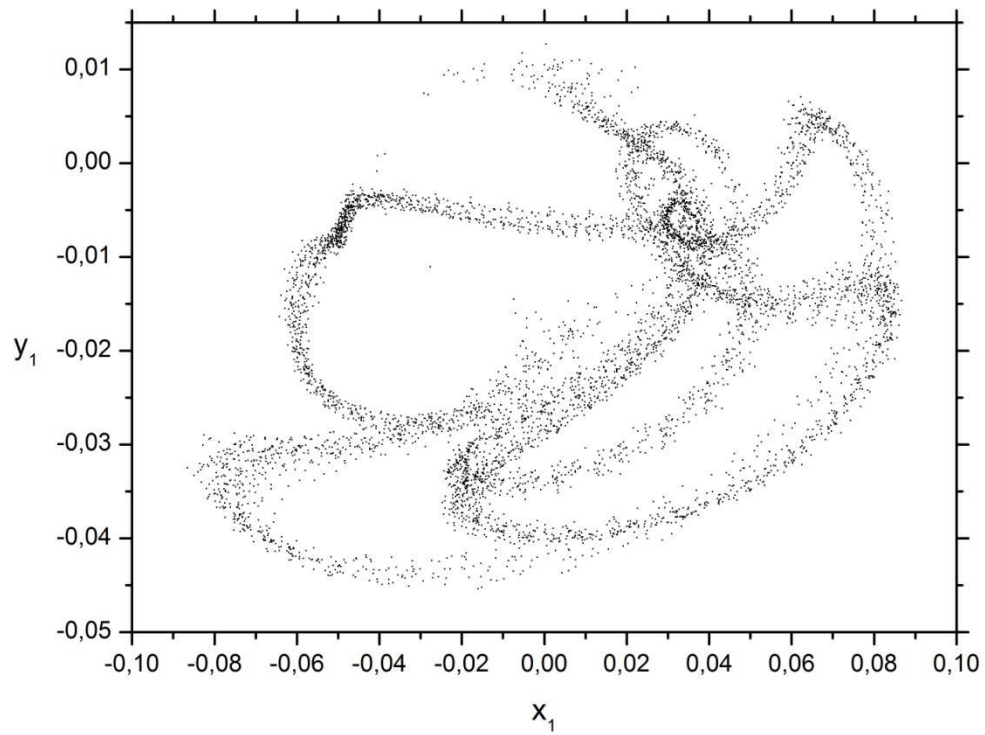


Fig. 4.3.11. Poincaré map for the coupling parameter $\sigma=0.0700$ – a circuit of seven real Duffing oscillators.

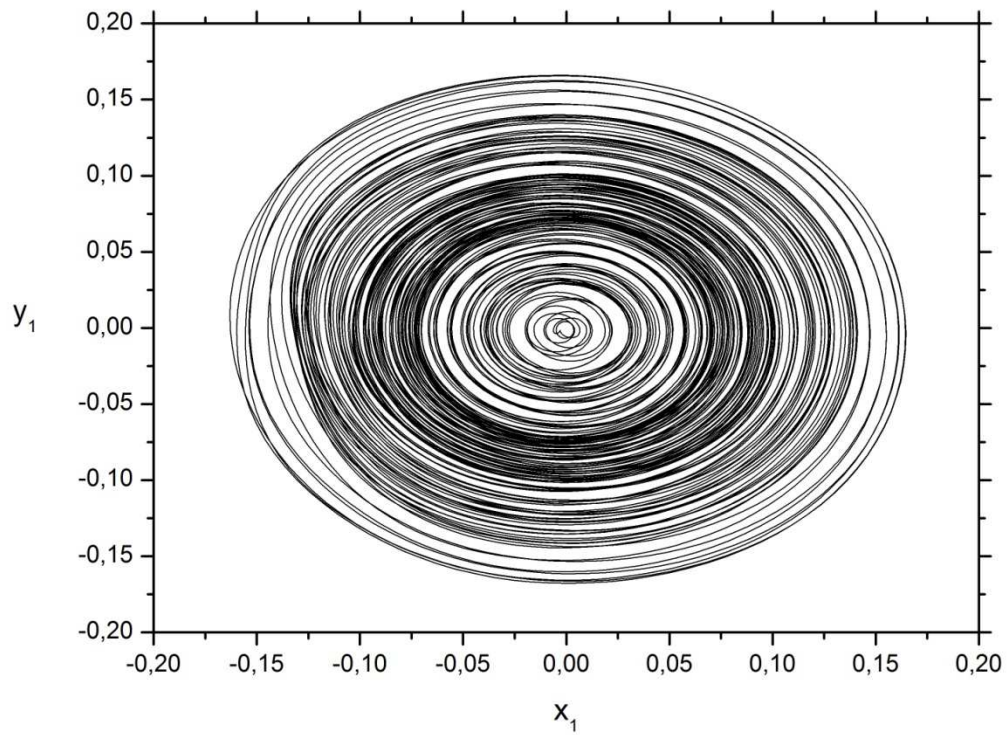


Fig. 4.3.12. Phase portrait for the coupling parameter $\sigma=0.0730$ – a circuit of seven real Duffing oscillators.

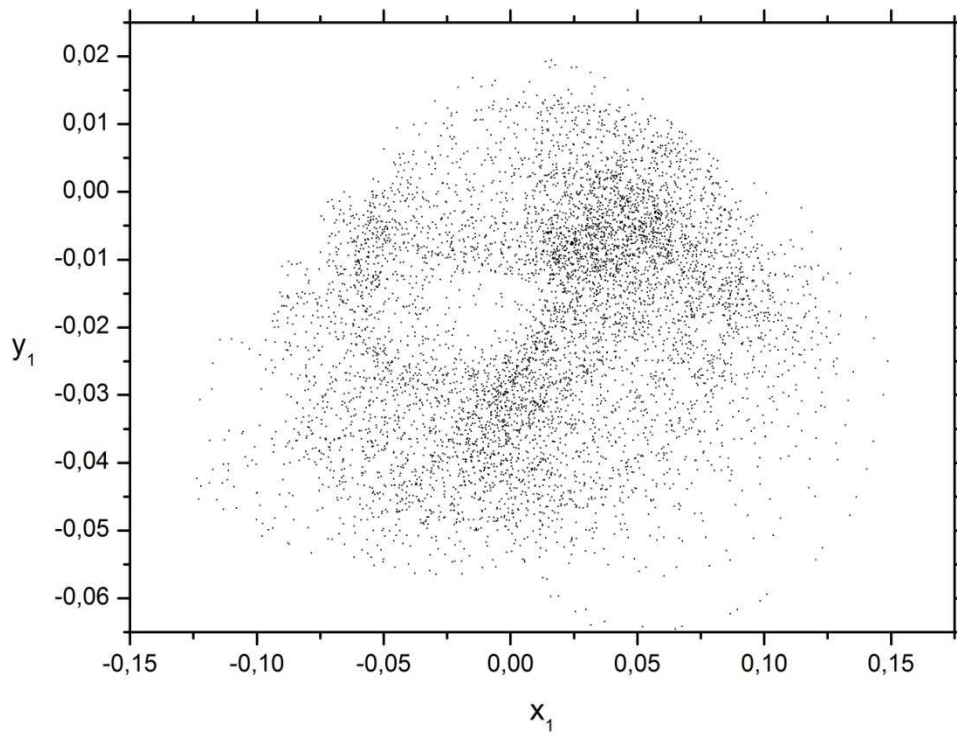


Fig. 4.3.13. Poincaré map for the coupling parameter $\sigma=0.0730$ – a circuit of seven real Duffing oscillators.

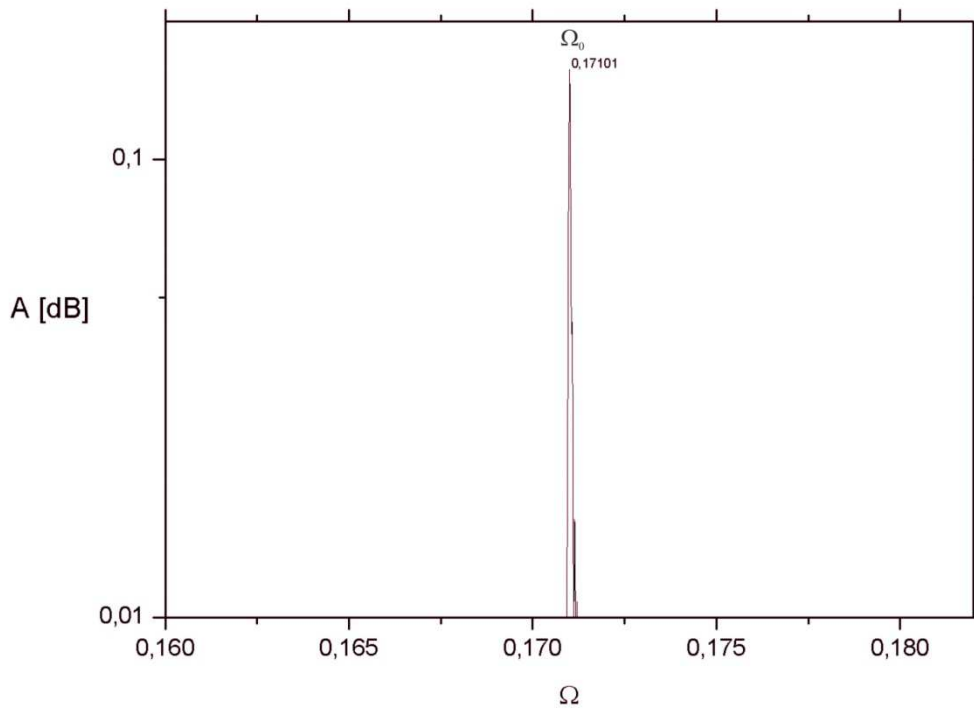


Fig. 4.3.14. FFT spectrum analysis for the coupling parameter $\sigma=0.0490$ – a circuit of seven real Duffing oscillators.

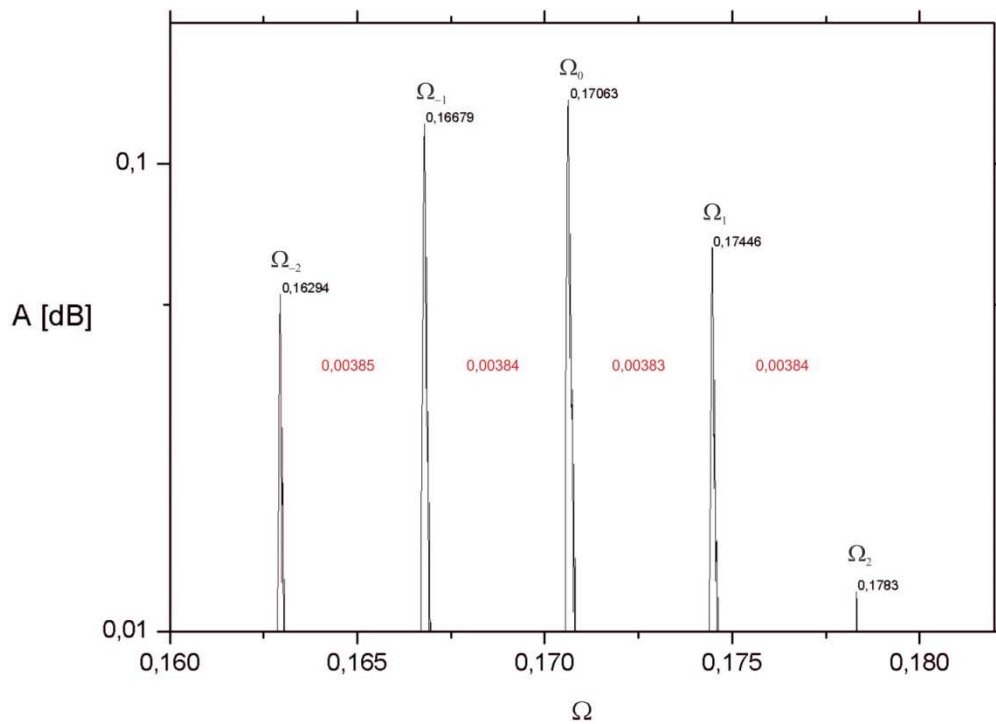


Fig. 4.3.15. FFT spectrum analysis for the coupling parameter $\sigma=0.0660$ – a circuit of seven real Duffing oscillators.

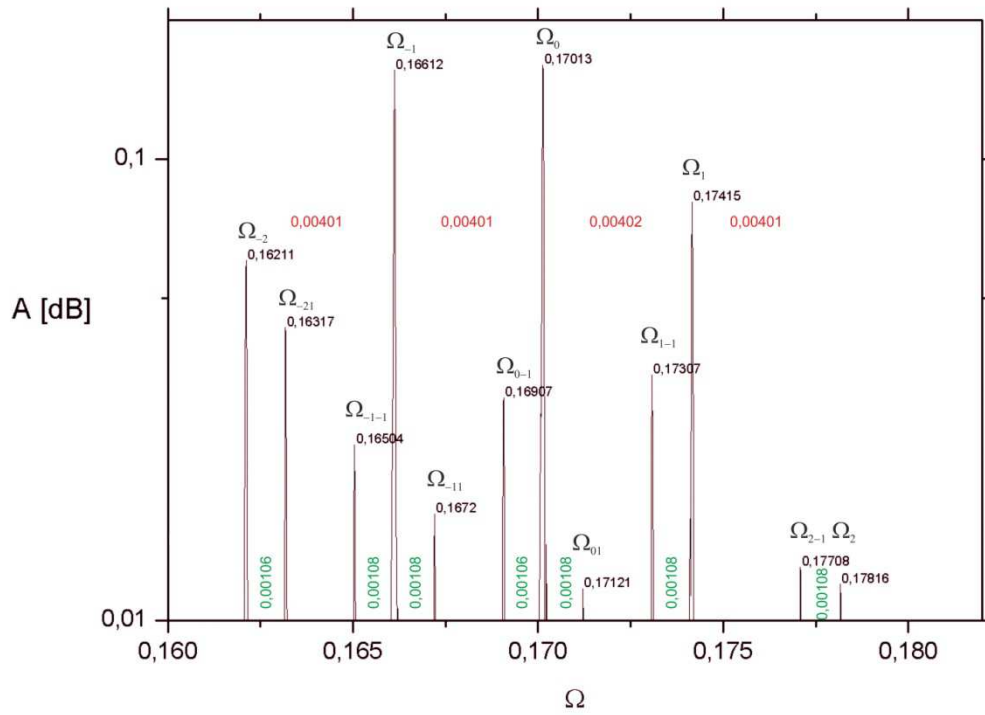


Fig. 4.3.16. FFT spectrum analysis for the coupling parameter $\sigma=0.0680$ – a circuit of seven real Duffing oscillators.

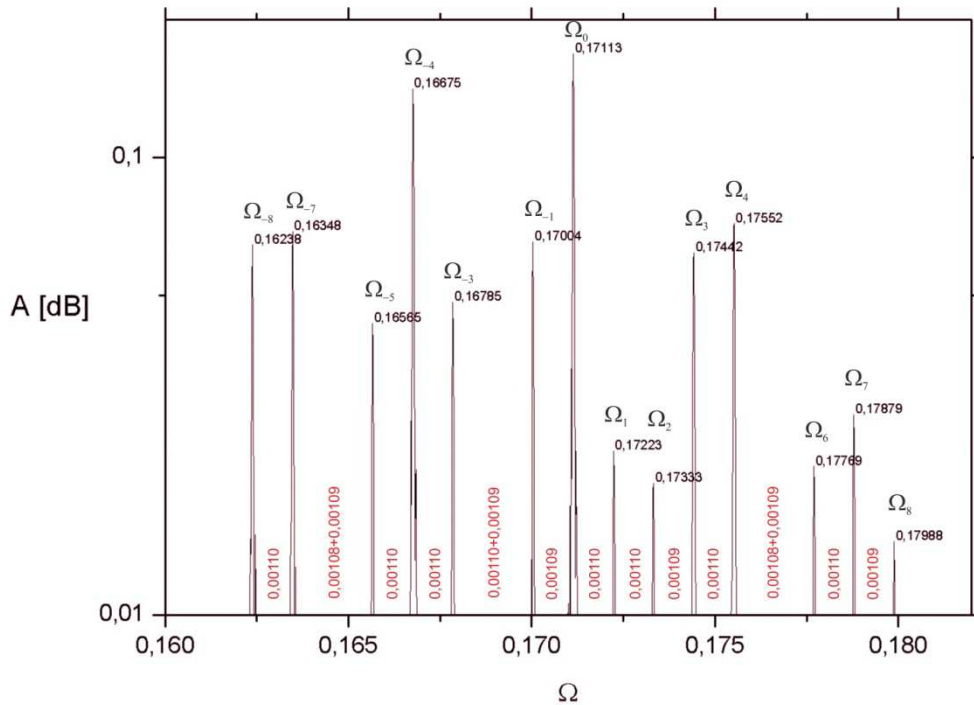


Fig. 4.3.17. FFT spectrum analysis for the coupling parameter $\sigma=0.0700$ – a circuit of seven real Duffing oscillators.

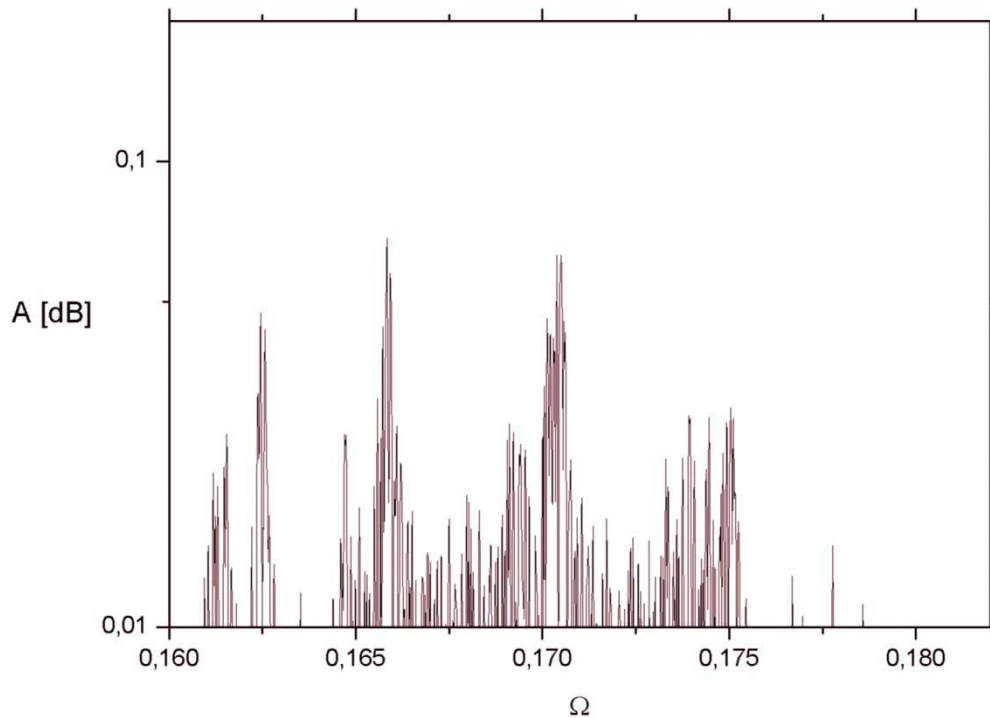


Fig. 4.3.18. FFT spectrum analysis for the coupling parameter $\sigma=0.0730$ – a circuit of seven real Duffing oscillators.

4.4. FFT analysis of the electrical circuit

As in the case of the numerical FFT spectral analysis, all frequencies on the FFT spectrum graphs (Fig. 4.3.14-4.3.18) were divided by the value of ω_{04} . This made the use of the concept of dimensionless frequency Ω of the signal possible.

For the coupling parameter $\sigma = 0.0490$, the first Hopf-type bifurcation occurs and a single main frequency Ω_0 appears on the spectrum (see Fig. 4.3.14) representing the limit cycle (Fig. 4.3.4, 4.3.5) existing in a relatively narrow range of the coupling parameter. This solution is represented by a single, main frequency Ω_0 on the FFT spectral analysis graph. An increase in the coupling parameter $\sigma > 0.0490$ leads to the second Hopf-type bifurcation and a 2D torus (Fig. 4.3.6, 4.3.7) appears, which is represented by two disproportionate frequencies Ω_0 and Ω_1 . In Fig. 4.3.15, newly formed peaks in addition to the main frequencies can be seen. As in the case of the spectral analysis for the numerical circuit, the distance between the newly formed peaks and the main peak has a constant value or is a multiplication of this constant. As a result, the first frequency is characterized by the peak Ω_0 and the second

one, disproportionate to the first frequency, is associated with a fixed value (marked in red on the graphs) shift of the peaks to the peak Ω_0 , equal to:

$$\Omega_n = \Omega_0 + n\beta_1 \quad (4.4.1)$$

where:

β_1 (≈ 0.00002) – constant offset between the peaks,

n – number of the analyzed frequency.

For example, the frequency Ω_{-1} in Fig. 4.3.15 is:

$$\Omega_{-1} = \Omega_0 - \beta_1 = 0.17063 - 0.00384 = 0.16679$$

The 2D torus dominates in a wide range of the coupling parameter - $\sigma \in (0.0490 \div 0.0680)$. For the coupling parameter $\sigma = 0.0680$, the third Hopf-type bifurcation and a transition from the 2D torus to a 3D torus (Fig. 4.3.8, 4.3.9) takes place. The FFT spectral analysis graph (Fig. 4.3.16) shows three frequencies disproportionate to each other. The first frequency is represented by the peak Ω_0 . The second frequency – Ω_n – is associated with a fixed distance (marked in red) relative to the peak Ω_0 , while the third one – Ω_{nm} – is associated with a fixed distance (marked in green) relative to the peaks representing the first and second disproportionate frequency. Similarly as for the numerical circuit of oscillators, the third disproportionate frequency can be described by the equation:

$$\Omega_{nm} = \Omega_n + m\beta_2 \quad (4.4.2)$$

where:

β_2 (≈ 0.00002) - constant offset between the peaks,

n, m - number of the analyzed frequency.

Using formula (4.4.2), the frequency Ω_{-1-1} visible in Fig. 4.3.16 can be calculated as follows:

$$\Omega_{-1-1} = \Omega_{-1} - \beta_2 = \Omega_0 - \beta_1 - \beta_2 = 0.17013 - 0.00401 - 0.00108 = 0.16504$$

The 3D torus is stable up to $\sigma = 0.0700$, where a 2D torus appears again but with a multiplied period (Fig. 4.3.10, 4.3.11), which can be an effect of the frequency (modes) synchronization or a 2D torus period-doubling bifurcation after the reverse Hopf bifurcation. In Fig. 4.3.17, as well as in the numerical analysis, the first frequency is characterized by the peak Ω_0 and the second frequency, disproportionate to the first one, is associated with a fixed value (marked in red on the graphs) shift of the peaks to the peak Ω_0 . To calculate the frequency, we use formula (4.4.1), for example:

$$\Omega_2 = \Omega_0 + 2 * \beta_1 = 0.17113 + 2 * 0.00110 = 0.17333$$

For the coupling parameter $\sigma = 0.0730$, a transition to a chaotic solution (Fig. 4.3.12, 4.3.13) characterized by a continuous FFT spectrum graph (see Fig. 4.3.18) occurs.

NUMERICAL ANALYSIS OF A DUFFING OSCILLATOR WITH A TIME DELAY LOOP

In this Chapter, a numerical analysis of a single Duffing oscillator with a time delay loop is demonstrated. An influence of changes in the value of time delay on the system dynamics is analyzed. The numerical simulations carried out are compared with the numerical results obtained for the circuit of unidirectionally coupled Duffing oscillators, which was presented in Chapter 3.

A single Duffing oscillator with a time delay loop is described by Eq. (1.3). Substituting $x = u, y = \dot{u}$, a single second-order equation was converted into two first-order equations:

$$\begin{aligned}\dot{x}(t) &= y(t) \\ \dot{y}(t) &= -cy(t) - ax(t) - bx(t)^3 + p[x(t - \tau) - x(t)]\end{aligned}\tag{5.1}$$

where the parameters are:

$$c = 0.03162$$

$$a = 1$$

$$b = 10$$

$$p = 30$$

Comparing Eq. (5.1) with the generalized equation defining a ring of unidirectionally coupled Duffing oscillators (Eq. (2.1)), we can see that the mathematical structure of these system is very close to each other. For Eq. (5.1), the time delay is obtained by changing the parameter τ , while in Eq. (2.1), the resulting time delay is related to the phase shift between neighboring oscillators. Thus, the mechanism of oscillation excitation in both cases is caused by a unidirectional feedback which is realized by a structure of connected oscillators or by a delay feedback loop.

To compare the results, in both considered cases, i.e., for a ring of coupled oscillators and a single Duffing oscillators with a feedback loop, the parameters a , b , c have the same values.

5.1. Numerical results

The numerical investigations of a single Duffing oscillator with a time delay loop were carried out with the MATLAB R2009b software. The bifurcation parameter is the time delay τ . The obtained results were illustrated by:

- bifurcation diagrams (Fig. 5.1),
- phase portraits (Figs. 5.2, 5.4, 5.6, 5.8),
- Poincaré maps (Figs. 5.3, 5.5, 5.7, 5.9),
- FFT spectrum analysis (Figs. 5.10-5.13).

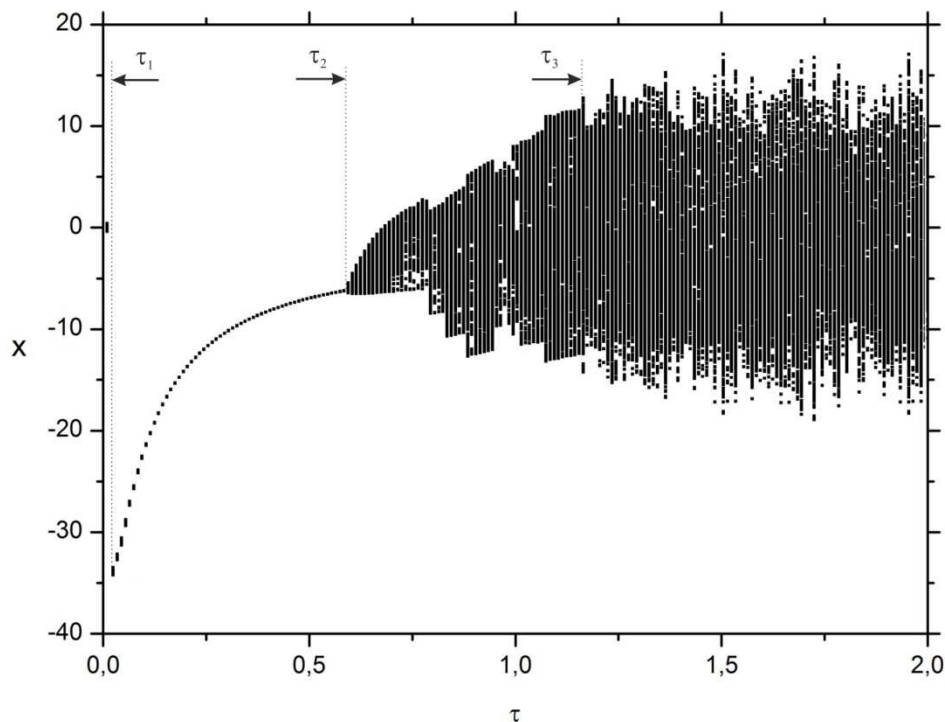


Fig. 5.1. Bifurcation diagram of the displacement x versus the delay parameter τ for a single Duffing oscillator with a time delay loop.

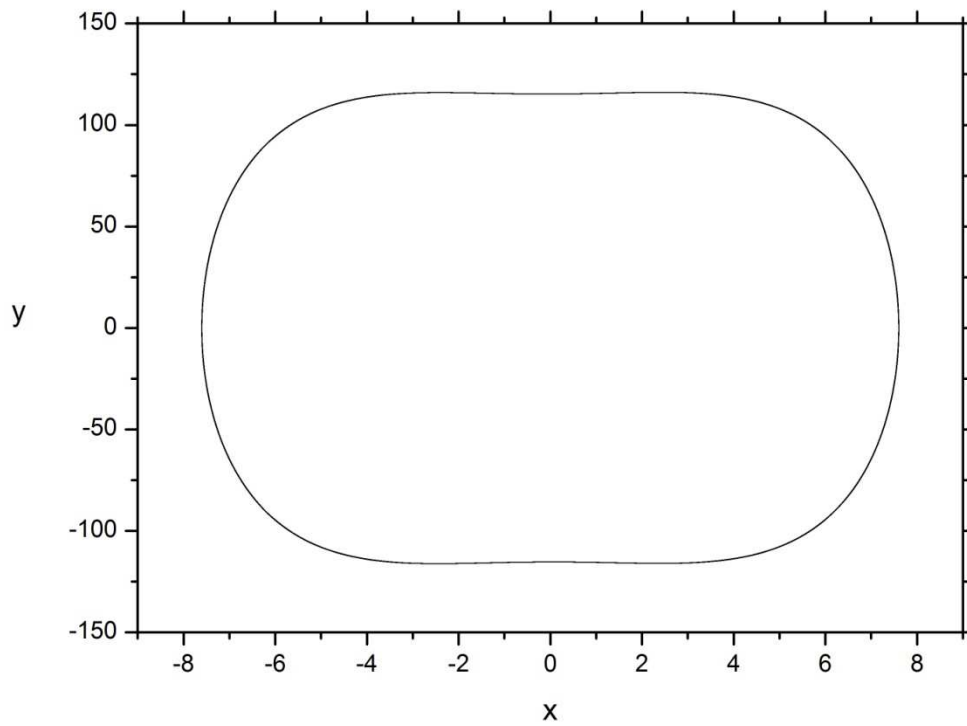


Fig. 5.2. Phase portrait for the delay parameter $\tau=0.50$ – a single Duffing oscillator with a time delay loop.

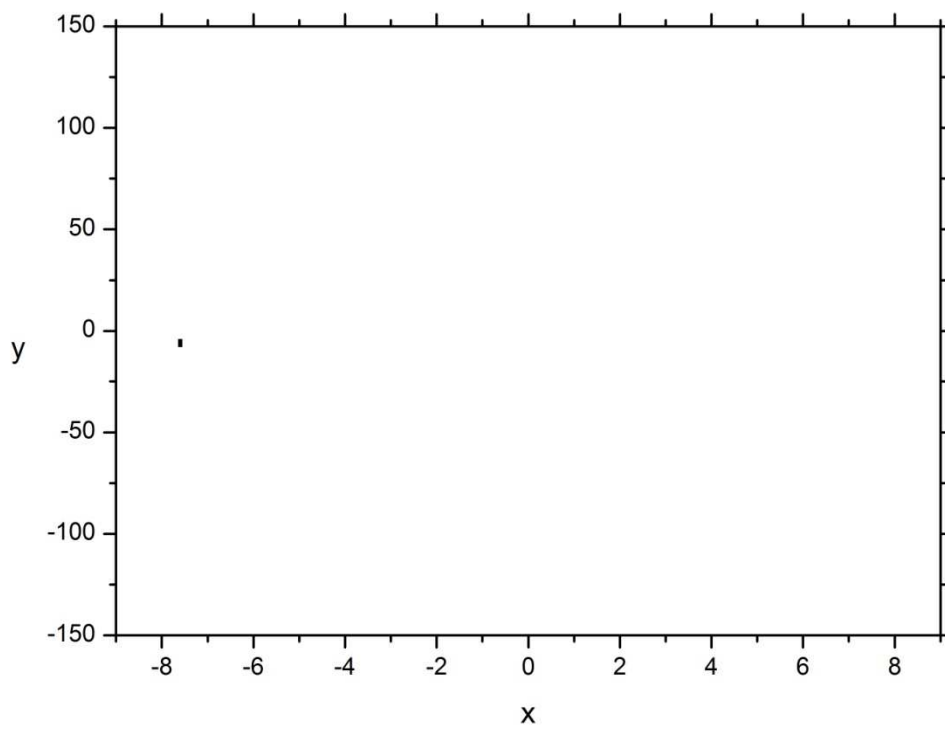


Fig. 5.3. Poincaré map for the delay parameter $\tau=0.50$ – a single Duffing oscillator with time delay loop.

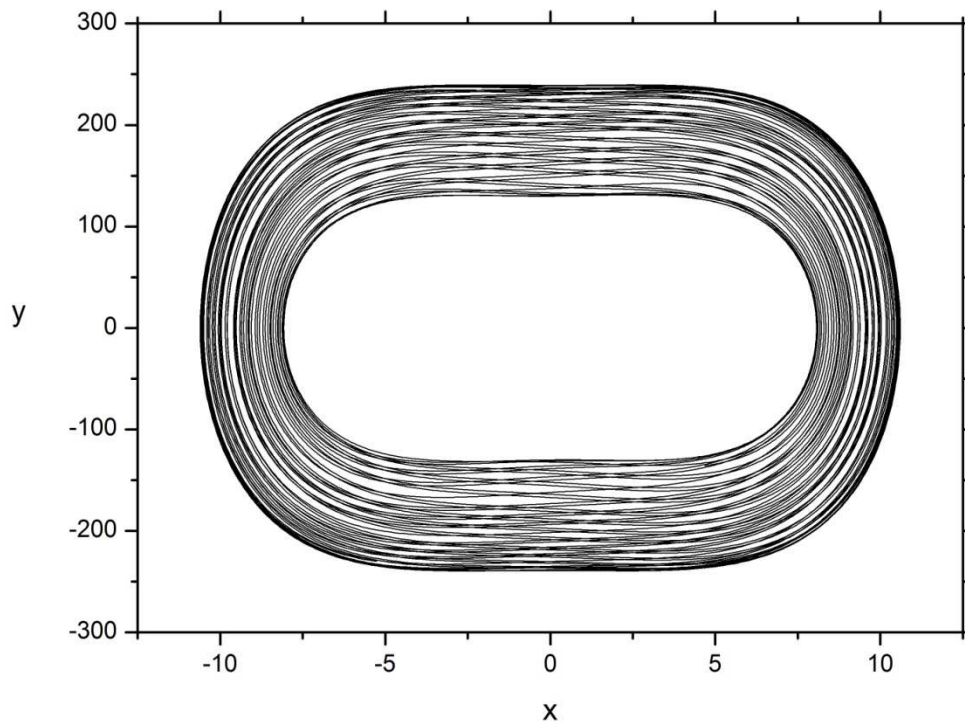


Fig. 5.4. Phase portrait for the delay parameter $\tau=0.72$ – a single Duffing oscillator with a time delay loop.

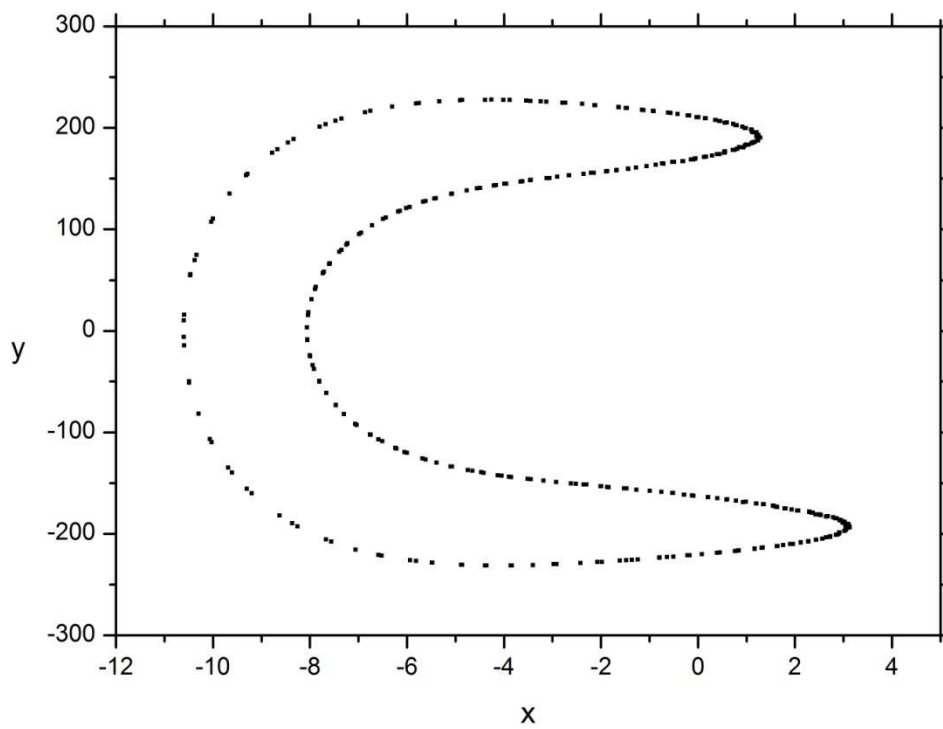


Fig. 5.5. Poincaré map for the delay parameter $\tau=0.72$ – a single Duffing oscillator with a time delay loop.

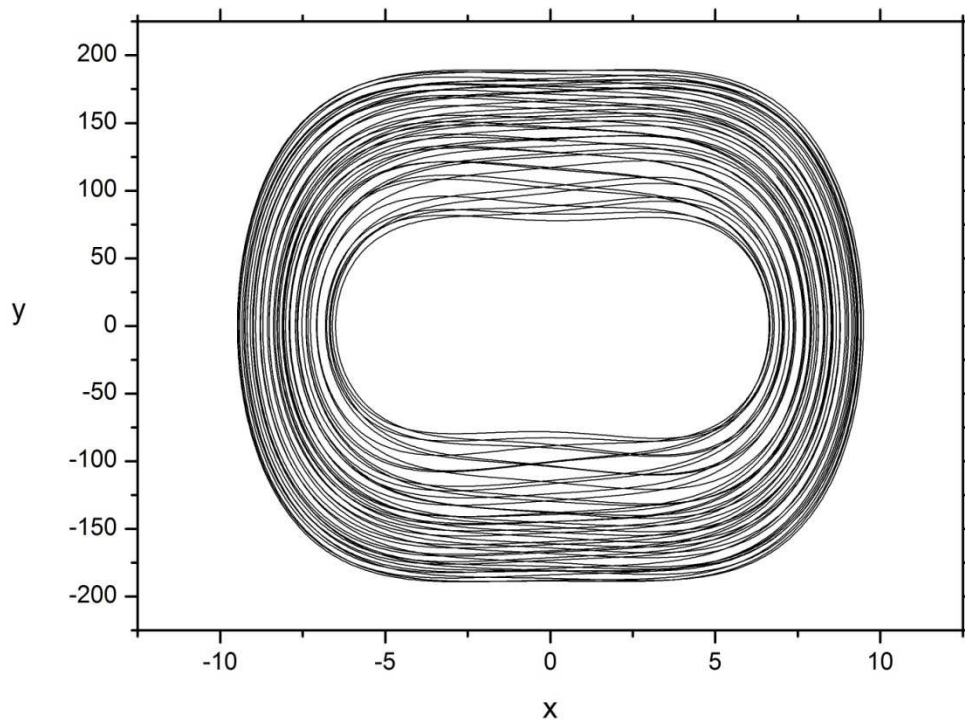


Fig. 5.6. Phase portrait for the delay parameter $\tau=1.05$ – a single Duffing oscillator with a time delay loop.

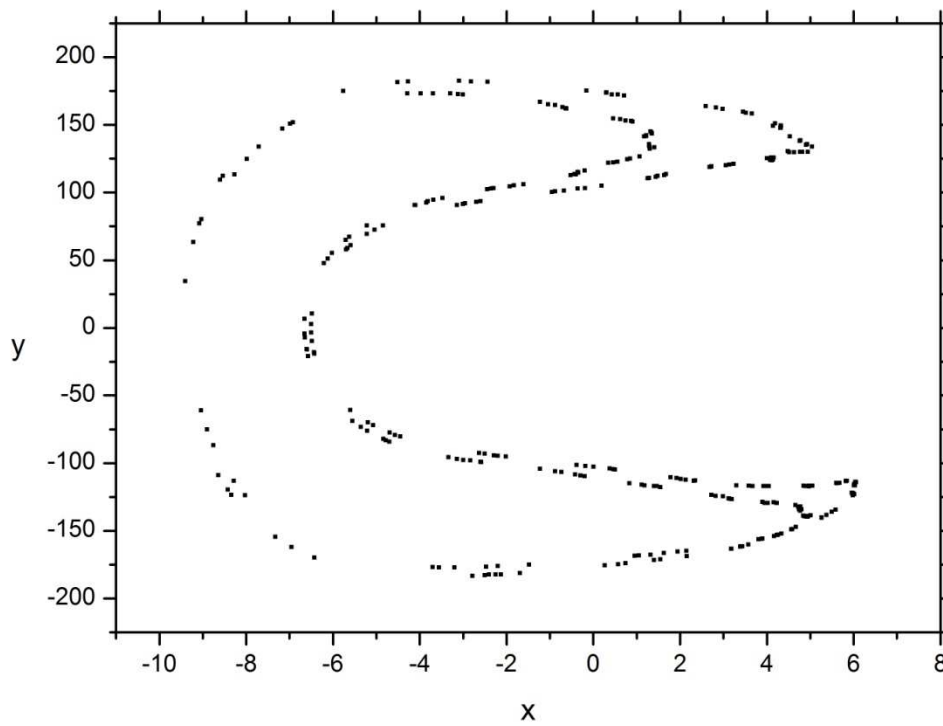


Fig. 5.7. Poincaré map for the delay parameter $\tau=1.05$ – a single Duffing oscillator with a time delay loop.

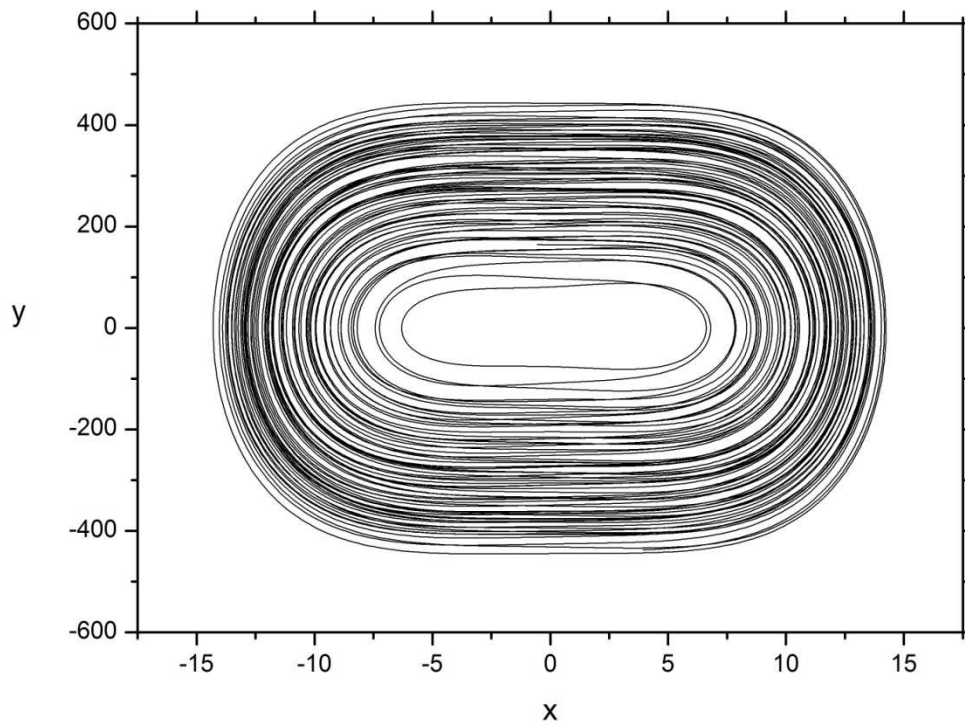


Fig. 5.8. Phase portrait for the delay parameter $\tau=1.40$ – a single Duffing oscillator with a time delay loop.

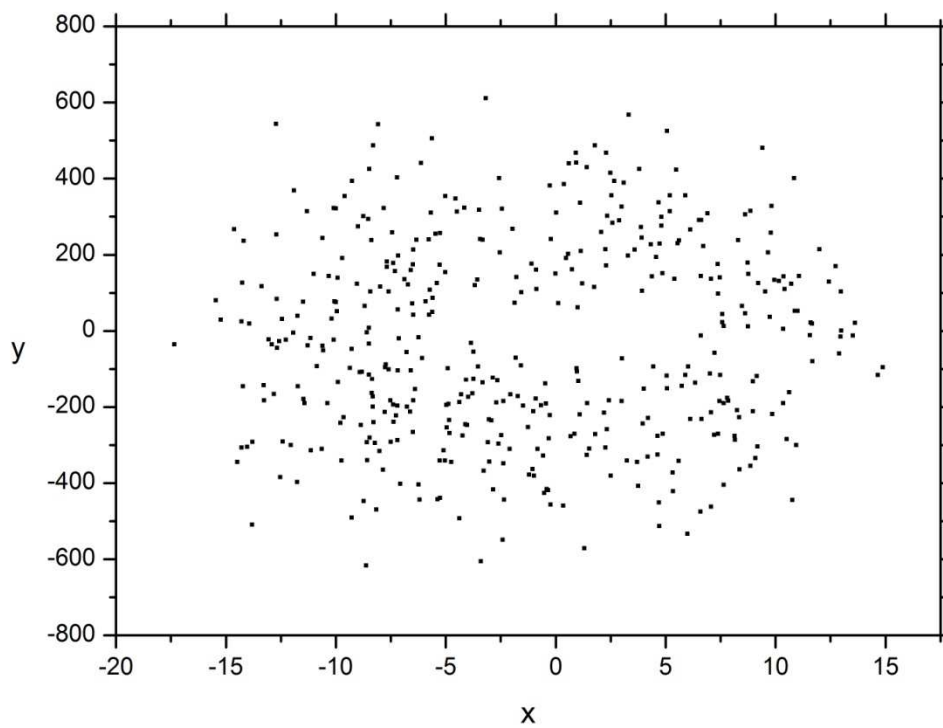


Fig. 5.9. Poincaré map for the delay parameter $\tau=1.40$ – a single Duffing oscillator with a time delay loop.

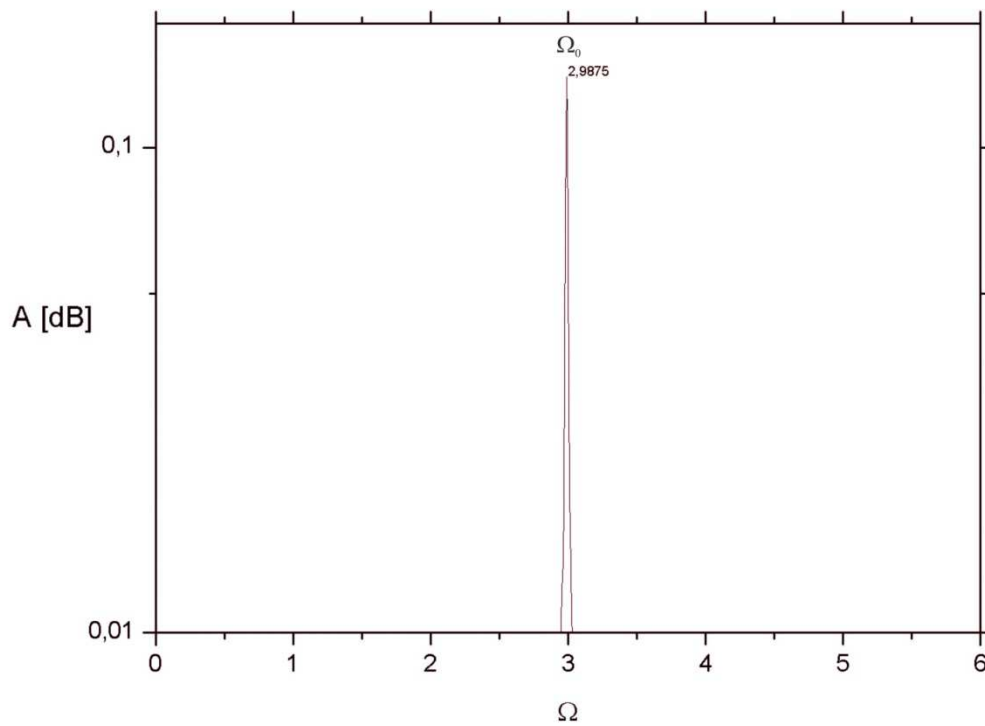


Fig. 5.10. FFT spectrum analysis for the delay parameter $\tau=0.50$ – a single Duffing oscillator with a time delay loop.

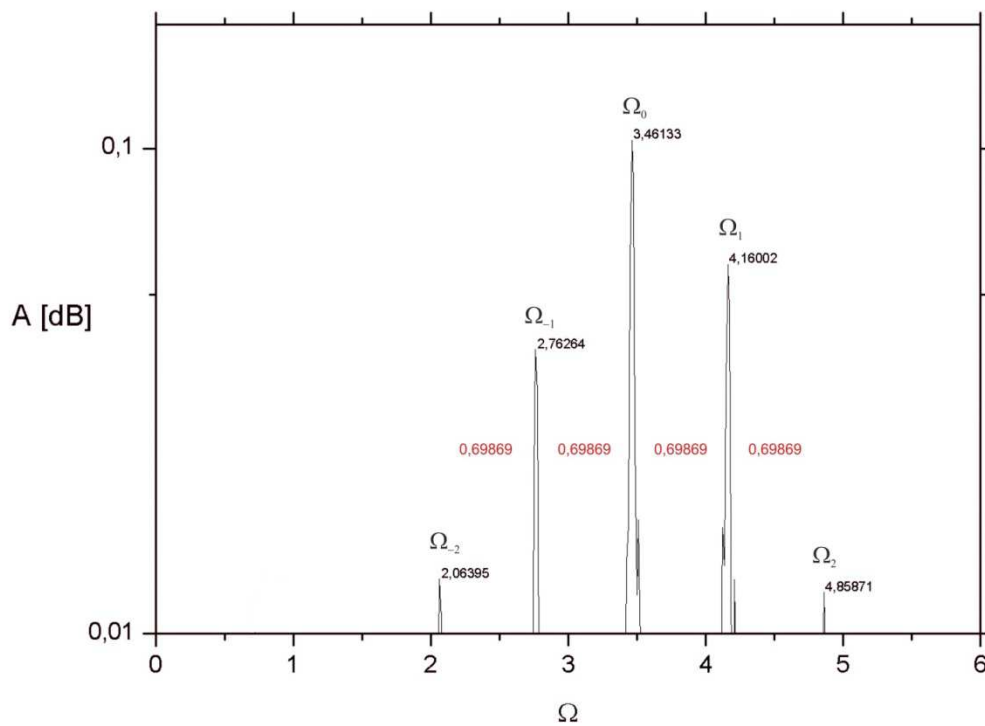


Fig. 5.11. FFT spectrum analysis for the delay parameter $\tau=0.72$ – a single Duffing oscillator with a time delay loop.

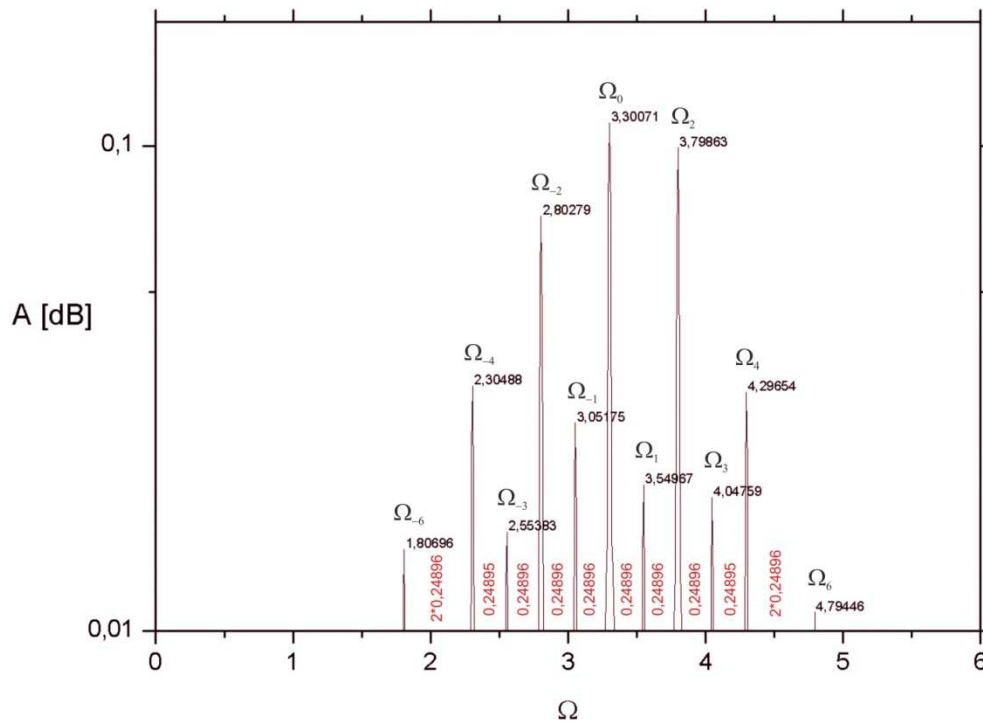


Fig. 5.12. FFT spectrum analysis for the delay parameter $\tau=1.05$ – a single Duffing oscillator with a time delay loop.

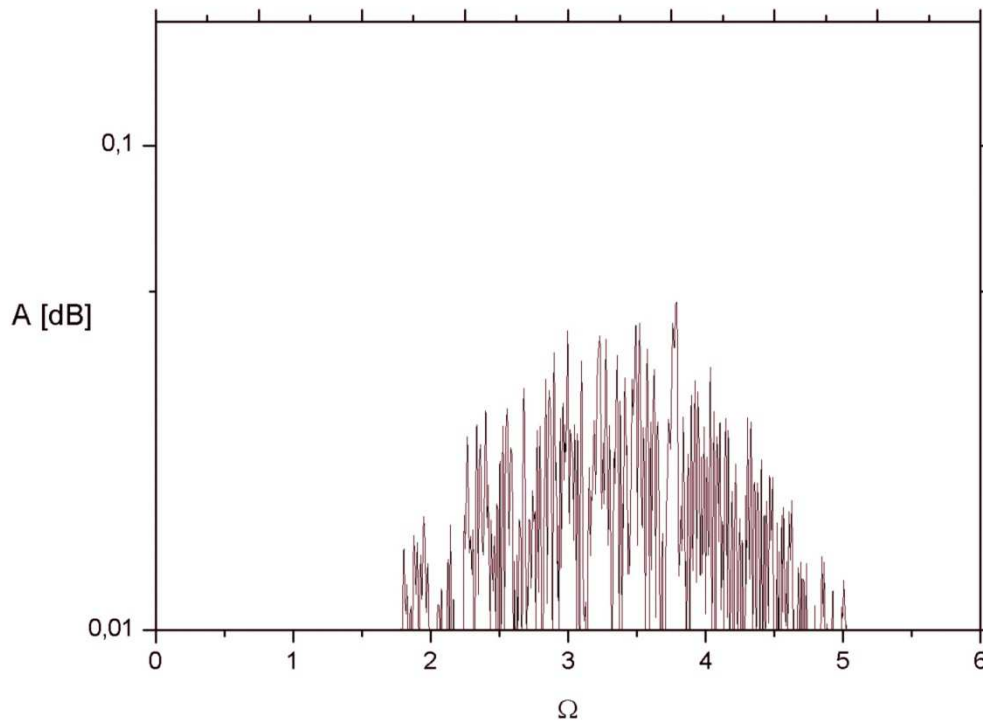


Fig. 5.13. FFT spectrum analysis for the delay parameter $\tau=1.40$ – a single Duffing oscillator with a time delay loop.

5.2. FFT analysis of the studied system

For the delay parameter $\tau > 0.01$, the first Hopf bifurcation occurs. The investigated system passes from a stationary to periodic solution and the first frequency of oscillation appears. In Fig. 5.10, this frequency, as for the ring of seven coupled Duffing oscillators, is represented by the single peak Ω_0 . The limit cycle exists in quite a wide range of the delay parameter $\tau \in \langle 0.01; 0.67 \rangle$. For $\tau = 0.68$, the second Hopf bifurcation takes place. The limit cycle transforms into a quasi-periodic solution (Fig. 5.4, 5.5). In Fig. 5.11, this 2D torus is presented by two main disproportionate frequencies Ω_0, Ω_1 and their sub-harmonics. Similarly as in Chapters 3 and 4, the newly formed frequencies can be calculated using the formula:

$$\Omega_n = \Omega_0 + n\beta_1 \quad (5.2)$$

where:

$\beta_1 (\approx 0.00002)$ – constant offset between the peaks,

n – number of the analyzed frequency.

For example, the frequency Ω_2 in Fig. 5.11 is:

$$\Omega_2 = \Omega_0 + 2\beta_1 = 3.46133 + 2 * 0.69869 = 4.85871$$

For $\tau = 1.02$, a period-doubling bifurcation of the 2D torus (Fig. 5.6, 5.7) takes place. Figure 5.12 shows that between the peaks $\Omega_{-6}, \Omega_{-4}, \Omega_{-2}, \Omega_0, \Omega_2, \Omega_4, \Omega_6$, representing the 2D torus, there are new peaks which divide the distance between the previous ones exactly in half. They appear as an effect of the torus period-doubling. For example, according to formula (5.2), the frequency Ω_{-3} in Fig. 5.12 is:

$$\Omega_{-3} = \Omega_0 - 3\beta_1 = 3.30071 - 3 * 0.24896 = 2.55383$$

A further increase in the delay parameter leads to a chaotic solution (Fig. 5.8, 5.19). Dominant frequencies cannot be specified on the graph of the FFT spectral analysis (Fig. 5.13). All peaks are located very close to each other and in a chaotic manner. As a consequence, an analysis and interpretation of the results is impracticable.

CHAPTER 6

ANALYSIS OF THE RESULTS AND CONCLUSIONS

In Chapters 2-4 of this dissertation, results of the analytical, numerical and experimental investigations of a circuit of seven, nominally identical, unidirectionally coupled Duffing oscillators were presented. On the other hand, a numerical bifurcation analysis of the analogous single Duffing oscillator with a time delay loop was demonstrated in Chapter 5. Comments, conclusions and hypotheses, which are described below, have been formulated on the basis of these data.

The stability analysis of the equilibrium position (critical point) of the linearized system of unidirectionally coupled oscillators (Chapter 2) showed that small differences in parameters between them had a minimal impact on the instability threshold of the equilibrium position. The critical point loses its stability due to the Hopf bifurcation caused by an increase in the coupling parameter. This instability results in an appearance of a *harmonic rotating wave* (HRW), which is confirmed in the next chapters.

Analyzing the results of the experiment (Chapter 4) and comparing them with the results of the numerical simulations (Chapter 3) of a circuit of seven real (non-identical) Duffing oscillators, we can see the same scenario of a transition to chaotic behavior. The results achieved in the experiment confirm the results of the numerical studies. However, some differences in the values of the coupling parameter, for which corresponding bifurcations occur, can be observed. For the corresponding bifurcation, the value of the coupling parameter in the experimental system (Fig. 4.3.3÷4.3.13) is higher in comparison with the numerical model (Fig. 3.1.8, 3.1.11, 3.1.12, 3.1.15, 3.1.16, 3.1.19÷3.1.22, 3.1.25, 3.1.26). Slight differences also exist in the values of dimensionless frequencies in the FFT spectrum analysis graphs (Fig. 4.3.14÷4.3.18 and 3.1.28, 3.1.30, 3.1.32, 3.1.33, 3.1.35). This may be an effect of a transition of one (or several) of integrating amplifiers into saturation. As a result, the amplifier stops to operate in the linear range. Consequently, in order to compensate for the possible saturation effect (for this working amplifier or amplifiers), it was necessary to increase a value of the coupling parameter in order to achieve the same system dynamics as in the case of the numerical investigations. Besides, slight additional resistance formed on the paths connecting various elements in the electric circuit. There was also a slight

change in the resistance and capacitance of elements, which formed during soldering components on a printed circuit board.

The demonstrated (in Chapters 3 and 4) results of the experimental and numerical investigations indicate that the stable three-frequency quasi-periodicity is a typical phenomenon for rings of unidirectionally coupled autonomous Duffing oscillators and it can occur in a wide range of system parameters. Definitely, this trend seems to be in contradiction to the classical NRT theorem. In agreement with the hypotheses proposed earlier (see Chapter 1), such an unexpected effect of the 3D torus stability can be explained by some properties of the spatiotemporal or rotational symmetry of identical oscillators coupled unidirectionally in the ring configuration [72,91,92]. However, the analysis proves that this solution remains, in spite of some symmetry breaking caused by the parameter mismatch. On the other hand, its relatively considerable influence on the real system dynamics (Figs. 3.1.3, 3.1.4, 3.1.6) in comparison with the case of identical oscillators (Figs. 3.1.1, 3.1.2, 3.1.5) is clearly visible. This influence manifests with some shift in the sequence of bifurcations in both the cases, reducing the range of the 3D torus existence for the disturbed version of the ring under consideration. Moreover, a qualitatively different evolution to chaotic motion can be observed. In the case of identical nodes, a direct transition from a 3D torus to chaos takes place (Fig. 3.1.5), whereas for slightly different parameters of nodes, a return conversion from the 3D to 2D quasi-periodic attractor analysis occurs before a transition to chaos via consecutive torus period-doubling bifurcations (Fig. 3.1.6).

The analytic investigations presented in Chapter 1 show that a RW appears simultaneously with the first Hopf bifurcation of the equilibrium position $U(0,0)$ in the system under consideration. Obviously, this is a PRW, strictly speaking a *harmonic rotating wave* (HRW). The threshold of the coupling strength σ_l required for its occurrence has been determined by an eigenvalue analysis of the linearized system (2.1.1) demonstrated in Chapter 2. This value amounts to $\sigma_l = 0.0332$ for identical nodes (see Figs. 2.1.1 and 3.1.1, 3.1.2) and $\sigma_l = 0.0365$ for real oscillators (see Figs. 2.2.1 and 3.1.3, 3.1.4). According to this analysis, the Hopf bifurcation activating the HRW takes place when an increase in the coupling coefficient σ causes that the largest real part of eigenvalues (2.1.1) becomes positive. In the case of identical nodes, they start to oscillate harmonically (Fig. 6.1) in accordance with the solution:

$$x_j = Ae^{i(\omega_0 t + j\phi)}, \quad (6.1)$$

where A is an amplitude and $\phi = 2\pi/N$ is a unit phase shift between two neighbor oscillators. Substituting this solution into (2.1), with an assumption of the equality of parameters and approximating the nonlinear component with the formula $bx_j^3 = bx_j|x_j^2| = bA^2x_j$, we obtain the characteristic equation

$$-\omega_0^2 + id\omega_0 + a + bA^2 + \sigma(1 - e^{-i\phi}) = 0. \quad (6.2)$$

Separation of Eq. (6.2) into real (6.3a) and imaginary (6.3b) parts:

$$-\omega_0^2 + a + bA^2 + \sigma(1 - \cos\phi) = 0, \quad (6.3a)$$

$$d\omega_0 + \sigma\sin\phi = 0, \quad (6.3b)$$

makes it possible to determine analytically the unknown frequency:

$$\omega_0 = \sqrt{a^2 + bA^2 + \sigma(1 - \cos\phi)}, \quad (6.4)$$

and amplitude of oscillations:

$$A = \sqrt{\frac{\sigma^2 \sin^2 \phi - d^2 a^2 - d^2 \sigma(1 - \cos\phi)}{d^2 b}} \quad (6.5)$$

Including the mismatch of parameters into the considered system, we have N harmonic solutions of individual nodes $x_j = A_j e^{i(\omega_0 t + \phi_j)}$ after the first Hopf bifurcation, differing in the amplitudes A_j and the phase shifts ϕ_j (see Fig. 6.4). The characteristic equation for each oscillator is now as follows:

$$-\omega_0^2 + id_j\omega_0 + a_j + b_j A_j^2 + \sigma k_j [1 - \left(\frac{A_{j-1}}{A_j}\right) e^{-i(\phi_j - \phi_{j-1})}] = 0. \quad (6.6)$$

Separating real and imaginary components of Eq. (6.6) for all ring items, we obtain $2N$ algebraic equations. They can be written in the general form:

$$C_{Re}(\omega_0, A_j, \phi_j) = 0, \quad (6.7a)$$

$$C_{Im}(\omega_0, A_j, \phi_j) = 0. \quad (6.7b)$$

Equation (6.7a-b) together with the formula

$$\sum_{j=1}^N (\phi_j - \phi_{j-1}) = 2\pi, \quad (6.7c)$$

allows us to calculate all unknown parameters ω_0 , A_j and ϕ_j .

Consequently, the RW phenomenon still persists for slightly non-identical parameters of oscillators also in the case of more complex dynamical responses of the system (quasi-periodic or chaotic). In Figs. 6.1-6.6, time traces of all seven oscillators representing regular responses of ideal (Figs. 6.1-6.3) and real (Figs. 6.4-6.6) circuits, i.e., periodic and two- or three-frequency quasi-periodic cases, respectively, can be seen. For identical nodes, we can observe an obvious equality of their amplitudes and phase shifts (see Figs. 6.1-6.3) resulting from the symmetry of the ring. The parameter mismatch causes some discrepancy of amplitudes and phases (Figs. 6.4-6.6) but the RW effect with the dominant frequency ω_0 is preserved, in spite of more complex periodicity of oscillations, especially clearly visible in cases of quasi-periodic motion (see Figs. 6.5, 6.6).

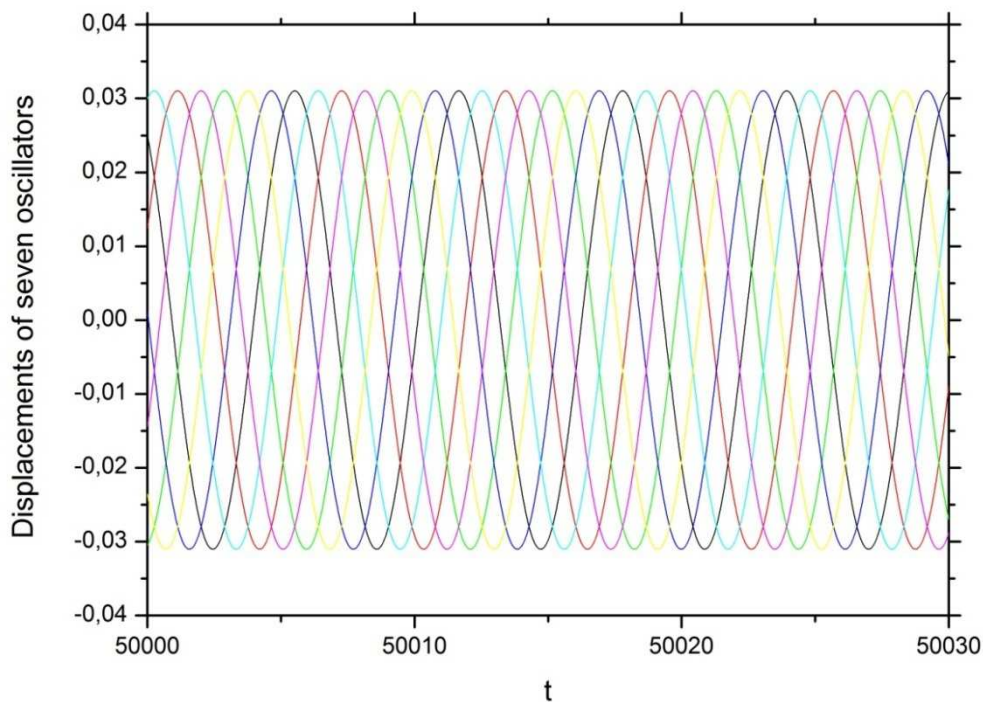


Fig. 6.1. Overlapped time traces of all seven oscillators, an ideal circuit, harmonic motion.

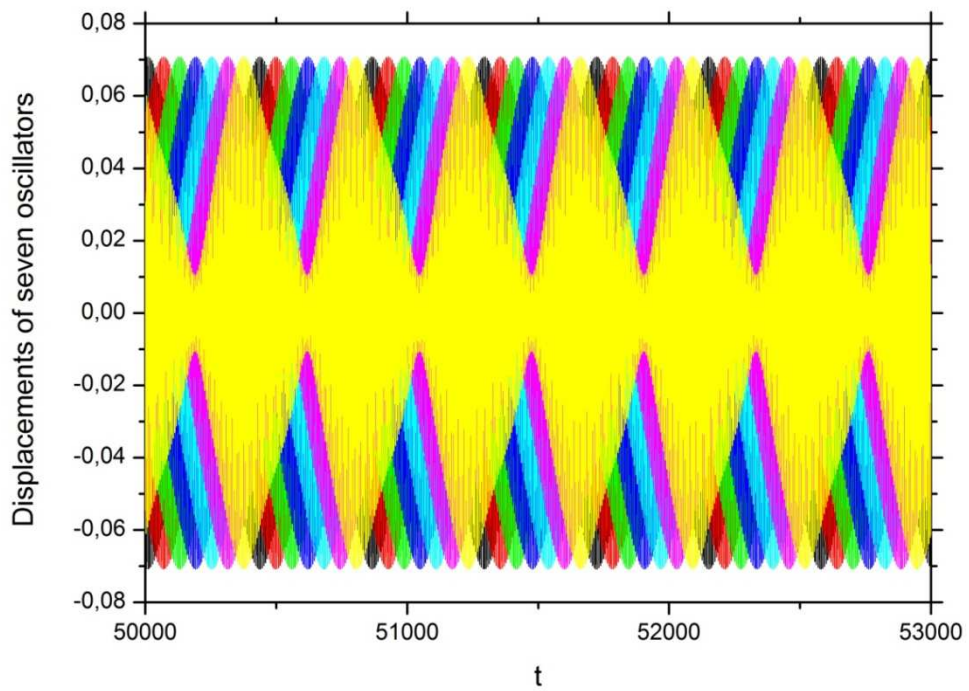


Fig. 6.2. Overlapped time traces of all seven oscillators, an ideal circuit, two-frequency quasi-periodicity.

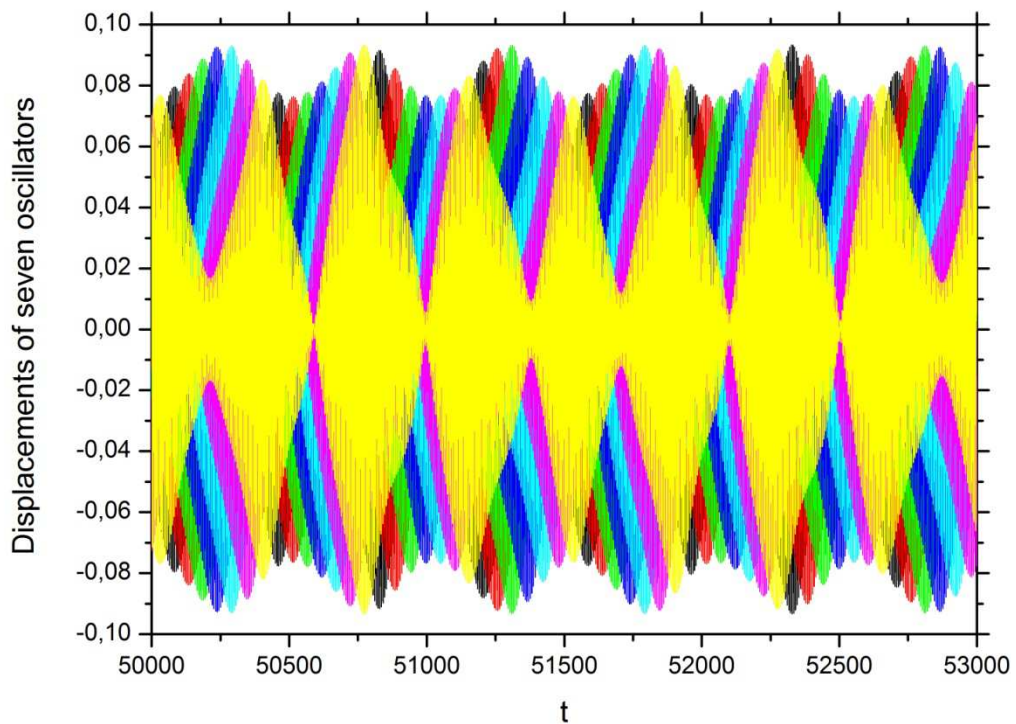


Fig. 6.3. Overlapped time traces of all seven oscillators, an ideal circuit, three-frequency quasi-periodicity.

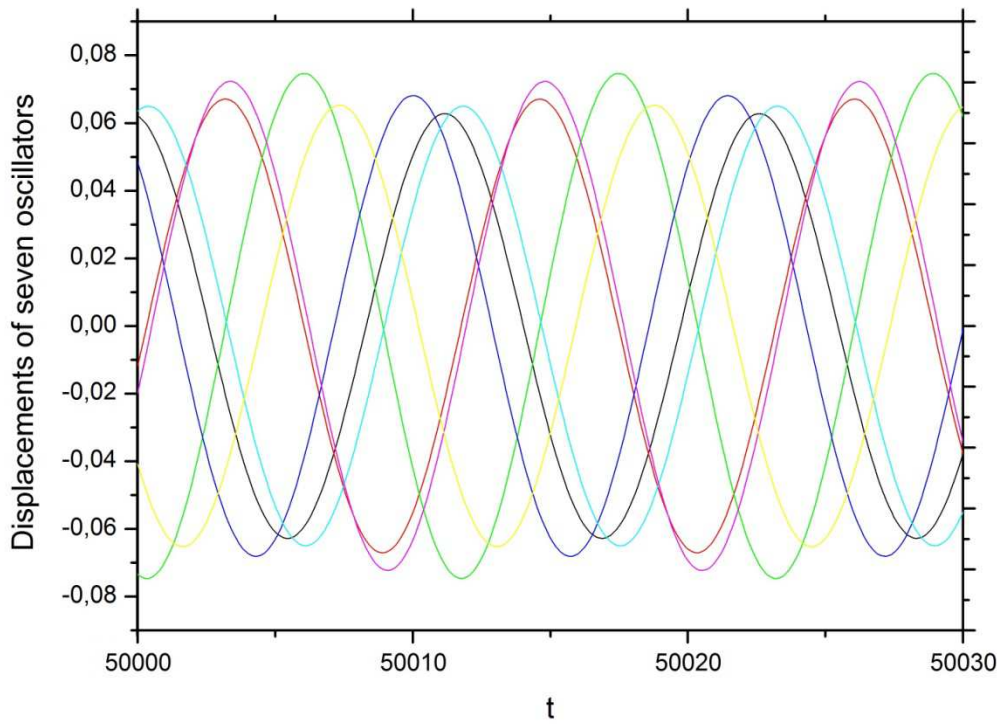


Fig. 6.4. Overlapped time traces of all seven oscillators, a real circuit, harmonic motion.

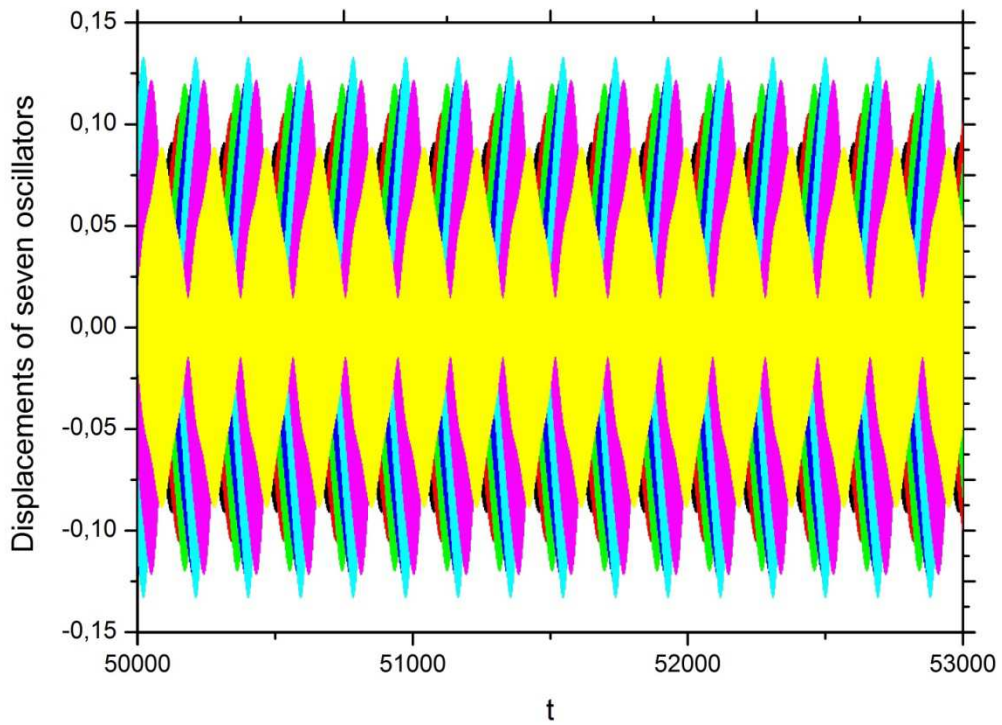


Fig. 6.5. Overlapped time traces of all seven oscillators, a real circuit, two-frequency quasi-periodicity.

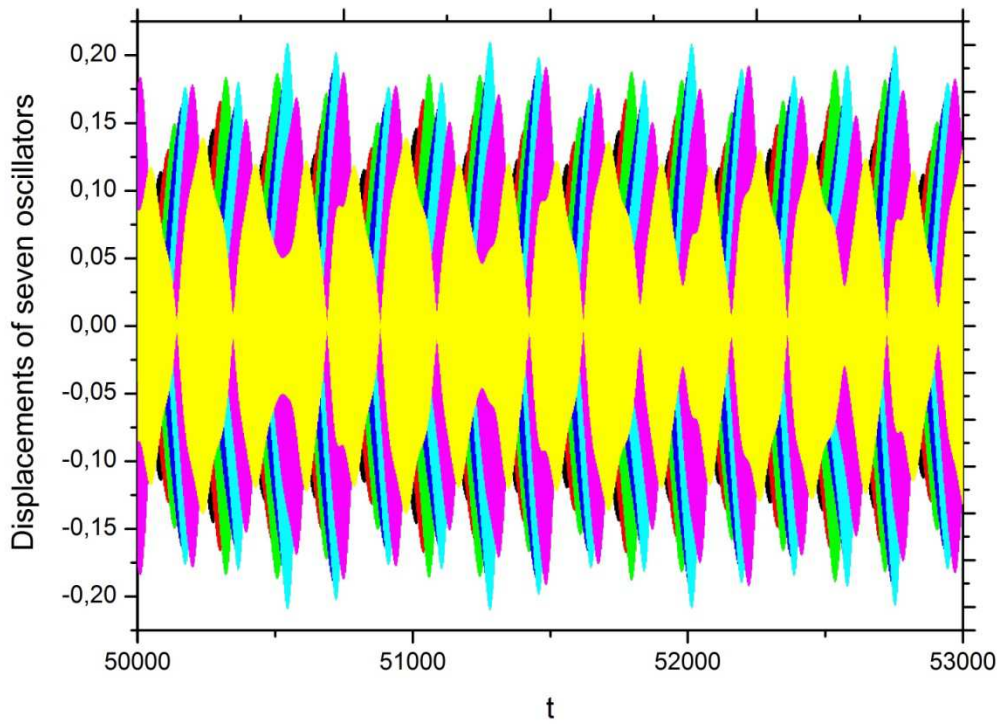


Fig. 6.6. Overlapped time traces of all seven oscillators, a real circuit, three-frequency quasi-periodicity.

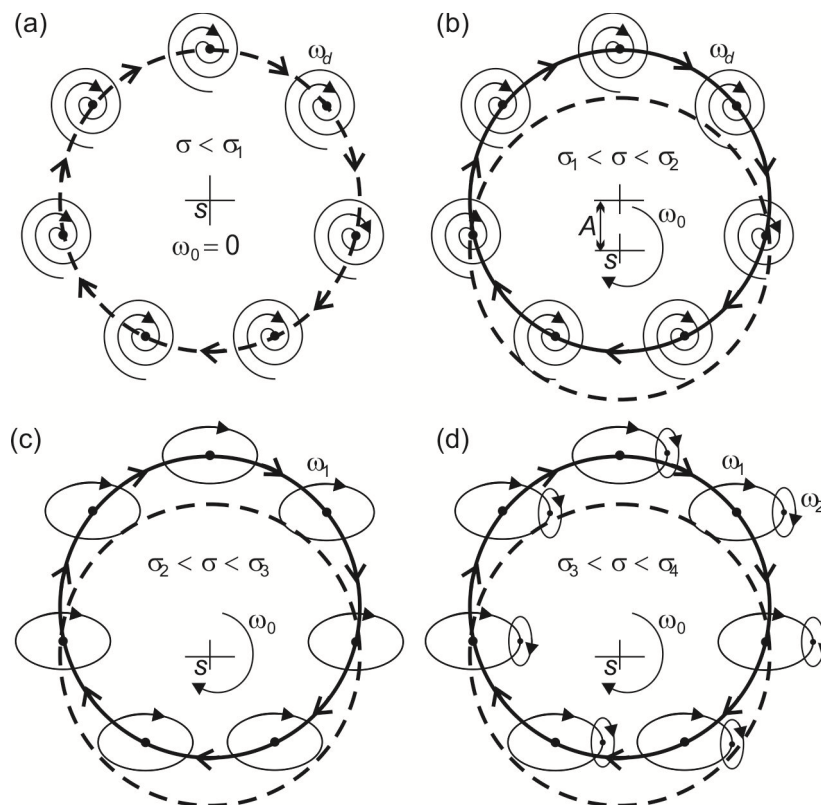


Fig. 6.7. Illustration of the conjecture explaining robust stability of the 3D torus.

Analyzing these solutions, we can formulate a conjecture explaining the observed behavior of the system under consideration, which is illustrated in Fig. 6.7 for the case of identical nodes. According to this approach, a rotational, let us say *tangent* (to the ring), degree of freedom (DoF) resulting from the unidirectional connectivity scheme is independent of an individual node, let us say *transverse* (to the ring) degrees of freedom. A small coupling ($\sigma < \sigma_1$) does not enable an initiation of the RW and damped oscillations of each item in the *transverse* direction with the frequency ω_d take place (Fig. 6.7a), i.e., the global equilibrium position (dotted circle in Fig. 6.7a) is stable. The first Hopf bifurcation at $\sigma_1 = 0.0332$ activates the rotational degree of freedom (HRW) but transverse vibrations are still damped. Thus, now we can observe a transversally stable equilibrium floating harmonically with the amplitude A (Fig. 6.7b), defined by Eq. (6.5) and shown in Fig. 6.1, due to rotational forcing. In the scheme shown in Fig. 6.7b, it is manifested with an eccentricity of the distance A (amplitude of such floating) between solid and dotted circles. Rotations of the solid circle cause harmonic oscillations around the stable position represented by the dotted circle. Just after a slight increase in the coupling strength, the second Hopf type bifurcation at $\sigma_2 = 0.0337$ takes place, which is the first one in the *transverse* DoF. It activates a limit cycle (LC) of the frequency ω_1 in the *transverse* direction (Fig. 6.7c), which is disproportionate to ω_0 , i.e., the frequency of the HRW. As a result, we can see the T^2 solution as a combination of the HRW and the LC – see Fig. 6.7. After the next Hopf type bifurcation at $\sigma_3 = 0.0436$, the third incommensurate frequency ω_2 appears and, consequently, the stable three-frequency quasi-periodic solution T^3 can be observed (Fig. 6.7d and 6.3). However, according to the theorem represented by us, the third Hopf bifurcation is only the second in the transverse DoF and then the T^3 solution can be considered as a superposition of the T^2 transverse solution and the independent HRW (see Fig. 6.4). Finally, chaos dominates after crossing the limit $\sigma_4 = 0.0478$ (Figs. 3.1.1, 3.1.2 and 3.1.5). From the viewpoint of global ring dynamics, it looks like a transition to chaos after the fourth Hopf bifurcation but from the transverse DoF point of view, this is a realization of the classical NRT scenario where a chaotic attractor appears as a product of the 3D torus destruction just after the third consecutive Hopf bifurcation. Thus, global dynamics of the ring is a superposition of harmonic rotational forcing (manifested with the HRW) and a transversal response of individual oscillators.

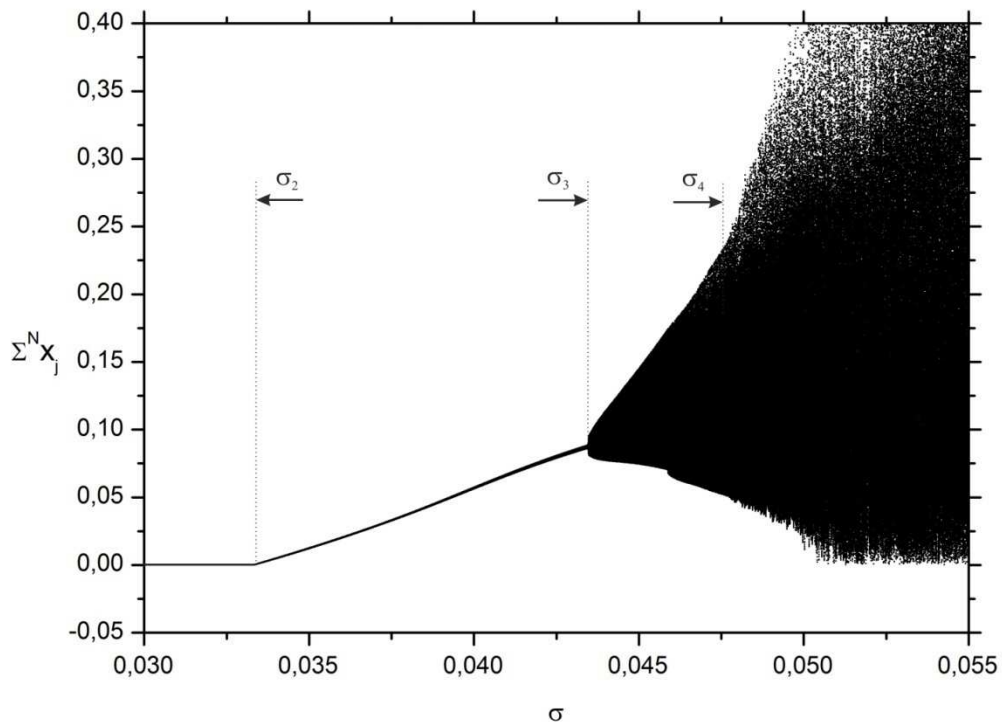


Fig. 6.8. Bifurcation diagram of the sum $\Sigma^N x_j$ versus the coupling parameter σ .

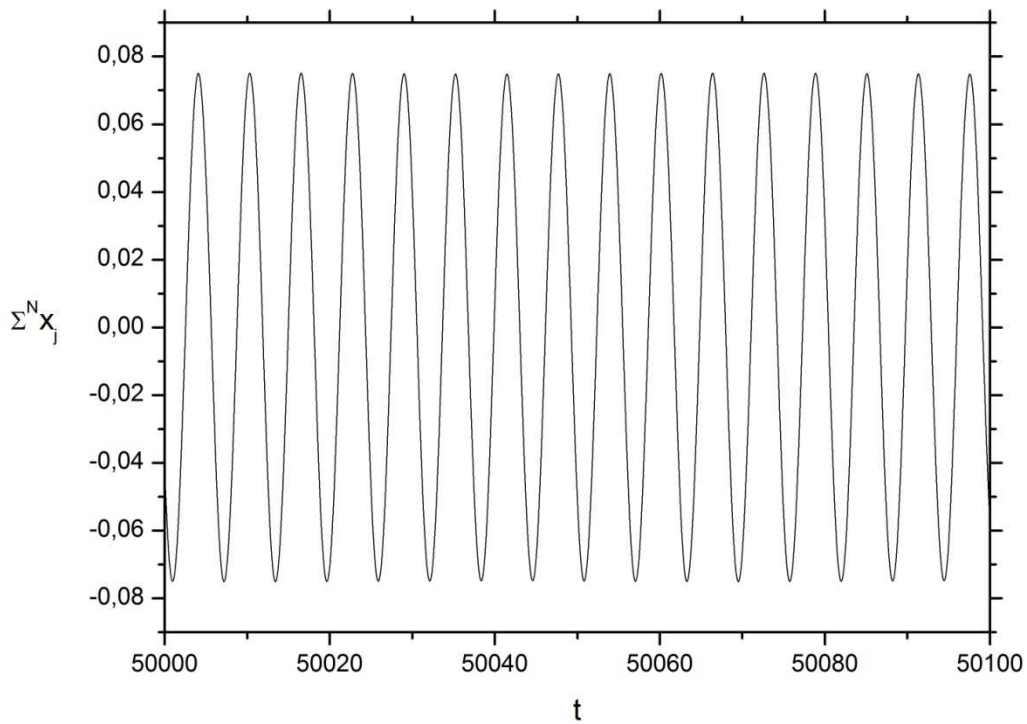


Fig. 6.9. Time diagram of the sum $\Sigma^N x_j$ for the coupling parameter $\sigma=0.0420$.

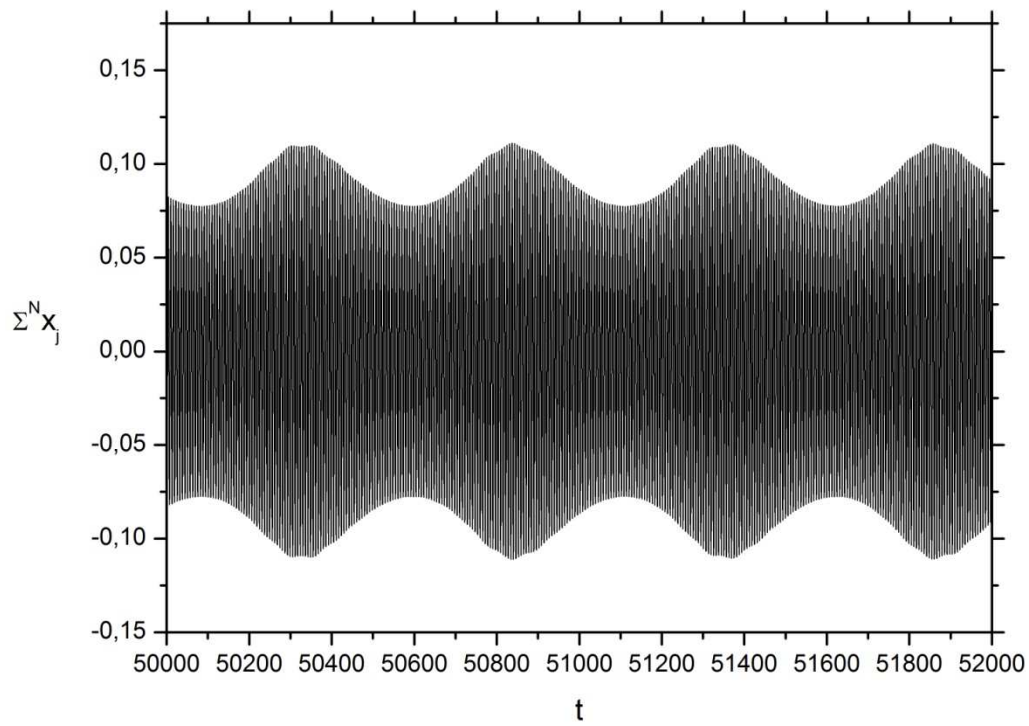


Fig. 6.10. Time diagram of the sum $\Sigma^N x_j$ for the coupling parameter $\sigma=0.0440$.

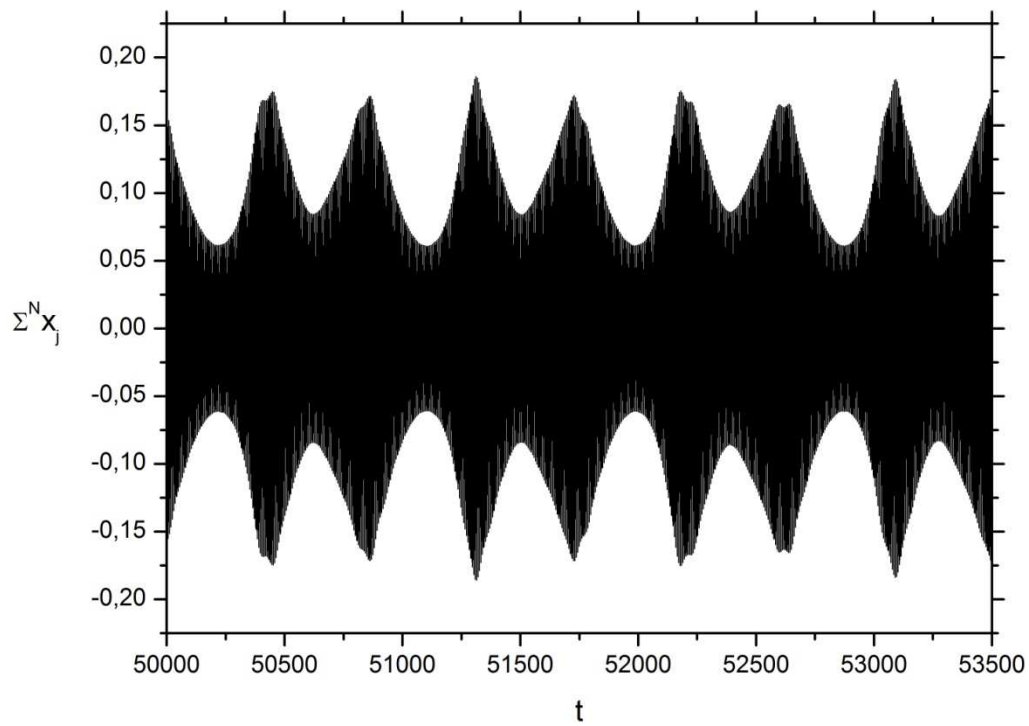


Fig. 6.11. Time diagram of the sum $\Sigma^N x_j$ for the coupling parameter $\sigma=0.0465$.

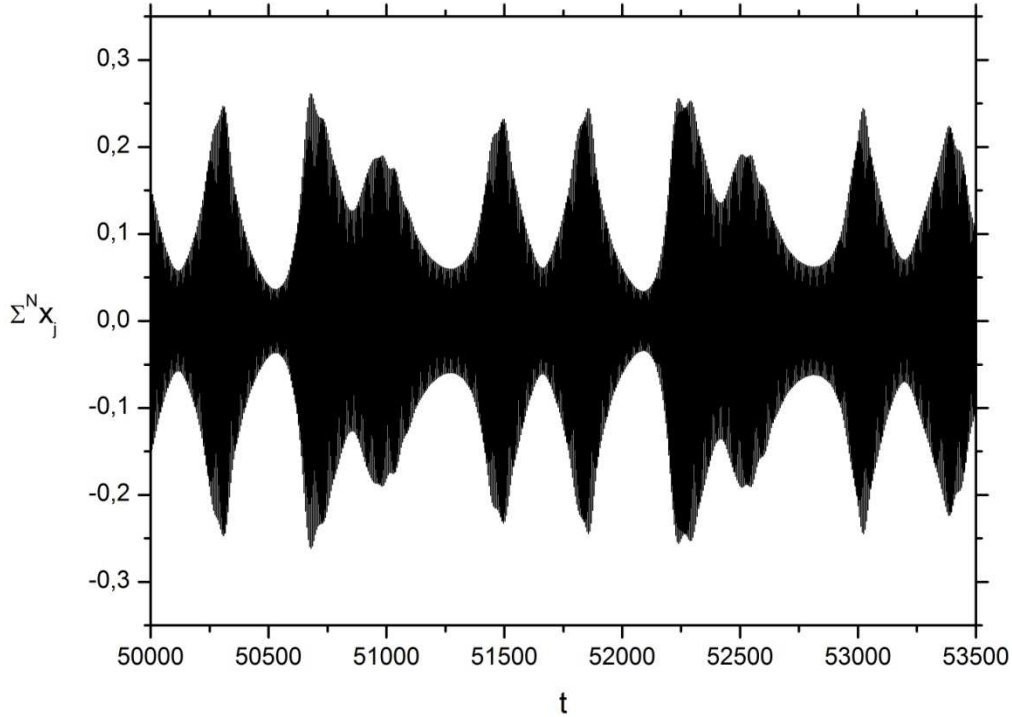


Fig. 6.12. Time diagram of the sum $\Sigma^N x_j$ for the coupling parameter $\sigma=0.0490$.

A good way to illustrate this idea on the example of the system under consideration is to extract the transverse response from the global ring dynamics and present its analysis. This can be achieved by elimination of the HRW components (clearly visible in Fig. 6.1) from the registered global ring signal. The same components are hidden in the skeleton of quasi-periodic and chaotic solutions. These HRW modes can be simply removed from responses of identical oscillators by summing up their signals. Due to the symmetry of their phase distribution along the ring, their sum is equal to zero in each moment of the system evolution. Thus, such a sum signal does not contain the frequency ω_0 (6.4) in the spectrum, so it is representative for the transverse dynamics of ring oscillators. In Fig. 6.8, a bifurcation diagram of the sum $\Sigma^N x_j$ versus σ , corresponding to Figs. 3.1.1 and 3.1.2, and the related time courses of this sum (Figs. 6.9-6.12) are demonstrated. The equilibrium remains stable up to the value σ_2 , where the first transverse Hopf-type bifurcation takes place (Fig. 6.8). Next, a stable LC in the range $\sigma_2 < \sigma < \sigma_3$, corresponding to the T^2 solution from Figs. 3.1.1 and 3.1.2, is observed (see its time diagram in Fig. 6.9). Consequently, the Hopf-type bifurcation at σ_3 leads to the existence of a transverse 2D torus (Fig. 6.10) and its period-doubling (Fig. 6.11) in the interval $\sigma_3 < \sigma < \sigma_4$. This sequence of bifurcations is also reflected in Figs. 3.1.1 and 3.1.2 for the global three-frequency quasi-periodicity. The last Hopf-type bifurcation at σ_4

destabilizes the transverse 2D torus and chaotic motion becomes dominant (Fig. 6.12). Thus, in the transverse DoF, we observe a typical NRT scenario of a transition to chaos.

In the case of the mismatch of parameters between ring oscillators, the HRW of the frequency ω_0 also exists but it is non-symmetric in accordance with the solutions to Eqs. (6.7a-c), as shown in Fig. 6.4. This is the reason why the rotational DoF cannot be effectively eliminated from the global signal by a sum of the HRW components, so the visualization of transverse modes by this method, analogous to that one shown in Figs. 6.8-6.12, is impractical. Nevertheless, the conjecture presented above on the superposition effect explaining the robust stability of the observed 3D torus is definitely still applicable in the real circuit with the parameter mismatch, in spite of some obvious differences in sequences of bifurcations between identical and real circuits (compare Figs. 3.1.1, 3.1.2, 3.1.5 with Figs. 3.1.3, 3.1.4, 3.1.6).

After analyzing the results of the numerical simulations of a single Duffing oscillator with a time delay loop (Chapter 5) and comparing them with the results for a circuit of seven identical unidirectionally coupled Duffing oscillators (Chapter 3), we can say that they exhibit a considerable similarity. In both cases, there is the first and second Hopf bifurcation. A transition from the stationary to periodic solution and then to the quasi-periodic solution (2D torus) can be seen. However, in contrast to the unidirectionally coupled oscillators, a stable three-frequency torus is not observed in the system with time delay. For a single Duffing oscillator with time delay, a period-doubling bifurcation of the 2D torus takes place after the second Hopf bifurcation. A further increase in the control parameter (time delay) leads to a chaotic solution.

Summing up, a robustly stable three-frequency quasi-periodic solution in the ring of unidirectionally coupled Duffing oscillators has been confirmed numerically and verified experimentally. The mechanism of such robust stability has been explained as an effect of the structural separation of rotational and transverse DoFs. Moreover, it has been shown that initiation and propagation of the RW is possible also in unidirectional rings of slightly non-identical oscillators. This fact can shed a new light on the nature of the RW phenomenon. On the other hand, an absence of a 3D torus in the single Duffing oscillator with a time delay loop may be explained by an absence of the RW, which occurs in the ring of unidirectionally coupled oscillators. Therefore, a superposition effect of rotational and transversal vibrations forms, which stabilizes three-frequency quasi-periodic solutions according to the above hypothesis, is not possible in this system. Hence, mathematical and physical properties of the RW will be a subject of further investigations in the nearest future.

NUMERYCZNA I EKSPERYMENTALNA ANALIZA EFEKTÓW SPRZEŻENIA I OPÓŹNIENIA CZASOWEGO W SZEREGACH NIELINIOWYCH OSCYLATORÓW

Przedmiotem niniejszej pracy jest analiza klasycznego oscylatora typu Duffinga w dwóch konfiguracjach systemowych:

1. jako układ węzłowy w domkniętym szeregu (pierścieniu) jednokierunkowo sprzężonych oscylatorów,
2. jako układ z pętlą opóźnienia czasowego.

Głównym celem pracy było pokazanie analogii dynamicznych pomiędzy szeregami jednokierunkowo sprzężonych oscylatorów, a układami z opóźnieniem czasowym, głównie w kontekście podobieństwa scenariuszy bifurkacyjnych, prowadzących od stanu stacjonarnego poprzez ruch regularny do dynamicznego hiper-chaosu. Szczególny nacisk zostanie położony na identyfikację mechanizmu destabilizacji stanu stacjonarnego oraz rozwiązania okresowego w rezultacie wzrostu parametru sprzężenia lub wielkości opóźnienia czasowego.

Natomiast teza pracy brzmi: *Możliwe jest występowanie statecznego, trój-częstościowego rozwiązania quasi-okresowego w szeregach jednokierunkowo sprzężonych oscylatorów oraz istnieje wiele analogii pomiędzy zachowaniami dynamicznymi takich układów a oscylatorami z opóźnionym sprzężeniem zwrotnym.*

W pierwszej części pracy (rozdziały 2 i 3) dokonano numerycznej analizy bifurkacyjnej szeregu siedmiu identycznych oraz rzeczywistych, tzn. z uwzględnieniem zmierzonych na stanowisku doświadczalnym różnic parametrów, sprzężonych jednokierunkowo oscylatorów Duffinga. Dokonano również porównania rezultatów symulacji numerycznych dla identycznych oraz rzeczywistych oscylatorów.

W kolejnej części pracy (rozdział 4) zaprezentowano stanowisko doświadczalne, przeprowadzono identyfikację jego parametrów oraz badania eksperymentalne celem potwierdzenia symulacji numerycznych dla badanego obwodu. Wyniki eksperymentu porównano z rezultatami numerycznymi.

W ostatniej części pracy dokonano analizy numerycznej pojedynczego oscylatora Duffinga z wprowadzoną pętlą opóźnienia czasowego (rozdział 5). Wyniki eksperymentu numerycznego zostały porównane z wynikami dla szeregów identycznych, sprzężonych oscylatorów w kontekście podobieństwa scenariuszy bifurkacyjnych.

Podsumowując, w pracy potwierdzono i zweryfikowano doświadczalnie istnienie statecznego trój-częstościowego rozwiązania quasi-okresowego w obwodzie jednokierunkowo sprzężonych oscylatorów Duffinga. Mechanizm takiej trwałej stateczności torusa 3D został w pracy wyjaśniony hipotezą o strukturalnej separacji rotacyjnego (fala rotacyjna) i transwersalnych (odpowiedzi oscylatorów) stopni swobody. Z drugiej strony, wykazano, że inicjacja i propagacja fali rotacyjnej jest możliwa również w obwodach jednokierunkowo sprzężonych oscylatorów rzeczywistych, czyli przy braku idealnej zgodności wartości parametrów. Fakt ten może rzucić nowe światło na charakter i dynamikę zjawiska fali rotacyjnej.

Natomiast, zgodnie ze sformułowaną hipotezą, brak rozwiązania w postaci torusa 3D w układzie pojedynczego oscylatora typu Duffinga z wprowadzoną pętlą opóźnienia czasowego może być spowodowane niewystępowaniem fali rotacyjnej, która pojawia się w szeregach sprzężonych jednokierunkowo oscylatorów.

Matematyczne i fizyczne właściwości fali rotacyjnej generowanej w układach jednokierunkowo sprzężonych oscylatorów będą przedmiotem dalszych badań w najbliższej przyszłości.

BIBLIOGRAPHY

- [1] Chua, L. O., and S. Parker. "Chaos: A tutorial for engineers." *Proc. IEEE* 75 (1987): 982-1008.
- [2] Hadamard, Jacques Salomon. *Sur le billard non Euclidien*. Impr. Gauthier-Villars, 1898.
- [3] Poincaré, Henri. *Science and hypothesis*. Science Press, 1905.
- [4] Birkhoff, G. D. (1920). Recent advances in dynamics. *Science*, 51, 51-55.
- [5] Cartwright, M. L. (1952). Non-Linear Vibrations: A Chapter in Mathematical History. Presidential Address to the Mathematical Association, January 3, 1952. *The Mathematical Gazette*, 36(316), 81-88.
- [6] Smale, S. (1961). On gradient dynamical systems. *The Annals of Mathematics*, 74(1), 199-206.
- [7] Kolmogorov, A. N. (1962). A refinement of previous hypotheses concerning the local structure of turbulence in a viscous incompressible fluid at high Reynolds number. *J. Fluid Mech*, 13(1), 82-85.
- [8] Kolmogorov, A. N. (1991). The local structure of turbulence in incompressible viscous fluid for very large Reynolds numbers. *Proceedings of the Royal Society of London. Series A: Mathematical and Physical Sciences*, 434(1890), 9-13.
- [9] Sparrow, Colin. *The Lorenz equations: bifurcations, chaos, and strange attractors*. Vol. 41. New York: Springer-Verlag, 1982.
- [10] Rössler, Otto E. "An equation for continuous chaos." *Physics Letters A* 57.5 (1976): 397-398.
- [11] Chen, Guanrong, and Tetsushi Ueta. "Yet another chaotic attractor." *International Journal of Bifurcation and Chaos* 9.07 (1999): 1465-1466.
- [12] Rapp, Paul E. "Chaos in Biology: Chaos in the neurosciences: cautionary tales from the frontier." *BIOLOGIST-INSTITUTE OF BIOLOGY* 40 (1993): 89-89.
- [13] Weiss, James N., et al. "Chaos and chaos control in biology." *Journal of Clinical Investigation* 93.4 (1994): 1355.
- [14] Coffey, Donald S. "Self-organization, complexity and chaos: the new biology for medicine." *Nature Medicine* 4.8 (1998): 882-885.
- [15] Epstein, Irving R. "Oscillations and chaos in chemical systems." *Physica D: Nonlinear Phenomena* 7.1 (1983): 47-56.

- [16] Scott, Stephen K. *Oscillations, waves, and chaos in chemical kinetics*. Oxford: Oxford University Press, 1994.
- [17] Epstein, Irving R., and Kenneth Showalter. "Nonlinear chemical dynamics: oscillations, patterns, and chaos." *The Journal of Physical Chemistry* 100.31 (1996): 13132-13147.
- [18] Benhabib, Jess. *Cycles and chaos in economic equilibrium*. Princeton University Press, 1992.
- [19] Brock, William A. "Pathways to randomness in the economy: emergent nonlinearity and chaos in economics and finance." *Estudios Economicos* (1993): 3-55.
- [20] Invernizzi, Sergio, and Alfredo Medio. "On lags and chaos in economic dynamic models." *Journal of Mathematical Economics* 20.6 (1991): 521-550.
- [21] Sagdeev, Roald & D. Z., Daniël Alekseevič Usikov, and George M. Zaslavsky. *Nonlinear Physics: from pendulum to turbulence and chaos*. Vol. 4. CRC Press LLC, 1988.
- [22] Bohigas, Oriol, and H. A. Weidenmüller. "Aspects of chaos in nuclear physics." *Annual Review of Nuclear and Particle Science* 38.1 (1988): 421-453.
- [23] Blümel, Reinhold, and William P. Reinhardt. *Chaos in atomic physics*. Vol. 10. Cambridge University Press, 2005.
- [24] Hagedorn, Peter. "Non-linear oscillations." *Oxford and New York, Clarendon Press, 1981. 298 p. Translatio* 1 (1981).
- [25] Tseng, W-Y., and J. Dugundji. "Nonlinear vibrations of a buckled beam under harmonic excitation." *Journal of Applied Mechanics* 38 (1971): 467.
- [26] Pezeshki, C., and E. H. Dowell. "An examination of initial condition maps for the sinusoidally excited buckled beam modeled by the Duffing's equation." *Journal of sound and vibration* 117.2 (1987): 219-232.
- [27] Kovacic, Ivana, and Michael J. Brennan. *The duffing equation: Nonlinear oscillators and their behaviour*. Wiley, 2011.
- [28] Chakravarthy, S. K., and C. V. Nayar. "Series ferroresonance in power systems." *International Journal of Electrical Power & Energy Systems* 17.4 (1995): 267-274.
- [29] Van Der Pol, Balth. "VII. Forced oscillations in a circuit with non-linear resistance.(Reception with reactive triode)." *The London, Edinburgh, and Dublin Philosophical Magazine and Journal of Science* 3.13 (1927): 65-80.
- [30] Van der Pol, Balth, and J. Van der Mark. "Frequency demultiplication." *Nature* 120 (1927): 363-364.
- [31] Bennett, Matthew, et al. "Huygens's clocks." *Proceedings: Mathematics, Physical and Engineering Sciences* (2002): 563-579.

- [32] Altintas, Y., and M. Weck. "Chatter stability of metal cutting and grinding." *CIRP Annals-Manufacturing Technology* 53.2 (2004): 619-642.
- [33] Kapitaniak, Tomasz. *Chaos for engineers: theory, applications, and control*. Vol. 3. Springer Verlag, 2000.
- [34] Peleš, Slaven, and Kurt Wiesenfeld. "Synchronization law for a van der Pol array." *Physical Review E* 68.2 (2003): 026220.
- [35] Pyragas, Kestutis. "Continuous control of chaos by self-controlling feedback." *Physics Letters A* 170.6 (1992): 421-428.
- [36] Garfinkel, Alan, et al. "Controlling cardiac chaos." *Science* 257.5074 (1992): 1230-1235.
- [37] Chen, Guanrong. *Controlling chaos and bifurcations in engineering systems*. CRC Press LLC, 2000.
- [38] Chen, Guanrong, and Xinghuo Yu. *Chaos control*. Vol. 292. Springer verlag, 2003.
- [39] Schöll, Eckehard, and Heinz Georg Schuster, eds. *Handbook of chaos control*. Wiley-Vch, 2008.
- [40] Afraimovich, V. S., N. N. Verichev, and M. I. Rabinovich. "Stochastic synchronization of oscillation in dissipative systems." *Radiophysics and Quantum Electronics* 29.9 (1986): 795-803.
- [41] Awrejcewicz J. "Chaos i synchronizacja w układach fizycznych." *Wydawnictwo Politechniki Łódzkiej, Łódź, 1995*.
- [42] Fujisaka, Hirokazu, and Tomoji Yamada. "Stability theory of synchronized motion in coupled-oscillator systems." *Progress of Theoretical Physics* 69.1 (1983): 32-47.
- [43] Kapitaniak, T. "Synchronization of chaos using continuous control." *Physical Review E* 50.2 (1994): 1642.
- [44] Pecora, Louis M., and Thomas L. Carroll. "Synchronization in chaotic systems." *Physical review letters* 64.8 (1990): 821-824.
- [45] Landau, Lev D. "On the problem of turbulence." *CR Acad. Sci. URSS* 44.31 (1944): 1-314.
- [46] Hopf, Eberhard. "A mathematical example displaying features of turbulence." *Communications on Pure and Applied Mathematics* 1.4 (1948): 303-322.
- [47] Newhouse, Sheldon, David Ruelle, and Floris Takens. "Occurrence of strange Axioma attractors near quasi periodic flows on T^m , $m \geq 3$." *Communications in Mathematical Physics* 64.1 (1978): 35-40.
- [48] Ruelle, David, and Floris Takens. "On the nature of turbulence." *Communications in mathematical physics* 20.3 (1971): 167-192.

- [49] Feigenbaum, Mitchell J. "Quantitative universality for a class of nonlinear transformations." *Journal of statistical physics* 19.1 (1978): 25-52.
- [50] Feigenbaum, Mitchell J. "The universal metric properties of nonlinear transformations." *Journal of Statistical Physics* 21.6 (1979): 669-706.
- [51] Hénon, Michel. "A two-dimensional mapping with a strange attractor." *Communications in Mathematical Physics* 50.1 (1976): 69-77.
- [52] Pomeau, Yves, and Paul Manneville DPh G. PSRM. "Intermittent transition to turbulence in dissipative dynamical systems." *Communications in Mathematical Physics* 74.2 (1980): 189-197.
- [53] Manneville, Paul, and Yves Pomeau. "Different ways to turbulence in dissipative dynamical systems." *Physica D: Nonlinear Phenomena* 1.2 (1980): 219-226.
- [54] Grebogi, Celso, Edward Ott, and James A. Yorke. "Are three-frequency quasiperiodic orbits to be expected in typical nonlinear dynamical systems?." *Physical Review Letters* 51.5 (1983): 339-342.
- [55] Grebogi, Celso, Edward Ott, and James A. Yorke. "Attractors on an N-torus: Quasiperiodicity versus chaos." *Physica D: Nonlinear Phenomena* 15.3 (1985): 354-373.
- [56] Battelino, Peter M. "Persistence of three-frequency quasiperiodicity under large perturbations." *Physical Review A* 38.3 (1988): 1495.
- [57] Gollub, J.P., and S. V. Benson. "Many routes to turbulent convection." *J. Fluid Mech* 100.3 (1980): 449-470.
- [58] Linsay, Paul S., and Andrew W. Cumming. "Three-frequency quasiperiodicity, phase locking, and the onset of chaos." *Physica D: Nonlinear Phenomena* 40.2 (1989): 196-217.
- [59] Alaggio, Rocco, and Giuseppe Rega. "Characterizing bifurcations and classes of motion in the transition to chaos through 3D-tori of a continuous experimental system in solid mechanics." *Physica D: Nonlinear Phenomena* 137.1 (2000): 70-93.
- [60] Feudel, Ulrike, Wolfgang Jansen, and Jürgen Kurths. "Tori and chaos in a nonlinear dynamo model for solar activity." *International Journal of Bifurcation and Chaos* 3.01 (1993): 131-138.
- [61] Anishchenko, V. S., , M. A., Feudel, U., & Kurths, J. "Bifurcations and transition to chaos through three-dimensional tori." *International Journal of Bifurcation and Chaos* 4.03 (1994): 595-607.
- [62] Feudel, U., Safonova, M. A., Kurths, J., & Anishchenko, V. S. "On the destruction of three-dimensional tori." *International Journal of Bifurcation and Chaos* 6.07 (1996): 1319-1332.

- [63] Yang, Junzhong. "Quasiperiodicity and transition to chaos." *Physical review. E, Statistical physics, plasmas, fluids, and related interdisciplinary topics* 61.6 Pt A (2000): 6521-6526.
- [64] Lopez, J. M., and F. Marques. "Dynamics of three-tori in a periodically forced Navier-Stokes flow." *Physical Review Letters* 85.5 (2000): 972-975.
- [65] Marques, F., J. M. Lopez, and J. Shen. "A periodically forced flow displaying symmetry breaking via a three-tori gluing bifurcation and two-tori resonances." *Physica D: Nonlinear Phenomena* 156.1 (2001): 81-97.
- [66] Matías, M. A., Güémez, J., Pérez-Munuzuri, V., Marino, I. P., Lorenzo, M. N., & Pérez-Villar, V. "Size instabilities in rings of chaotic synchronized systems." *EPL (Europhysics Letters)* 37.6 (1997): 379.
- [67] Sánchez, Esteban, and Manuel A. Matías. "Transition to chaotic rotating waves in arrays of coupled Lorenz oscillators." *International Journal of Bifurcation and Chaos* 9.12 (1999): 2335-2343.
- [68] Pazó, Diego, Esteban Sánchez, and Manuel A. Matías. "Transition to high-dimensional chaos through quasiperiodic motion." *International Journal of Bifurcation and Chaos* 11.10 (2001): 2683-2688.
- [69] Pazó, Diego, and Manuel A. Matias. "From quasiperiodicity to high-dimensional chaos without intermediate low-dimensional chaos." *arXiv preprint arXiv:0909.1260* (2009).
- [70] Bi, Qinsheng. "Dynamical analysis of two coupled parametrically excited van der Pol oscillators." *International journal of non-linear mechanics* 39.1 (2004): 33-54.
- [71] Wu, Wenjuan, Zengqiang Chen, and Zhuzhi Yuan. "The evolution of a novel four-dimensional autonomous system: among 3-torus, limit cycle, 2-torus, chaos and hyperchaos." *Chaos, Solitons & Fractals* 39.5 (2009): 2340-2356.
- [72] Turing, A. M. "Philosophical transactions of the Royal Society of London. Series B." *Biological Sciences* 237.641 (1952): 37-72.
- [73] Erneux, Th, and M. Herschkowitz-Kaufman. "Rotating waves as asymptotic solutions of a model chemical reaction." *The Journal of Chemical Physics* 66 (1977): 248.
- [74] Auchmuty, J. F. G. "BIFURCATING WAVES*." *Annals of the New York Academy of Sciences* 316.1 (1979): 263-278.
- [75] Noszticzius, Zoltan, et al. "Sustained chemical waves in an annular gel reactor: a chemical pinwheel." *Nature* 329.6140 (1987): 619-620.
- [76] Matias, M. A., et al. "Observation of a fast rotating wave in rings of coupled chaotic oscillators." *Physical review letters* 78.2 (1997): 219-222.

- [77] Sánchez, Esteban, Diego Pazó, and Manuel A. Matías. "Experimental study of the transitions between synchronous chaos and a periodic rotating wave." *Chaos: An Interdisciplinary Journal of Nonlinear Science* 16.3 (2006): 033122-033122.
- [78] Perlikowski, P., Yanchuk, S., Wolfrum, M., Stefanski, A., Mosiolek, P., & Kapitaniak, T. "Routes to complex dynamics in a ring of unidirectionally coupled systems." *Chaos: An Interdisciplinary Journal of Nonlinear Science* 20.1 (2010): 013111-013111.
- [79] Perlikowski, P., Jagiello, B., Stefanski, A., & Kapitaniak, T. "Experimental observation of ragged synchronizability." *Physical Review-Section E-Statistical Nonlinear and Soft Matter Physics* 78.1 (2008): 17203.
- [80] Perlikowski, P., Stefański, A., & Kapitaniak, T. "1: 1 Mode locking and generalized synchronization in mechanical oscillators." *Journal of Sound and Vibration* 318.1 (2008): 329-340.
- [81] Verichev, Nikolai N., Stanislav N. Verichev, and Marian Wiercigroch. "Asymptotic theory of chaotic synchronization for dissipative-coupled dynamical systems." *Chaos, Solitons & Fractals* 41.2 (2009): 752-763.
- [82] Mackey, M. C., & Glass, L. (1977). Oscillation and chaos in physiological control systems. *Science*, 197(4300), 287-289.
- [83] Doyné Farmer, J. (1982). Chaotic attractors of an infinite-dimensional dynamical system. *Physica D: Nonlinear Phenomena*, 4(3), 366-393.
- [84] Lu, H., & He, Z. (1996). Chaotic behavior in first-order autonomous continuous-time systems with delay. *Circuits and Systems I: Fundamental Theory and Applications, IEEE Transactions on*, 43(8), 700-702.
- [85] Maccari, A. (2003). Vibration control for the primary resonance of the Van der Pol oscillator by a time delay state feedback. *International journal of non-linear mechanics*, 38(1), 123-131.
- [86] Yu, P., Yuan, Y., & Xu, J. (2002). Study of double Hopf bifurcation and chaos for an oscillator with time delayed feedback. *Communications in Nonlinear Science and Numerical Simulation*, 7(1), 69-91.
- [87] Xu, J., & Chung, K. W. (2003). Effects of time delayed position feedback on a Van der Pol–Duffing oscillator. *Physica D: Nonlinear Phenomena*, 180(1), 17-39.
- [88] Yanchuk, Serhiy, and Matthias Wolfrum. "Destabilization patterns in chains of coupled oscillators." *Physical Review E* 77.2 (2008): 026212.
- [89] Pecora, Louis M., and Thomas L. Carroll. "Master stability functions for synchronized coupled systems." *Physical Review Letters* 80.10 (1998): 2109-2112.

- [90] Robinson, F. N. H. "Experimental observation of the large-amplitude solutions of Duffing's and related equations." *IMA Journal of Applied Mathematics* 42.2 (1989): 177-201.
- [91] Collins, J. J., & Stewart, I. (1994). A group-theoretic approach to rings of coupled biological oscillators. *Biological cybernetics*, 71(2), 95-103.
- [92] Rand, D. (1982). Dynamics and symmetry. Predictions for modulated waves in rotating fluids. *Archive for Rational Mechanics and Analysis*, 79(1), 1-37.